UNIVERSITY OF NOVA GORICA
GRADUATE SCHOOL

VISUALIZATION AND DYNAMICS OF FLAVIVIRAL RNA IN LIVING CELLS

DISSERTATION

Lisa Miorin

Mentor: Alessandro Marcello PhD.

Nova Gorica, 2011

ABSTRACT

RNA viruses induce host cell membranes' rearrangements to replicate efficiently and possibly to escape from innate immunity. In this work we developed a powerful tool to track flaviviral RNA in living cells in order to dissect the dynamic interaction between viral genomes and the host cell machinery. We engineered tick-borne encephalitis virus (TBEV) replicons with an array of binding sites for the phage MS2 core protein. The modified TBEV replicons were competent for RNA replication and accumulated in cytoplasmic compartments enriched in non-structural viral proteins as well as in the double-stranded RNA (dsRNA) intermediate of replication. These compartments appeared organized in a network of interconnected vesicles that originates from the endoplasmic reticulum and protects viral dsRNA from being digested by RNase treatment. The MS2-based system was then further exploited in order to address the relationship between the formation of these membrane wrapped replication compartments and the subversion of the innate immune response. We observed a consistent delay of interferon induction following virus replication. This delay correlated with a defect in pattern recognition receptor's signaling. However, viral proteins could not directly inhibit the pathway suggesting an indirect mechanism. Then, we explored protein and viral RNA trafficking in the living cells. We found that cytoplasmic sites of replicated viral RNA accumulation are able to exchange proteins with the cytosol. However, viral RNA trafficking to the cytosol was significantly impaired. Therefore, we conclude that the initial escape from innate immunity involves the formation of replication vesicles that may prevent the direct interaction between pattern recognition receptors and their agonists or impair signalling to downstream adaptor molecules.

POVZETEK

Virusi RNA spreminjajo strukturo celične membrane gostiteljskih celic zaradi zagotavljanja lastne replikacije in verjetno tudi zaradi izogibanja prirojenemu imunskemu odzivu. V našem raziskovalnem delu smo razvili učinkovito orodje za sledenje flavivirusne RNA v živih celicah, ki omogoča proučevanje dinamičnih interakcij med virusnimi genomi in gostiteljsko celico. Konstruirali smo replikon virusa klopnega meningoencefalitisa (TBEV) z mrežo vezavnih mest za središčni protein faga MS2. Modificirani replikon TBEV je bil zmožen replikacije RNA in kopičenja v citoplazemskih razdelkih, ki so bili obogateni z nestrukturnimi virusnimi proteini in z dvoverižnimi itermediati RNA (dsRNA) replikacije. Ti razdelki so organizirani v mrežo med seboj povezanih veziklov, ki izvirajo iz endoplazemskega retikuluma in ki ščitijo virusno dsRNA pred razgradnjo z RNA-zami. Konstrukt MS2 smo v nadaljevanju uporabili za proučevanje razmerja med nastankom membranskih replikacijskih razdelkov in izogibanjem prirojenemu imunskemu odzivu. Opazili smo dosledno zakasnitev proženja interferonskega odziva, ki nastane kot odgovor na virusno podvojevanje. Ta zakasnitev je bila povezana z nepravilnostmi v signaliziranju preko receptorjev za prepoznavanje patogenih motivov. Vendar virusni proteini niso neposredno inhibirali te poti, kar kaže na posredni mehanizem delovanja. V naslednjem koraku smo raziskovali razmeščanje proteinov in virusne RNA v živih celicah. Ugotovili smo, da so citoplazemski razdelki, kjer se kopiči podvojena RNA, sposobni izmenjave proteinov s citosolom. Nasprotno pa je bilo potovanje virusne RNA v citosol zelo omejeno. Zaključili smo, da je začetno izogibanje prirojenemu imunskemu odzivu povezano z nastankom replikacijskih razdelkov, ki najverjetneje preprečijo neposredno interakcijo med receptorji za prepoznavanje patogenih motivov in njihovimi agonisti, oziroma ovirajo prenašanje signalov do znotrajceličnih adaptorskih molekul.

PUBLICATIONS

This thesis is based in these publications:

Miorin, L., Maiuri, P., Hoenninger, V.M., Mandl, C.W., and Marcello, A. (2008). Spatial and Temporal Organization of Tick-Borne Encephalitis Flavivirus Replicated RNA in Living Cells, Virology *379*, 64-77.

Hoenninger, V.M., Rouha, H., Orlinger, K.K., Miorin, L., Marcello, A., Kofler, R.M., and Mandl, C.W. (2008). Analysis of the effects of alterations in the tick-borne encephalitis virus 3'-noncoding region on translation and RNA replication using reporter replicons. Virology *377*, 419-430.

Miorin, L., Albornoz, A., Baba, M.M., D'Agaro, P., and Marcello, A. (2011). Formation of membrane-defined compartments by tick-borne encephalitis virus contributes to the early delay in interferon signalling. (Submitted to Journal of General Virology)

CONTENTS

LIST OF FIGURES

LIST OF TABLES

1. INTRODUCTION

1.1. Family Flaviviridae

Flaviviridae are enveloped, positive single-stranded RNA viruses responsible for causing severe disease and mortality in humans and animals. This family of viruses consists of three genera: Flavivirus (from the Latin *flavus*, yellow), Pestivirus (from the Latin *pestis*, plague) and Hepacivirus (from the Greek *hepar, hepatos*, liver). In addition to these genera, two groups of unassigned viruses, GBV-A and GBV-C, await formal classification within the family (Figure 1). Although they belong to different genera and they have different biological properties, the members of this family share similarity in terms of virion morphology, genome organization and replication strategies (Fernandez-Garcia et al., 2009; Gould and Solomon, 2008; Lindenbach et al., 2007; Mukhopadhyay et al., 2005).

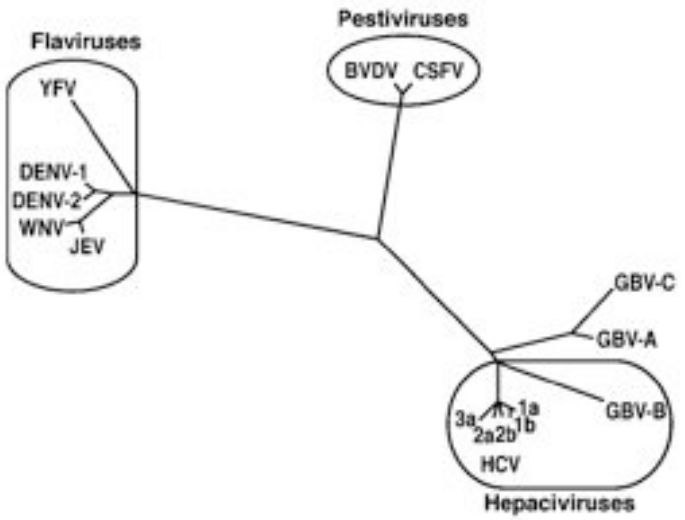

Figure 1 The family Flaviviridae. Phylogenetic tree based on analysis of NS3 helicase regions. Members of the Flavivirus genus are shown: yellow fever virus (YFV), dengue-1 (DENV-1), dengue-2 (DENV-2), West Nile virus (WNV) and Japanese encephalitis (JEV); the Pestivirus genus: bovine viral diarrhea virus (BVDV) and classical swine fever (CSFV); several Hepacivirus (HCV) isolates, including GBV-B; and the unclassified viruses GBV-A and GBV-C. Figure from (Lindenbach et al., 2007).

The Flavivirus genus is the largest in the family and consists of more than 70 members. Flaviviruses are among the most important emerging viruses known to man and are mostly transmitted by mosquitoes or ticks (arthropod-borne viruses). As described more in the details in the Chapter 1.2, they include important human

pathogens such as yellow fever virus (YFV), the dengue viruses (DV), Japanese encephalitis virus (JEV), West Nile virus (WNV) and tick-borne encephalitis virus (TBEV).

The Pestivirus genus contains three important animal viruses: the type member, bovine viral diarrhea virus (BVDV), as well as classical swine fever virus (CSFV), and border disease virus (BDV) of sheep. Within the family, Pestiviruses show greater similarities in genome structure and mechanism of translation initiation to the Hepaciviruses than to the Flaviviruses.

Hepatitis C virus (HCV) is the unique blood-borne virus in the family and its origin is still unknown. HCV is the type member of the Hepacivirus genus, which also include GB virus B (GBV-B). HCV infections were referred as non-A, non-B hepatitis until the causative agent was identified in 1989 (Choo et al., 1989). They represent the major cause of chronic hepatitis, liver cirrhosis and hepatocellular carcinoma (HCC) worldwide. Currently more than 170 million people, roughly 3 % of the human population, are indeed infected with HCV and epidemiologic studies have revealed that about 80% of infected individuals fail to eradicate the virus and subsequently develop a lifelong persistent infection (Bode et al., 2007; Leyssen et al., 2000).

1.2. Genus Flavivirus

Flaviviruses are a group of arboviruses belonging to the Flaviviridae family with a high impact on public health. The majority of flaviviruses are transmitted to humans through the bite of two groups of vectors, mosquitoes and ticks. According to the arthropod vector, within the genus, viruses can be further divided in three clusters: the mosquito-borne cluster, the tick-borne cluster and the nonvector-borne cluster. Prominent viral species of the first group include yellow fever virus, dengue virus, Japanese encephalitis virus, and West Nile virus. Tick-borne encephalitis virus is instead the most important member of the tick-borne cluster (Gubler et al., 2007; Mackenzie et al., 2004; Mandl, 2005). Flaviviruses are highly prevalent particularly in the developing world, however, are becoming a global severe problem due to climatic and socio-economic changes that lead to the spread of the viruses to new

geographic regions. Hemorrhagic disease, encephalitis, biphasic fever, and flaccid paralysis are typical manifestations of diseases after flavivirus infection (Gould and Solomon, 2008; Solomon and Mallewa, 2001). Surprisingly, despite the large number of humans that suffer severe flavivirus infections annually, there are no available antiviral therapies. Furthermore, although excellent advances have been made in the development of new prophylactic measurements, the need of safe, stable, and low cost vaccine for the dissemination in the endemic area is still an important issue in flaviviral research. Hence, an in-depth understanding of the molecular mechanisms involved in the disease progression and pathogenesis will certainly contribute to the development of new effective therapeutics to combat flavivirus-mediated diseases.

1.2.1. Virion morphology and composition

Flaviviruses are icosahedral enveloped 50 nm viruses with a positive-strand RNA genome packaged by the viral capsid protein (C). The spherical nucleocapsid core of about 30 nm is covered by a host-derived lipid bilayer with two surface glycoproteins, membrane (M, which is expressed as prM, the precursor to M) and envelope (E), that have double-membrane anchors at the C-terminus.

The C protein, consistently with its role in packaging the viral RNA, is a highly basic protein of approximately 11 kilodalton (KDa). Although sequence identity among flaviviruses capsid proteins is very little, their overall structural organization is conserved. They all share a “central” hydrophobic domain responsible for the interaction with the surrounding membranes, which has been proposed to play a role in virion assembly (Kofler et al., 2002; Ma et al., 2004), and a second hydrophobic region at the C-terminal end of the protein. This second stretch of hydrophobic amino acid residues serves as signal peptide for prM translocation into the lumen of the ER and is later removed from the mature protein C by the viral serine protease NS2B-NS3 (Lindenbach et al., 2007).

The prM glycoprotein (26KDa) is the precursor of the structural protein M. As mentioned above, prM is translocated into the ER by the C protein signal peptide. The N-terminal region of prM contains the glycosilation sites and six conserved cysteine residues whereas the trans-membrane domains are located at the C-terminal region (Lindenbach et al., 2007). The M protein is produced during maturation of the

viral particle within the secretory pathway after cleavage of prM by the cellular protease furin. This step is crucial to yield mature and fully infectious virions (Guirakhoo et al., 1991; Stadler et al., 1997).

The E protein is the major viral antigen and has the dual function of mediating receptor interaction and low pH-induced fusion during virus entry (Stiasny and Heinz, 2006) (Kaufmann and Rossmann, 2011). E is a type I membrane protein composed by a two-helix transmembrane region and an N-terminal ectodomain connected by a α-helical stem region. The ectodomain has three distinct, structurally defined domains (DI, DII and DIII) that are joined by short flexible hinges (Stiasny et al., 2009). DI, which forms a β-barrel, is the central domain and participates in the conformational changes induced by endosomal acidification during cell entry (Bressanelli et al., 2004); DII contains the highly conserved fusion peptide loop at its tip; and DIII appears to be involved in receptor binding (Rey et al., 1995).

As shown in Figure 2, immature particles display 60 prominent and irregular spikes on their surface, each spike consisting of a trimer of prM-E heterodimers. The prM proteins cap the fusion peptides on the E proteins and protect the virus from premature fusion before release (Yu et al., 2009; Yu et al., 2008). Depending on the pH of the cellular environment, the immature particle can exist reversibly in either "spiky" (pH 7) or "smooth" (pH 6) forms. During the maturation process, due to the low pH-conditions in the Trans-Golgi Network (TGN), the prM proteins expose a furin cleavage site and the 'pr' peptides are irreversibly cleaved. As a consequence, the trimer is disrupted and the E proteins rearrange in the characteristic and irreversible mature conformation, with 90 heterodimers lying flat on the viral surface in a head–to–tail orientation. The 'pr' peptides, which are still associated to the M-E complex, dissociate only when the virion is released into the neutral pH of the cellular environment (Yu et al., 2009; Yu et al., 2008).

In addition to mature virions, also non-infectious subviral particles (SVPs) can be released from flavivirus-infected cells. These particles are smaller than virions (about 14 nm diameter) and only contain E and M proteins anchored to a lipid membrane (Mukhopadhyay et al., 2005). Moreover, mammalian cells co-expressing E and prM proteins can also assemble capsid-less recombinant subviral particles (RSPs). These structures are highly antigenic and could represent a good candidate for a recombinant vaccine (Heinz et al., 1995).

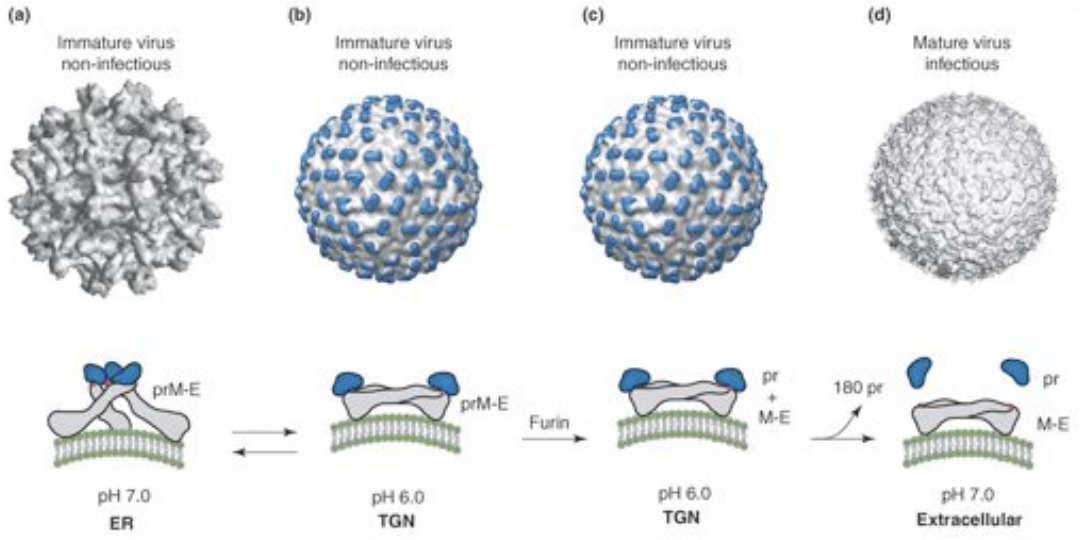

Figure 2 Structural organization of immature and mature flavivirus particles. (a) Cryo-EM reconstruction of the DV immature virion at neutral pH. In this structure the E protein exists as a heterodimer with prM, and these heterodimers form 60 trimeric spikes that extend away from the surface of the virus. This proteins arrangement represents the initial particle that buds into the ER. The conformation of the E protein (grey) within a spike is shown below the virion. The 'pr' peptide is shown in blue protecting the fusion peptide on E (shown as a red star). **(b)** Cryo-EM reconstruction of the immature virion at low pH. During its transit through the secretory pathway, the virus encounters low pH in the Trans-Golgi Network (TGN). Under these conditions, the prM-E heterodimers dissociate from their trimeric organization and form 90 dimers that lie flat on the viral surface. This orientation gives a 'smooth' morphology to the virion. **(c)** While in the TGN, the prM protein is cleaved by the host protease furin to generate the 'pr' peptide and the M protein. The cleaved 'pr' peptide maintains its position as a 'cap' on E. **(d)** Cryo-EM reconstruction of the mature virion. Following furin cleavage, the mature virion is secreted into the extracellular milieu and the 'pr' peptide released from mature particle. Taken from (Perera and Kuhn, 2008)

1.2.2. Genome structure and expression

The flavivirus genome is an 11-kilobase single-stranded RNA molecule of positive polarity that encodes a single long open reading frame (ORF). (Figure 3 shows a schematic representation of the genome structure and polyprotein organization). The 5' end of the genome carries a type I cap (m7GpppAmpN2), but unlike cellular messenger RNA (mRNA) the 3' end mostly lacks a polyadenylate structure. The ORF of all flaviviruses is flanked by 5' (about 100 nucleotides) and 3' (400-700 nucleotides) untranslated regions (UTR) carrying RNA sequence motifs and secondary structures that function as cis-acting regulatory elements for genome amplification, translation or packaging (Lindenbach et al., 2007).

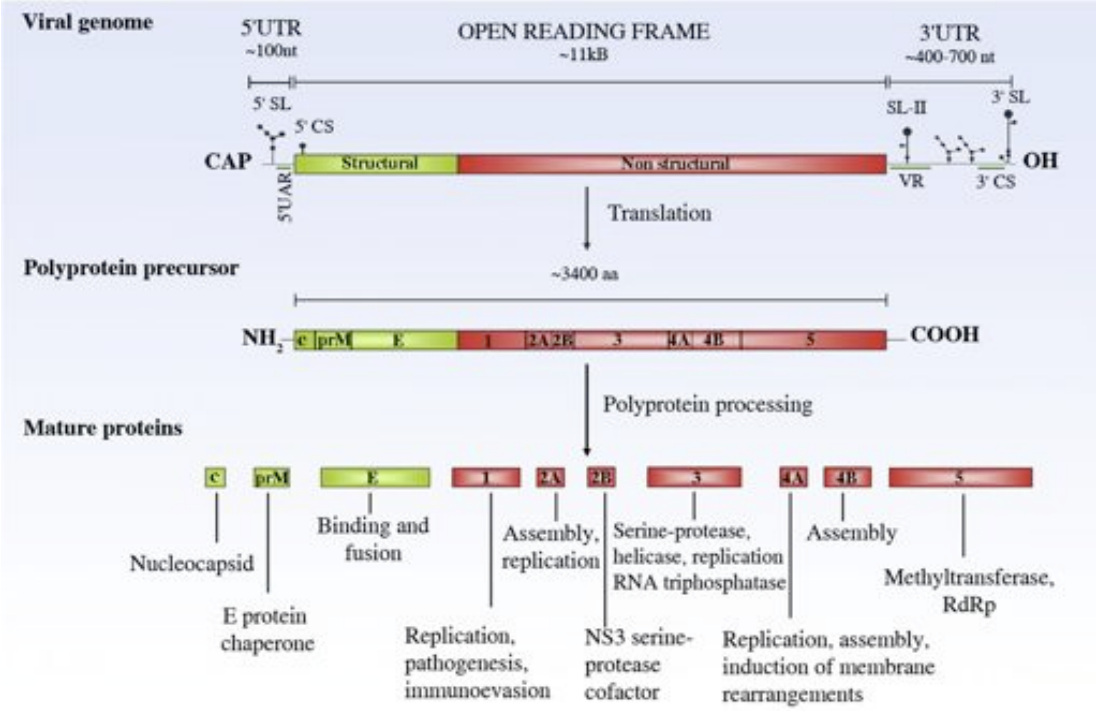

Figure 3 Flavivirus genome structure and expression. The single open reading frame (~11 Kb) with the structural and non-structural protein coding regions (coloured in green and red respectively), the 5'-Cap and the 5' and 3' untranslated regions (UTR) are shown on the top diagram. Simplified RNA secondary and tertiary structures within UTRs are also indicated. The polyprotein precursor and the putative functions of the viral proteins during infection are described in the middle and bottom diagrams respectively. Aa, amino acids; C, capsid protein; CS, cyclization sequence; E, envelop; M, membrane; RdRp, RNA-dependent RNA polymerase; UAR, upstream AUG region; VR, variable region; SL, stem loop. Taken from (Fernandez-Garcia et al., 2009).

Although the sequence of the 5'-UTR is not well conserved, common secondary structures and essential RNA elements are present in both mosquito-borne and tick-borne flaviviruses (Mandl et al., 1993; Markoff, 2003). These consist of a Y-shaped stem-loop structure at the beginning of the genome that functions as a promoter for polymerase recognition and activity (Gritsun and Gould, 2007) and of one or more cyclization elements that interact with complementary sequences in the 3'-UTR during replication (Alvarez et al., 2005b; Hahn et al., 1987; Khromykh et al., 2001; Kofler et al., 2006). The organization of the 3'-UTR is also quite heterogeneous between mosquito-borne and tick-borne flaviviruses. Within this region the most conserved structure consists of a long 3' stem-loop (3'SL) that has been involved in the modulation of both viral translation and replication (Alvarez et al., 2005b; Holden and Harris, 2004). Just upstream of the 3'SL are instead located the 3' cyclization sequences (3' CS).

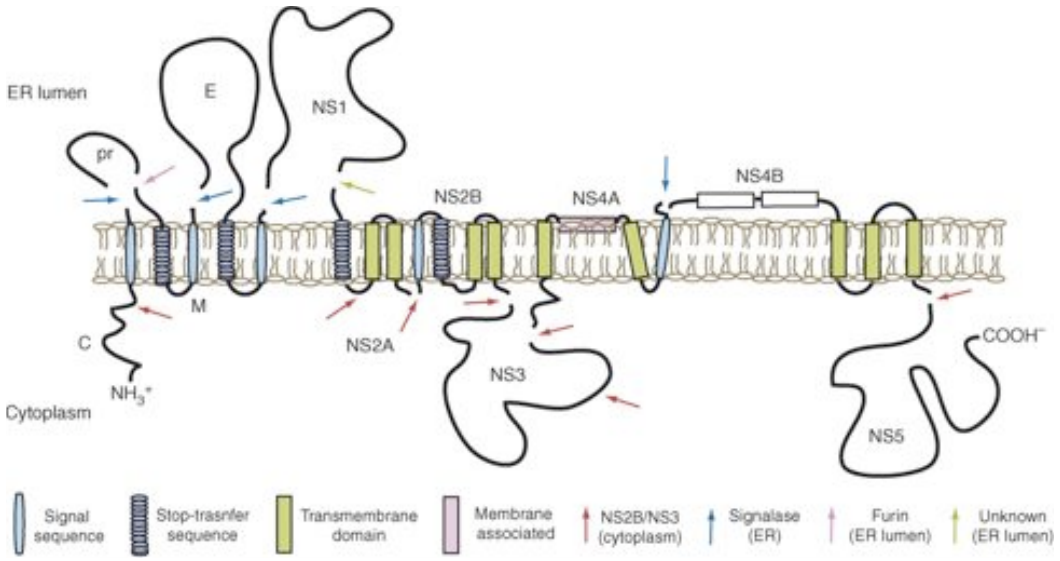

Figure 4 Membrane topology of the flaviviral polyprotein. The proposed topology of the flavivirus polyprotein cleavage products with respect to the ER membrane is shown. Taken from (Perera and Kuhn, 2008).

Therefore, as it has been described for TBEV (Wallner et al., 1995), within the 3'-UTR it is possible to distinguish two distinct domains, a variable region and a highly conserved core element. The core element was shown to be located at the most 3'-terminal region of the genome and contains all the sequence motifs and structures required for RNA replication previously described. The variable region is instead located between the stop codon of the genome and the core element and appeared to be superfluous for TBEV replication (Mandl et al., 1998). Consistently, engineered replicons whose entire variable region was replaced with an expression cassette were still competent for replication in cell culture (Gehrke et al., 2005).

Translation of the genome by the host cell machinery produces a long polyprotein precursor that is co- and post-translationally cleaved into at least 10 proteins. The N-terminal end of this polyprotein encodes the structural proteins (C-prM-E) followed by seven non-structural (NS) proteins (NS1-NS2A-NS2B-NS3-NS4A-NS4B-NS5) each of which is an essential component of the viral replication complex (RC).

Signal sequences within the nascent polyprotein translocate NS1 and the ectodomain of prM and E into the lumen of the endoplasmic reticulum (ER); the C protein, NS3 and NS5 localise in the cytoplasm and NS2A, NS2B, NS4A and NS4B remain predominantly transmembrane (Figure 4). Processing of the polyprotein occurs

before the translation is completed and is carried out by both host proteases and the viral protease NS3 together with its cofactor NS2B in the lumen of the ER.

1.2.3. Features of the non-structural proteins

The majority of the flaviviral non-structural proteins are multifunctional and appear to play different roles in the replication process. However little is known about the interactions between the different non-structural proteins and between these proteins and host proteins that may also be involved in the formation of active replication complexes and innate immune evasion.

NS1 is a glycoprotein of 40-46 KDa that is translocated into the ER lumen during polyprotein synthesis. The E/NS1 junction is cleaved by the host signal peptidase whereas a still unknown ER-resident enzyme is responsible for the cleavage of the NS1/NS2A junction. Newly synthesized NS1 appears as a monomer but in about 30 minutes dimerises and acquires affinity for membranes. NS1 is found intracellularly, on cell surface and, as soluble form, can also be secreted by mammalian cells. Intracellular NS1 is likely to play an important role in RNA replication. Mutations in the gene can lead to dramatic defects on RNA accumulation (Muylaert et al., 1996; Muylaert et al., 1997). Furthermore, NS1 has also been shown to localize within viral replicative compartment together with other proteins involved in viral RNA replication (Mackenzie et al., 1996; Westaway et al., 1997). The role of the NS1 extracellular form is not yet completely understood. However, since high levels of the protein in the serum of DV-infected patients correlate with severe disease, it has been implicated in viral pathogenesis (Avirutnan et al., 2006). Flavivirus NS1 also has a direct immune evasion functions and antagonizes complement activation (Avirutnan et al., 2010; Wilson et al., 2008). Additionally, anti-NS1 antibodies protect from flavivirus-induced disease (Chung et al., 2006).

Therefore, flaviviruses by modulating their intracellular, surface and secreted NS1 levels can balance particular proviral functions (cofactor for replication and complement antagonism) with host antiviral responses (antibody recognition and clearance of infected cells).

NS2A is a small, hydrophobic, membrane-associated protein involved in RNA replication. NS2A binds with high specificity to the 3'UTR of viral RNA and to other components of the RC (Mackenzie et al., 1998). Recently, NS2A has been

shown to be also involved in virus assembly and modulation of the interferon (IFN) response, however further studies are needed to elucidate the exact mechanisms by which this protein operates (Kummerer and Rice, 2002; Leung et al., 2008; Liu et al., 2004; Munoz-Jordan et al., 2003).

NS2B has been shown to complex with and function as the cofactor for the viral serine protease (NS3) (Lindenbach et al., 2007) that, together with the RNA-dependent RNA polymerase (RdRp) NS5, is the most characterized non-structural protein. NS2B is a protein of about 14 KDa composed of a central hydrophilic part and two terminal hydrophobic regions. The hydrophilic region (residues 49-89) strongly interacts with the NS3 protease whereas both N- and C-terminal moieties form two hydrophobic helices that are responsible for membrane association of the NS2B-NS3 complex (Chambers et al., 1991; Falgout et al., 1993). Consistently with its role as a cofactor for the viral serine protease activity, NS2B substantially influences the NS3 secondary structure and contribute to the formation of substrate-recognition pockets (Erbel et al., 2006). Interestingly, a catalytically active NS2B-NS3 complex was recently shown to be involved in inhibition of the type I IFN response. DV-infected dendritic cells (DCs) significantly impaired signalling to interferon in response to several inducers. This effect depends on viral proteins translation and replication and, in agreement with what has been described for HCV (Li et al., 2005; Meylan et al., 2005), requires an active protease complex (Rodriguez-Madoz et al., 2010a). Although the precise mechanism by which the DV NS2B-NS3 protease exerts its inhibitory role is still unknown, this work reports the first evidence that also flaviviruses posses active mechanisms of pattern recognition receptors (PRRs) signaling inhibition.

NS3, as mentioned above, together with the cofactor NS2B, provides serine protease activity required for polyprotein processing. The protease domain (NS3pro) localizes at the N-terminus of the protein whereas the NS3 C-terminal portion (NS3hel) performs different related activities including nucleoside triphosphatase (NTPase), RNA triphosphatase (RTPase) and helicase activities (Lindenbach et al., 2007). NS3pro is a trypsin-like serine protease with the characteristic catalytic triad (Asp-His-Ser) and a highly specific substrate recognition sequence conserved in all flaviviruses. The cleavage sites consist of two basic amino acids followed by an amino acid with a short side chain (Chambers et al., 1990). NS3hel is a member of the DEAH/D box family of RNA helicases. NS3 helicase activity is thought to be

involved in initiation of RNA synthesis by unwinding RNA secondary structures in the 3'UTR of the genome, to facilitate polymerase processivity during elongation or to separate double-stranded RNA (dsRNA) intermediates generated during viral replication (Lindenbach et al., 2007). The NS3 RTPase activity is instead involved, together with the NS5 methyltransferase (MTase) domain in capping of the viral RNA (Wengler, 1993). Recently a new role for NS3 has also been proposed. DV NS3 was shown to bind to and redistribute fatty acid synthase (FASN) into viral replication compartments (Heaton et al., 2010). This interaction is likely responsible for the increased lipid biogenesis observed in DV-infected cells. The mechanism by which NS3 stimulates FASN-activity is currently under investigation, however newly synthesized fatty acids are supposed to be incorporated into the ER membrane in order to expand RCs and increase membrane fluidity.

NS4A is a small hydrophobic protein of about 16 KDa. NS4A localizes within cytoplasmic replicative vesicles (Welsch et al., 2009) and its interaction with the NS1 protein is required for efficient RNA amplification (Lindenbach and Rice, 1999). Over-expression studies demonstrated that regulated cleavages of the NS4A/2K/NS4B junctions play an essential role in the induction of membrane rearrangements that form the scaffold for the viral RCs (Miller et al., 2007; Roosendaal et al., 2006).

NS4B is another flaviviral hydrophobic protein, which localizes in ER membranes. Yeast two-hybrid assays and immunoprecipitation studies have shown the association between NS4B and the NS3-NS5 complex. Full length NS4B interacts with the C-terminal region of NS3. This observation suggested a role for NS4B in viral replication by helping the dissociation of the NS3 helicase from the RNA, and allowing binding of another duplex. Alternatively, NS4B might hold the separated RNA strand apart as the replication complex moves along the duplex (Umareddy et al., 2006). Furthermore, together with NS4A and NS2A, NS4B has also been suggested to take part in IFN antagonism (Evans and Seeger, 2007; Munoz-Jordan et al., 2003).

NS5 is located at the C terminus of the viral polyprotein and is the largest and most highly conserved flaviviral protein. It has two distinct enzymatic activities; the N-terminal is an MTase involved in capping of the viral RNA, whereas the C-terminus contains the RdRp domain. Consistently with the presence of a nuclear localization signal between the MTase and polymerase domains, NS5 has been detected in both

the cytoplasm and the nucleus of infected cells (Buckley et al., 1992; Uchil et al., 2006) suggesting that the host cell nucleus can provide an additional site for viral replication. In addition, studies on TBEV, DV and JEV demonstrated that NS5 antagonizes IFN signalling by inhibiting the JAK-STAT (Janus kinase-signal transducer and activator of transcription) signal transduction pathway (Ashour et al., 2009; Best et al., 2005; Lin et al., 2006b; Mazzon et al., 2009; Werme et al., 2008). Hence, NS5 may be a common IFN antagonist that plays a crucial role in flavivirus pathogenesis in addition to its central function in viral RNA replication.

1.2.4. Flavivirus life cycle

Flavivirus infection is initiated when mature viral particles attach to the target cell surface through interaction of the large glycoprotein E with cellular receptors (Figure 5). The nature of the receptors involved is still largely unresolved, however binding to highly sulphated glycosaminoglycans such as heparan sulphate has been suggested to play an important role during this initial step of the viral life cycle (Kroschewski et al., 2003; Mandl et al., 2001). After attachment, the virus is internalized by receptor-mediated endocytosis and delivered to the endosome. The low pH in the endosomal compartment induces a conformational change in the surface protein E that triggers the fusion of the viral and host cell membrane (Heinz and Allison, 2003; Krishnan et al., 2007). This process results in the release of the nucleocapsid and viral RNA into the cell cytoplasm. At this stage, the uncoated genome can be translated by the cell machinery to generate the polyprotein precursor described in figure 4.

Processing of the polyprotein by host and viral proteases then lead to the generation of 10 individual viral proteins and to the initiation of genome replication. The RdRp NS5 copies complementary minus-strand RNA from genomic RNA, which then serves as template for the synthesis of new positive strand viral RNAs. Appearance of the minus-strand template RNA has been detected as early as 3 hours after infection. Viral RNA synthesis appears to be asymmetric, with the plus-sense RNA synthesized in excess over minus-sense RNA (Chu and Westaway, 1985; Cleaves et al., 1981; Wengler and Gross, 1978). The newly synthesized plus-sense RNA is subsequently used for translation of further viral proteins or synthesis of additional minus-sense RNA, or it becomes incorporated into new viral particles.

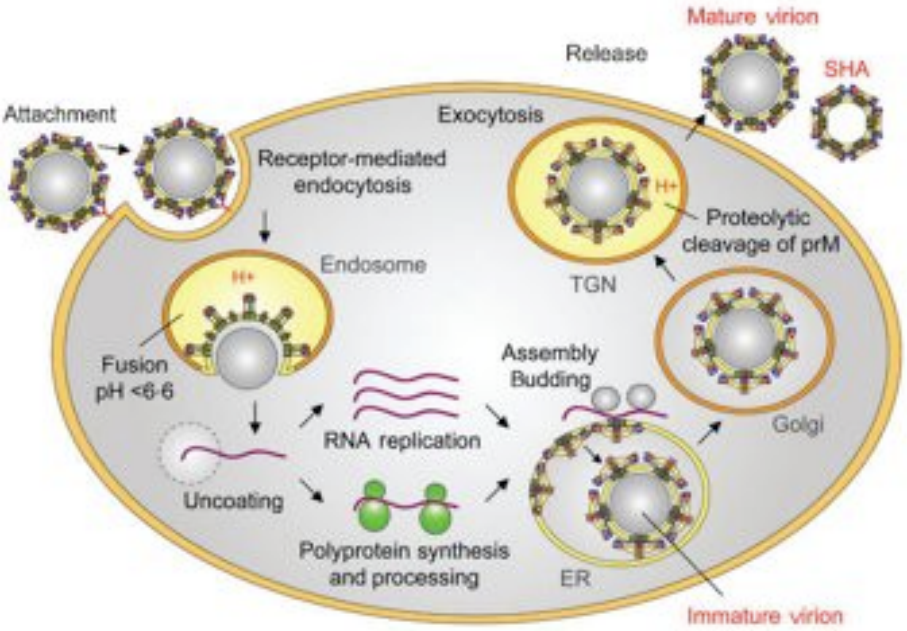

Figure 5 Flavivirus life cycle. Flaviviruses are internalized by receptor-mediated endocytosis and trafficked to early endosome, where the acidic environment induces fusion between the virus and the host membrane resulting in genome release. Translation of the viral RNA is followed by processing of the resulting polyprotein by host and virus-encoded proteins. Upon translation, a replication complex is assembled and associated to virus-induced membranes where viral replication takes place. Progeny positive-strand RNA genomes can either initiate a new translation cycle or be assembled into virions. Assembly occurs on the surface of the endoplasmic reticulum (ER), followed by budding of the structural proteins and newly synthesized RNA into the lumen of the ER. The resultant immature virions are transported to the trans-Golgi where furin-mediated cleavage of prM to M generates mature infectious particles that are released by exocytosis. Taken from (Stiasny and Heinz, 2006)

Thus, the genome RNA has at least three different functions (translation, replication, and association with nascent viral particles), which need to be tightly regulated and coordinated during the viral replication cycle.

Flavivirus replication occurs in close association with virus-induced intracellular membrane structures, predominantly in the perinuclear region. It has been speculated that membranes may limit diffusion of viral/host proteins and viral RNA, thereby increasing the concentration of components required for RNA synthesis, or that may facilitate replication by providing a scaffold for anchoring the replication complex (RC) (Miller and Krijnse-Locker, 2008). In addition, membranes-associated replication factories may also hide dsRNA replication intermediates from host cellular surveillance (Fernandez-Garcia et al., 2009; Hoenen et al., 2007; Overby et al., 2010).

Although genome packaging and viral particle biogenesis are still the most obscure steps of the flavivirus life cycle it has been recently proposed that association of the DV C protein with ER derived lipid droplets (LDs) is crucial for infectious particle formation (Samsa et al., 2009). Immature particles are then formed by assembly of nucleocapsid and prM-E proteins and budding into the lumen of the endoplasmic reticulum (ER) membrane (Lorenz et al., 2003; Welsch et al., 2009). After transport through the secretory pathway, viral maturation occurs in the TGN where the host protease furin mediates the cleavage of the prM protein (Stadler et al., 1997). Infectious particles are then released into the extracellular medium.

1.3. The RNA replication compartment

Viruses are obligate intracellular parasites, therefore they must exploit the host cell machinery to efficiently replicate and produce infectious progeny. Flaviviruses, like all studied positive-strand RNA viruses, usurp and modify cytoplasmic membranes in order to build functional sites of protein translation, processing and RNA replication (Ahlquist, 2006; den Boon et al., 2010; Fernandez-Garcia et al., 2009; Gillespie et al., 2010; Mackenzie, 2005; Miller and Krijnse-Locker, 2008; Novoa et al., 2005). These sites, enriched in cellular membranes, viral RNA and virus- and host-encoded proteins, are generally defined as replication complexes. As already mentioned, membrane wrapping of the RC is thought to provide a physical framework in which RNA synthesis can occur and to ensure protection from host-response proteins recognizing the viral RNA.

The earliest visible event leading to RCs formation, detected by electron microscopy (EM), is the proliferation of the ER membranes followed by the appearance of smooth membrane structures around the time of early logarithmic virus production (Lindenbach et al., 2007; Ng and Hong, 1989). Studies with Kunjin virus-infected Vero cells showed that these structures are clusters of about 100 nm vesicles, also called vesicles packets (VPs), which accumulate during the course of the infection (Mackenzie et al., 1999; Westaway et al., 1997). Later on, also different structures described as convoluted membranes (CM) and paracrystalline arrays (PC) appear to be adjacent to VPs (Figure 6).

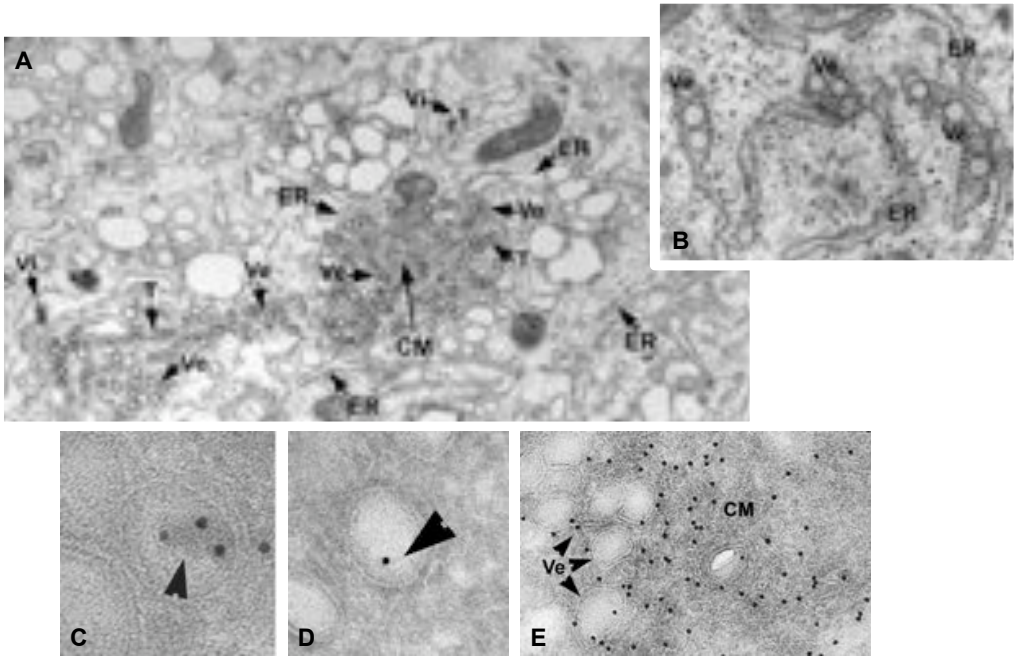

Figure 6 Ultrastructure of Flavivirus-induced membrane alteration. (A) Thin-section transmission electron microscopy (TEM) image of DV-infected, resin embedded Huh-7 cells fixed 24 hrs post-infection. Virus-induced vesicles (Ve) and occasionally membrane tubes (T) accumulates around stacks of convoluted membranes (CM). Ve and CM are tightly associated with the ER. Clusters of virus particles (Vi) reside in the periphery of virus induced membrane structures and are localized in the lumen of dilated ER cisternae. **(B)** Higher magnification view of Ve in the lumen of the ER. **(C-E)** DV-infected Huh-7 cells were fixed 24 hrs post-infection and thawed cryosections were labeled with antibodies against the replication intermediate dsRNA **(C)**, the RdRp NS5 **(D)** and the NS3 protein **(E)**. Adapted from (Welsch et al., 2009).

Interestingly, dsRNA and NS5 immunolabelling of cryosections prepared from flavivirus infected cells revealed that VPs are the sites of RNA replication, whereas the NS2B-NS3 protease localization indicated that CM and PC are possibly the sites of protein translation and proteolytic cleavage (Mackenzie et al., 1996; Mackenzie et al., 1998; Westaway et al., 1999). Recently, elegant three-dimensional EM tomography studies have also shown that vesicle packets and convoluted membranes are all part of a single ER-derived membrane network which is very similar to the one induced upon coronavirus infection (Gillespie et al., 2010; Knoops et al., 2008; Welsch et al., 2009). In these studies, VPs appeared as invaginations of the ER outer membrane bearing necked connections to the cytoplasm and between themselves (Figure 7). Hence, replication compartments are not made of clustered secluded vesicles surrounded by a double membrane as initially suggested by two-dimension images analysis. Indeed, some kind of connection to the cytoplasm and between

replication vesicles is necessary not only for the exchange of ribonucleotides and other cofactors of virus replication, but also to allow the transport of viral proteins and genomes between VPs interior, ribosome-containing membranes and virus assembly sites. As already mentioned, vesicles formation is probably induced by the flavivirus NS4A protein since its expression in cultured cells has been shown to induce membrane rearrangement similar to those observed in infected cells (Miller et al., 2007; Roosendaal et al., 2006). However, we are still far from understanding the exact role of the host's factors involved and the mechanisms responsible for the formation of these structures.

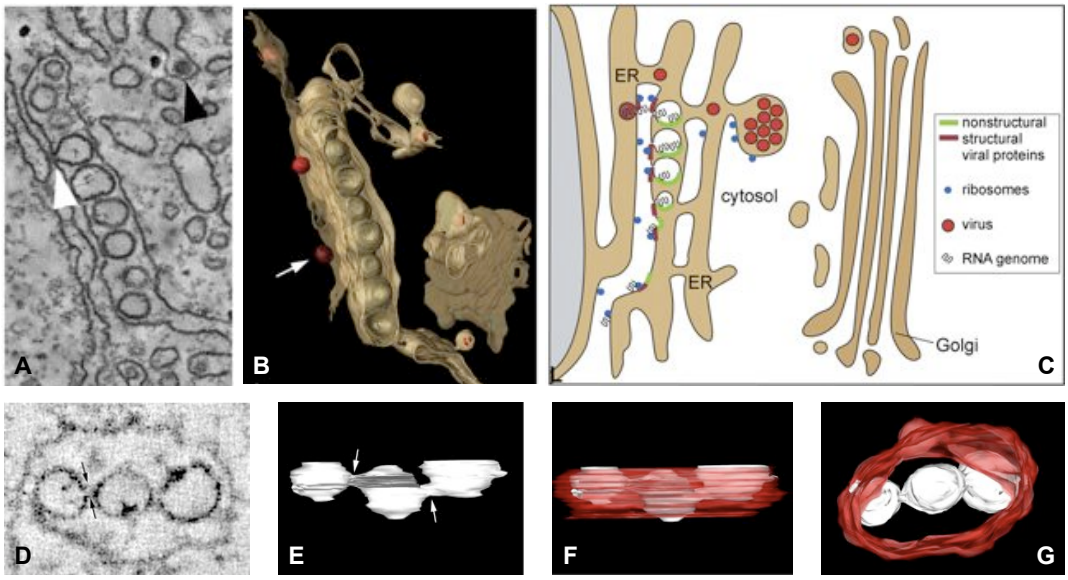

Figure 7 EM tomographic three-dimensional reconstruction of flavivirus-induced, ER-derived vesicle packets. Two-dimensional EM sectional view **(A)** and three-dimensional tomographic reconstruction **(B)** of DV-induced vesicle packets. Note the continuity of vesicles and ER membranes (white arrowhead). Virus particles, indicated with a black arrowhead in (A) and in red in (B), are localized in the ER and in a cisterna close to the Golgi stack. **(C)** Model of the relation between DV replication, assembly and virion release. Upon infection, the viral genome associates with the rough ER (ribosomes in blue), and the viral polyprotein, composed of the structural proteins (red) and the NS proteins (green), is synthesized on rough ER membranes. NS4A, together with other viral and perhaps cellular proteins, induces invaginations of the ER membrane, leading to the formation of vesicles that are connected to the cytosol via a pore. Inside these invaginations, RNA replication occurs. Viral capsid protein associates with progeny RNA genomes liberated through the pore-like structure into the cytosol. Virus budding occurs through the ER membrane located in close proximity to or opposite of the vesicles. Individual virions travel toward distal sites of the ER lumen, where they collect in dilated ER cisternae. They are transported, likely as individual virions, via secretory vesicles to the Golgi complex, where virion maturation occurs. Images A to C are adapted from (Welsch et al., 2009). Two-dimensional EM sectional view **(D)** and three-dimensional surface rendering **(E–G)** of vesicles within the WNV replication complex. Surface modelling revealed that vesicles are connected to each other directly via pores highlighted by arrows in panels D and E. The individual vesicles are indicated in white with the ER membrane depicted in red. Panel G is a 90° rotation of the VPs in panel F. Images D to G are adapted from (Gillespie et al., 2010).

1.4. Innate immunity pathways of RNA virus recognition

Mammalian cells have evolved a variety of defence mechanisms to detect, contain and clear viral infections. There are two fundamentally different types of responses to invading pathogens: the innate and the acquired immune response. The innate immune response offers the first early protection against foreign invaders and is mediated by a limited number of germline-encoded pattern-recognition receptors (PRRs). In contrast, acquired immunity is implicated in pathogens clearance during the late phase of the infection and involves lymphocytes (T and B cells) clonally expressing a large repertoire of rearranged antigen-specific receptors.

An effective innate immune response to viral infection involves two phases: an early phase of interferon production, triggered by the recognition of conserved "non-self" signatures, also known as pathogen-associated molecular patterns (PAMPs), by host PRRs, and a late phase of IFN signaling and interferon stimulated genes (ISGs) expression. Indeed, upon recognition, PRRs initiate signaling cascades that result in the activation of transcription factors critical for type I interferons (INFα and IFNβ) expression. Thereafter, as secreted factors, type I IFNs can regulate a variety of immune responses through interaction with the type I IFN receptor. These responses include induction of a protective antiviral state in the infected and neighbouring cells as well as initiation of the acquired immunity.

To date, two distinct families of sensors have been characterized as key players in the detection of RNA viruses: the Toll-like receptor (TLR) and the RIG-I (retinoic acid inducible gene-I)-like receptor (RLR) families.

1.4.1. RNA viruses detection by toll-like receptors

The TLR family is one of the best-characterized PRR families and is responsible for sensing a wide variety of invading pathogens outside of the cell as well as in intracellular endosomes and lysosomes. Toll-like receptors were initially identified through their homology to the Toll protein, a critical factor for the Drosophila innate immune response against fungal infection (Rock et al., 1998). To date, more than 11 mammalian members of the family have been recognized as receptors involved in PAMPs recognition (Akira et al., 2006; Kawai and Akira, 2011). These receptors are composed of an extracellular leucine-rich repeat (LRR) domain, directly involved in

pathogen recognition, a single transmembrane domain, and a conserved cytoplasmic signaling domain known as the Toll/IL-1R (TIR) domain with considerable homology to the interleukin-1 receptor (IL-1R) (Figure 8) (Akira and Takeda, 2004). They are expressed on various immune cells, including macrophages, dendritic cells (DCs) but also on non-immune cells such as fibroblast and epithelial cells.

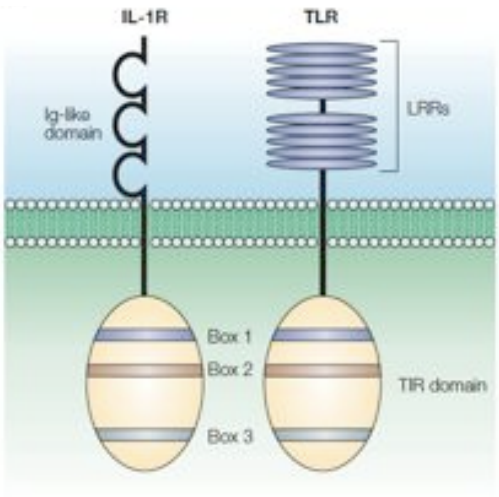

Figure 8 TLR structure. Toll-like receptors (TLRs) and interleukin-1 receptors (IL-1Rs) have a conserved cytoplasmic domain that is known as the Toll/IL-1R (TIR) domain. The TIR domain is characterized by the presence of three highly homologous regions (known as boxes 1, 2 and 3). Despite the similarity of the cytoplasmic domains of these molecules, their extracellular regions differ markedly: TLRs have tandem repeats of leucine-rich regions (known as leucine rich repeats, LRR), whereas IL-1Rs have three immunoglobulin (Ig)-like domains. Taken from (Akira and Takeda, 2004)

Accumulating evidences suggest that TLRs sub-cellular localization plays an important role in regulating ligand accessibility and can also affect downstream signaling events (Barton and Kagan, 2009). The TLRs localized within intracellular compartments such as endosomes, lysosomes and ER (TLR3, TLR7, TLR8 and TLR9) are mostly involved in non-self nucleic acids sensing, whereas receptors expressed on the cell surface (TLR1, TLR2, TLR4, TLR5 and TLR6) mainly recognize bacterial cell walls components or viral particles.

Bacterial or viral unmethylated DNA with CpG motifs is recognized by TLR9, whereas RNA viruses are specifically sensed by the other intracellular TLRs (TLR3, TLR7 and TLR8) (Akira and Takeda, 2004; Akira et al., 2006). TLR3 was the first characterized receptor involved in dsRNA recognition. As already described, dsRNA agonists can be generated during viral infection as a replication intermediate for single stranded RNA (ssRNA) viruses. Alternatively, dsRNAs may be derived from the genome of dsRNA viruses or be produced as a result of bidirectional

transcription of dsDNA viruses' genomes (Weber et al., 2006). Mice lacking TLR3 were shown to be more resistant to polyinosinic polycitdylic acid (Poly(I:C)) induced shock and TLR3 deficient macrophages exhibited reduced type I IFN production in response to dsRNA (Alexopoulou et al., 2001). However, the role of TLR3 in the generation of effective antiviral immune responses is still controversial. Experiments performed in TLR3 knockout mice infected with multiple RNA viruses failed to show increased mortality or altered viral burden phenotypes (Edelmann et al., 2004). Conversely, TLR3 was able to regulate cytokine production and protect against infection by mouse cytomegalovirus and encephalomyocarditis virus (EMCV) (Hardarson et al., 2007; Tabeta et al., 2004). Similar conflicting results emerged also upon infection with the flavivirus WNV. Two studies using the same TLR3 knockout mice described different phenotypes: one showed that WNV virulence was attenuated in knockout mice, most likely because of a decreased inflammatory response that diminished blood-brain barrier permeability and viral entry to the brain (Wang et al., 2004). In contrast, a second study reported an increased susceptibility to WNV in these mice. Interestingly, although TLR3 was shown to be dispensable in controlling viral replication in peripheral tissues, it appeared to be essential for restriction of WNV infection in neurons (Daffis et al., 2008). Therefore, a tissue and cell type specificity of PRR pathways may regulate viral pathogenesis *in vivo*.

TLR7 and TLR8 became activated by recognition of single-stranded RNA (ssRNA) from RNA viruses as well as small purine analog compounds (imidazoquinolines) (Akira et al., 2006). Accordingly, they are implicated in myeloid differentiation primary-response protein 88 (MyD88)-dependent recognition of different ssRNA and ssRNA-producing viruses including vesicular stomatitis virus (VSV), influenza A virus, human immunodeficiency virus (HIV) and WNV (Diebold et al., 2004; Heil et al., 2004; Lund et al., 2004; Town et al., 2009). TLR7 and TLR8 are mostly localized in endosomal compartments of plasmacytoid dendritic cells (pDCs). For this reason they are more easily activated by viruses that enter the cell through endosomes. Alternatively, they can also be activated by viral RNA uptake from the cytoplasm of infected cells. All together these studies demonstrated that TLR7 and TLR8 are essential for IFN induction in pDCs by RNA viruses.

However, in many other cell types, including macrophages and fibroblasts, deletion of both MyD88 and TRIF (TIR domain-containing adaptor inducing IFNβ) adaptor molecules, had no effect on virus-induced IFN production (Kato et al., 2005).

Therefore, a TLR-independent pathway highly effective in providing antiviral innate immunity must exist in those cells.

1.4.2. Toll-like receptors signaling pathways

Upon PAMPs recognition, TLRs trigger transcriptional upregulation of many distinct antiviral genes, depending on the receptor and the cell type involved. The differences in the response mediated by the individual TLRs are partially explained by the recruitment of different adaptor proteins to TLRs. There are four TIR-domain adaptors, namely MyD88, TRIF, TRIF-related adaptor molecule (TRAM) and TIR-domain containing adaptor protein (TIRAP). However, TLR signaling can be roughly divided into two different pathways depending on the recruitment of MyD88 or TRIF (Akira et al., 2006). A schematic representation of the MyD88- and TRIF-dependent signaling pathways is shown in Figure 9.

The MyD88-dependent signaling pathway

The MyD88 adaptor is essential for the induction of type I IFN and proinflammatory cytokines by various TLRs, including TLR7 and TLR8, Ligand binding to the LRRs induces receptor dimerization and MyD88 association to the TIR domain, which in turn recruits the interleukin-1 receptor associated kinase-4 (IRAK4) allowing IRAK1 phosphorylation. Subsequently, IRAKs dissociate from MyD88 and interact with tumor necrosis factor receptor- associated factor 6 (TRAF6) to trigger downstream activation of IFN regulatory factor 7 (IRF-7) and of the kinase complex IKKα/β/γ and the mitogen-activated protein kinase (MAPK) cascades. Nuclear factor-kB (NF-kB) and MAPK cascade activation both coordinate transcriptional regulation of genes involved in the inflammatory response whereas IRF7 phosphorylation and subsequent nuclear translocation activates type I IFN genes expression.

The TRIF-dependent signaling pathway

Stimulation of TLR3 by dsRNA results in a MyD88-independent induction of type I IFN. Upon activation, TLR3 recruits the adaptor protein TRIF. TRIF interacts with receptor-interacting protein 1 (RIP1), which is responsible for NF-kB activation, and activates the TRAF-family-member-associated NF-kB activator (TANK) binding kinase 1 (TBK1) via TRAF3.

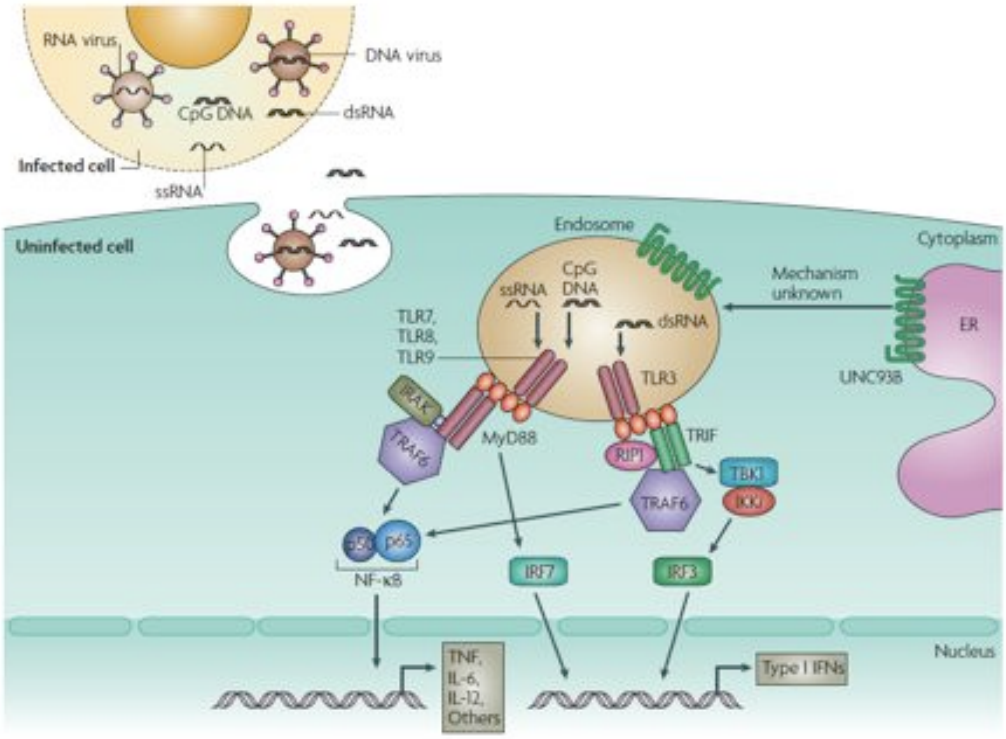

Figure 9 TLR receptors signaling in response to endosomal nucleic acids of viral origin. TLRs that sense nucleic acids can operate in non-infected cells of many types to detect the production of infection in other cells. Following the recognition of viral double-stranded RNA (dsRNA), single-stranded RNA (ssRNA) or CpG-containing DNA by TLR3 or TLR7, TLR8 and TLR9 that are expressed in the endosome, signalling proceeds through TRIF or MyD88, respectively. UNC93B is a multiple-transmembrane-spanning protein that is predominantly located in the endoplasmic reticulum (ER), but is known to associate with these endosomal TLRs and to be required for them to signal. TRIF, through the recruitment of TRAF6 and RIP1, as well as TBK1 and inducible IκB (inhibitor of nuclear factor-κB (NF-κB)) kinase (IKKi), activates IRF3 and NF-κB. MyD88 recruits TRAF6 and IRAK and activates IRF7 and NF-κB. NF-κB, IRF7 and IRF3 then translocate to the nucleus in order to induce the transcription of genes encoding cytokines such as TNF, IL-6 and type I IFNs. Taken from (Beutler et al., 2007).

TBK1 in turn phosphorylates IRF3 and IRF7 inducing their dimerization and nuclear translocation. Once in the nucleus, these transcription factors then regulates type I IFN induction and expression of IFN-inducible genes.

1.4.3. RIG-I-like receptors and virus recognition

Whereas TLRs detect viruses-derived nucleic acids within intracellular compartments of specific cell types, such as dendritic cells and macrophages, RLRs sense viral components that are present in the cytoplasm of most infected cells.

The RLR family is composed of three members: RIG-I, melanoma differentiation-associated gene 5 (MDA5) and laboratory of genetics and physiology 2 (LGP2) (Loo and Gale, 2011; Pichlmair and Reis e Sousa, 2007). RIG-I, the founding member of the family, was identified as a positive regulator of dsRNA-induced IFN genes activation by expression cloning experiments in 2004. In this study, a cDNA library was introduced into mouse L929 cells together with a reporter construct carrying IRF-binding sites. After poly(I:C) stimulation the cDNAs able to enhance reporter activity were selected. Among them, the clone encoding the N-terminal region of RIG-I was shown to constitutively activate the promoter (Yoneyama et al., 2004). Soon after, also the other two members of the family were identified for their homology with the RIG-I helicase domain (Yoneyama et al., 2005).

All RLRs proteins are DExD/H-containing RNA helicases and their primary structure can be divided into three basic domains: the N-terminal domain which consists of two caspase activation and recruitment domain (CARD), the central helicase domain and the C-terminal regulatory domain (RD) (Figure 10).

The N-terminal CARDs are essential for the interaction with the CARD of the IFNβ promoter stimulator (IPS)-1 adaptor protein (also known as mitochondrial anti-viral signaling protein (MAVS)) and for the downstream signaling cascade activation (Kawai et al., 2005; Seth et al., 2005). Consistently, when expressed alone, the CARD domain constitutively induces IFNβ expression (Yoneyama et al., 2004). As shown in figure 10, LGP2, the third member of the family, lacks the CARD domain, and it is unable to signal through MAVS. Therefore, LGP2 was initially proposed as a negative regulator of RLR signaling (Rothenfusser et al., 2005; Yoneyama et al., 2005). However, recent LGP2 knockout analyses indicate that this receptor acts as a positive regulator of both RIG-I- and MDA5-mediated viral recognition (Satoh et al., 2010). Hence, further biological studies will be necessary to better understand LGP2 role in the antiviral response.

The helicase domain contains six conserved DExD/H helicase motifs and is involved in two essential functions: the helicase/translocase activity and the ATPase activity. Mutation in the ATP-binding site resulted in loss-of-function phenotype and dominant negative activity suggesting that ATP hydrolysis is required for RLRs signaling (Yoneyama et al., 2004).

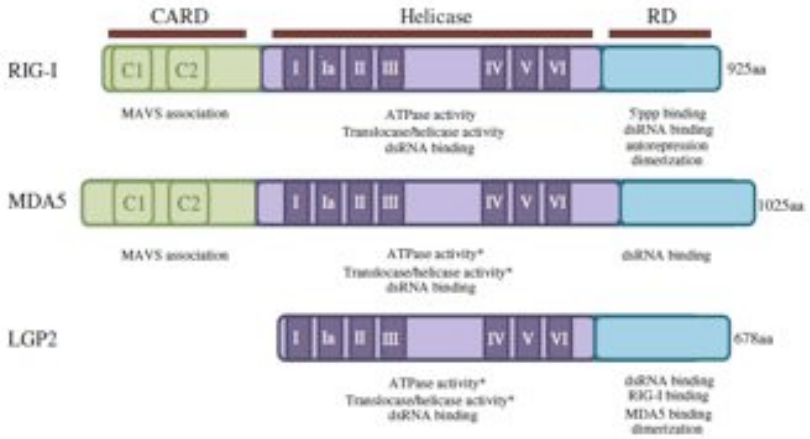

Figure 10 RLRs domains and their function. Schematic representation of the three RLRs basic domains. (1) The N-terminal CARD domain composed of two tandem CARDs. (2) The central helicase domain, belonging to the DExD/H family of RNA helicases. (3) The unique C-terminal domain containing multiple regulatory functions (RD). The CARD domain, present in RIG-I and MDA5 but absent in LGP2, is required for interaction with MAVS and downstream signaling. CARD1 (C1) is involved in physical interaction with the CARD domain of MAVS, whereas CARD2 (C2) of RIG-I undergoes ubiquitination required for RIG-I activation. The helicase domain contains six conserved DExD/H helicase motifs and is involved in translocation/unwinding of RNA and ATP hydrolysis required for RLR function. The helicase domain is also implicated in RNA binding for all three RLR members. The RD is required for recognition and binding of RNA substrates. This domain provides specificity for either 5'ppp containing RNA (RIG-I) or dsRNA (MDA5, LGP2). RD is also required for homo- (RIG-I, MDA5) and hetero- (LGP2) dimer formation, necessary for signaling by these receptors. The RD of RIG-I additionally provides a unique function of autorepression, and RIG-I constructs lacking the RD domain constitutively induce IFN in the absence of RNA stimuli. *Activity has not been shown directly and is assumed based on sequence similarity to the helicase domain of RIG-I. Taken from (Baum and Garcia-Sastre, 2010)

The role of the helicase/translocase function is still poorly understood. Indeed it is not clear yet whether RLRs unwind dsRNA *in vivo* or simply translocates on the RNA as recently reported for RIG-I (Myong et al., 2009).

Finally, the C-terminal RD of RIG-I and LGP2 have been shown to function as a repressor domain that keeps the protein inactive in the absence of viral stimulation (Saito et al., 2007). In addition, the RIG-I RD domain was also shown to be responsible for the recognition of specific viral RNA (Cui et al., 2008; Takahasi et al., 2008). Consistently, one side of the RD contains a basic cleft that serves as RNA binding surface, whereas the acidic region on the opposite side interacts with the CARD domain to preserve the RIG-I inactive conformation.

Originally, both RIG-I and MDA5 were thought to sense cytoplasmic dsRNA during viral infection (Yoneyama et al., 2005). However, through numerous studies, it has

been clearly demonstrated that, despite their structural and functional similarities, the two sensors are not redundant in their ability to recognize non-self RNA (Kato et al., 2006). Poly (I:C) as well as chemically synthesized RNA oligonucleotides annealed to a complementary strand trigger RIG-I (Kato et al., 2008; Takahasi et al., 2008). RNAs carrying a 5'-triphosphate (5'-PPP) moiety, generally produced during infection by influenza and other negative-strand RNA viruses, are RIG-I agonists as well (Hornung et al., 2006; Pichlmair et al., 2009). Long, possibly branched dsRNAs found for example in picornaviruses (Pichlmair et al., 2009) and mRNAs lacking 2'-O-methylation at their 5' cap structure (Daffis et al., 2010; Zust et al., 2011) are MDA5 agonists. Total RNA extracted from virally infected cells can also stimulate specific RLRs. However, the form of viral RNA that is recognized depends on the specific virus.

RLRs play also a crucial role in the recognition of Flavivirus infection. Stimulation of the type I IFN promoter in response to JEV infection was significantly reduced in cells over-expressing a dominant negative form of RIG-I and completely abolished in RIG-$I^{-/-}$ mouse embryonic fibroblasts (MEFs) (Chang et al., 2006; Kato et al., 2006). Furthermore, while RIG-I knockout mice demonstrated increased susceptibility to JEV infection compared to control mice, MDA5 deficient mice responded normally to infection (Kato et al., 2006) suggesting that RIG-I plays an essential role in triggering innate immune responses to JEV. In contrast, WNV and DV were shown to induce both RLRs-dependent pathways of PAMP recognition. Consistently, cells lacking either RIG-I and MDA5 or those deficient in IPS-1 alone were not able to properly counteract viral infection (Fredericksen and Gale, 2006; Fredericksen et al., 2008; Loo et al., 2008). Interestingly, IPS-1-deficient mice also exhibited enhanced inflammatory response and impaired adaptive immunity in response to WNV challenge highlighting RLR signaling regulatory functions *in vivo* (Suthar et al., 2010). The key role of both RIG-I and MDA5 PRRs in eliciting protective antiviral responses against flavivirus infection was also confirmed by a recent screening aimed at identifying the effects of hundreds of ISGs products on viral replication (Schoggins et al., 2011).

All together, these studies suggest that RIG-I plays an important role in establishing effective immune responses to all flaviviruses whereas MDA5 role appear to be virus-dependent.

1.4.4. RIG-I-like receptors signaling pathways

Binding of the viral RNA to the RLRs C-terminal domain induces an ATP-dependent conformational change of the receptor, which results in exposure of CARDs and initiation of downstream signalling events (Yoneyama and Fujita, 2009). Once activated, RIG-I and MDA5 interact with the CARD-containing adaptor protein IPS-1 (Figure 11). Interestingly, IPS-1 is localized on the mitochondrial membrane (Seth et al., 2005), suggesting a critical function of mitochondria as a signaling platform for antiviral innate immunity.

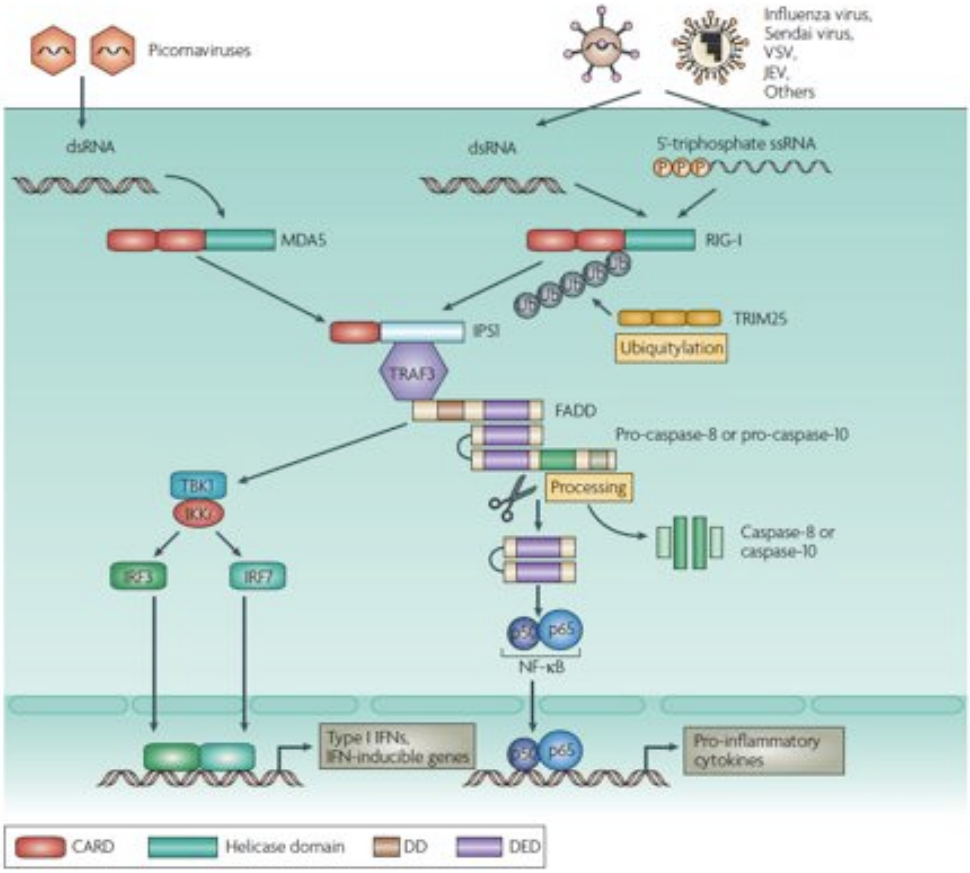

Figure 11 Signaling pathways activated by cytoplasmic helicases. Viral dsRNA in the cytoplasm is detected by one of two cytoplasmic helicases, MDA5 or RIG‑I. RIG‑I also detects 5′-triphosphate single-stranded RNA (ssRNA). IFNβ promoter stimulator 1 (IPS1; also known as mitochondrial antiviral signalling protein (MAVs), virus-induced signalling adaptor (VISA) and caspase-recruitment domain (CARD) adaptor inducing IFNβ (CARDIF)) is a central target of both MDA5 and RIG‑I. Through the recruitment of TRAF3, IPS1 activates FADD. FADD then associates with pro-caspase‑8 or pro-caspase‑10, resulting in its cleavage. The death-effector domains (DEDs) of caspase‑8 or caspase‑10 activate NF-κB, but not IRF3. However, the interaction between TRAF3 and TBK1 or inducible IκB (inhibitor of NF‑κB) kinase (IKKi) leads to IRF3 and IRF7 activation. Tripartite-motif-containing 25 (TRIM25) catalyses lysine-63-linked ubiquitylation of RIG‑I, which strongly enhances RIG‑I signalling. DD, death domain; JEV, Japanese encephalitis virus; VSV, vesicular stomatitis virus. Taken from (Beutler et al., 2007).

CARD-CARD interaction then triggers the recruitment of downstream signaling molecules that are involved in induction of type I IFN expression. In particular, IPS-1 associates with tumor necrosis factor (TNF) receptor-associated factor (TRAF) 3 leading to TBK1 and inhibitor of kB kinase (IkB) ε (IKKε) activation and subsequent IRF3 phosphorylation. Alternatively, IPS-1 recruits the adaptor Fas-associated death domain (FADD) and the kinases receptor- interacting protein 1 (RIP1) in order to trigger the NF-kB pathway. Upon activation, IRF3 and NF-kB translocate to the nucleus to drive type I IFN transcription and subsequent induction of the antiviral state (Yoneyama and Fujita, 2009).

1.5. Evasion to the interferon system by viruses

As mammalian hosts have evolved several sensors for viral infection, viruses, on the other hand, adapted multiple tricks to escape or at least counteract innate immune response. These can be distinguished in those that target PRR signaling, thus delaying the first induction of IFNs, and those that target IFNs signaling, thus limiting their antiviral potential (Suthar et al., 2009).

Typically, evasion of IFN induction is accomplished by viral proteins that directly inhibit the function of PRRs. The NS1 viral protein is the main IFN antagonist of influenza A viruses (Garcia-Sastre et al., 1998). NS1 acts both by preventing the nucleation of the IFN enhanceosome (Ludwig et al., 2002; Talon et al., 2000; Wang et al., 2000) and by targeting RIG-I activity (Gack et al., 2009). The HCV NS3/4A protease cleaves the IPS-1, the adaptor molecule that bridges RLRs to downstream effectors, affecting type I IFN production in infected cells (Li et al., 2005; Lin et al., 2006a; Loo et al., 2006; Meylan et al., 2005). A similar mechanism has been recently proposed also for the DV NS2B-NS3 protease. DV infection significantly affects type I IFN expression and IFNβ promoter activity in human DCs by preventing IRF3 phosphorylation. Mutation in the catalytic site of the DV protease complex impaired the inhibitory effect on type I IFN production supporting the hypothesis that the cleavage of some factor involved in PRRs signaling may represent a new active evasion mechanism evolved also by flaviviruses (Rodriguez-Madoz et al., 2010a; Rodriguez-Madoz et al., 2010b). Another still controversial example is the WNV

NS1-mediated inhibition of TLR3 signaling. In one study, using WNV replicon-bearing cells and IFN-cured derivative cells, NS1 significantly impaired NF-kB and IRF3 nuclear translocation preventing the establishment of an antiviral state (Wilson et al., 2008). However, more recently this hypothesis has been challenged since both ectopically expressed and virally encoded NS1 were unable to affect the expression of several interferon-related genes (Baronti et al., 2010).

As already mentioned, to prevent antiviral ISGs induction viral antagonists can also block at different levels IFN-α/β receptor (IFNAR) signaling and several flaviviruses are known to possess active mechanisms of immune evasion affecting this step of the response. Therefore, even when type I IFN is produced, it may not achieve the same inhibitory effect because of the attenuated signaling capacity. The first confirmation of DV's ability to circumvent type I IFN response was provided by Diamond and Harris (Diamond and Harris, 2001), who demonstrated that IFN pretreatment protects cells against *de novo* viral infection whereas it is not efficient at neutralizing an established infection. Thereafter, several groups focused on identifying the viral determinants and mechanisms mediating this effect. It has been demonstrated that DV-encoded NS2A, NS4A and NS4B enhance replication of IFN-sensitive viruses by blocking STAT1 nuclear translocation (Munoz-Jordan et al., 2003). The ability of NS4B to weaken JAK/STAT signaling appeared to be conserved among many mosquito-borne flaviviruses, indeed also WNV and YFV could block STAT1 activation and ISGs induction (Guo et al., 2005; Liu et al., 2005; Munoz-Jordan et al., 2005). NS5 is instead the key viral factor responsible for attenuating type I IFN signaling in JEV and tick-borne flaviviruses infected cells (Best et al., 2005; Lin et al., 2006b; Werme et al., 2008). The mechanism of NS5 inhibition appeared to have virus-specific features. For JEV, an intact NS5 N-terminus, but not the C-terminal residues, is required for the IFN-antagonistic activity. Furthermore, the inhibition is likely to occur through a protein-tyrosine phosphatase-dependent mechanism (Lin et al., 2006b). For TBEV, the interaction between a sequence in the MTase domain of the NS5 protein and the membrane protein Scribble is instead important for the JAK/STAT signaling inhibition (Werme et al., 2008). Conversely, for Langat virus (LGV), the critical residues for interferon antagonism were mapped within the RdRp domain (Park et al., 2007). In addition, cholesterol redistribution upon flavivirus infection has also been described as an active mechanism of innate immunity evasion. Recruitment of cholesterol to perinuclear region of WNV replication has

been indeed associated with the disruption of cholesterol-rich lipid rafts at the plasma membrane and with a reduction of the IFN antiviral signaling response (Mackenzie et al., 2007).

However, passive mechanisms of immune evasion have also been proposed. Some RNA viruses modify the potential agonist in order to avoid detection by PRRs. Examples include formation of a 5'-cap structure on the viral RNAs by the action of viral methyltransferases or cap snatching from cellular mRNAs (Plotch et al., 1981). Other strategies include masking of the 5'-end of viral transcripts by a viral protein (Flanegan et al., 1977; Lee et al., 1977) or removal of 5' triphosphates (Habjan et al., 2008). Since long dsRNA intermediates of replication act as MDA5 agonists, some RNA viruses encode cytoplasmic dsRNA-binding proteins that protect the dsRNA from recognition by PRRs (Cardenas et al., 2006; Donelan et al., 2003).

Coronaviruses like the murine hepatitis virus (MHV) are able to delay IFN induction in certain cell types (Roth-Cross et al., 2007; Zhou and Perlman, 2007). MHV infection cannot antagonize IFNβ induction by stimulatory viruses inferring that viral proteins are not able to directly disrupt the pathway. These observations led to the suggestion that MHV evades detection by sequestering dsRNA in membrane compartments that are inaccessible to PRRs (Versteeg et al., 2007). However, this view has been challenged by the observation that retransfection of RNA from MHV-infected cells didn't induce IFNβ (Rose and Weiss, 2009). IFN production is delayed also after productive infection of flaviviruses such as WNV and TBEV (Fredericksen and Gale, 2006; Overby et al., 2010). Similarly to what has been observed for MHV, also in these cases viral proteins are unable to inhibit induction by other agonists arguing against the presence of an active mechanism to inhibit cytoplasmic IFN induction as well.

All together, these results suggest that viruses by combining passive and active mechanisms may impose blocks in PAMP recognition or subsequent signal transduction.

1.6. MS2-based tagging of RNA

Labeling either by fusion with a fluorescent protein or with a fluorescent-dye moiety allows the dynamic study of a protein of interest in live cells. Imaging of nucleic acids *in vivo* is instead a less common technique since the DNA or RNA targets are typically not accessible for tagging *in vivo* and only recently non-invasive labelling approaches became available. So far, much of our knowledge about intracellular RNA dynamics mostly came from either *in situ* hybridization of fixed cells or from biochemical fractionation of sub-cellular components. However, these methods can only provide a static picture at the time of fixation or fractionation of the sample and are certainly not compatible for the monitoring of nucleic acids in live cells. Labelling of chromosomes *in vivo* can be achieved by fluorescent tagging of chromosome binding factors. Usage of the lac operator (lacO) DNA sequence that is inserted into the DNA of interest provides an elegant way to label specific chromatic regions (Robinett et al., 1996). The specific part of chromatin can be visualized by expression of a fluorescently tagged lac repressor (lacI) fusion protein, which specifically binds to lacO sequence. This approach has been used to study chromatin organization, chromosome dynamics and even genomes from DNA viruses (Fraefel et al., 2004; Janicki et al., 2004; Tsukamoto et al., 2000; Tumbar et al., 1999).

The mRNA, in order to be visualized, can also be conjugated to fluorescent dyes and directly microinjected to the cells, however this is a rather invasive procedure (Ainger et al., 1993). Several other techniques have been developed which include the use of fluorescently labeled probes for *in vivo* hybridization, the use of molecular "beacons" which are active only when bound to target RNA or the use of fluorescently tagged RNA-binding proteins (Cui et al., 2005; Politz et al., 1998; Tyagi and Kramer, 1996). However, none of those approaches provide information about the behaviour of a single RNA molecule in real-time in living cells.

An innovative approach was developed inserting a series of RNA aptamers–stem-loops into the transcript of interest. This RNA is then detected by high affinity specific interaction of RNA stem-loops and fluorescently labeled MS2 bacteriophage coat protein. Therefore, the RNA detection system is comprised of two elements, a tag protein fused to the MS2 and a reporter RNA containing MS2-binding sites repeated in tandem. MS2 binds specifically and avidly to an RNA stem–loop

structure consisting of 19 nucleotides (Figure 12). Thanks to this method tracking of the target RNA *in vivo* can be performed allowing a quantitative analysis of the kinetics involved.

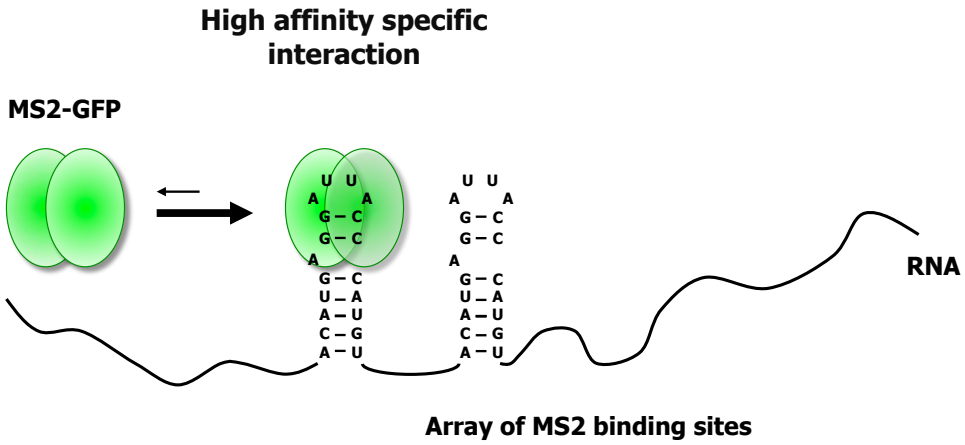

Figure 12 RNA detection MS2-based system. RNA molecules are detected using a fusion protein that comprises a fluorescent tag, such as green fluorescent protein (GFP) and the MS2 bacteriophage coat protein. MS2 has an extremely high affinity for a 19 nt RNA-recognition motif that is derived from the phage genome.

The MS2-based system has been effectively used for tracking specific cytoplasmic and nuclear mRNA in yeast, *Dictyostelium*, plants, flies and mammalian cells. For instance MS2-GFP has been used to demonstrate that *ASH1* mRNA is localized to the bud tip in *S. cerevisiae* in a zip-code dependent manner. Zip-codes are cis-acting elements often placed in 3'UTRs of mRNAs that specify the spatial information for mRNA targeting to a certain subcellular location. Proper *ASH1* mRNA targeting required the SHE protein complex, which is homologous to mammalian myosin motor proteins. Time-lapse imaging revealed that labeled mRNAs move to the bud tip at a rate of 0.2-0.44 μm/s in a directed fashion (Bertrand et al., 1998). Using the MS2-system in living mammalian cells, it was possible to demonstrate that cytoplasmic mRNAs exhibit directed, corralled, diffusive and static movements (Fusco et al., 2003). The β-actin zip-code increased the number and persistence of these directed movements relative to a non zip-code containing control reporter. Single particle tracking and time-lapse imaging revealed directed mRNA movements

along microtubules at an average rate of 1–1.5 μm/s. The MS2-system has also been used for the detection and kinetic studies of nuclear events such as transcription sites (Janicki et al., 2004). Visualization and trafficking of single mRNP in the nucleus revealed that diffusion is the primary mechanism by which these molecules translocate from transcription site to nuclear periphery (Shav-Tal et al., 2004). The mRNP particles moved an overage of 5 μm at velocities ranging from 0.03 to 0.08 μm/s. These movements were not affected by metabolic inhibitors of active transport and are consistent with diffusional rates. MS2-based approaches allowed the study of the dynamics of RNA polymerase II (RNAPII) *in vivo* (Darzacq et al., 2007). Photobleaching and photoactivation of fluorescent MS2 proteins used to label nascent messenger RNAs provided sensitive elongation measurements. It was shown that RNAPII elongated at 4.3 kb/min on a synthetic gene. These data were consistent with elongation rates measured on integrated human immunodeficiency virus (HIV-1) genes (Boireau et al., 2007; Maiuri et al., 2010; Molle et al., 2007). Photobleaching of nascent HIV RNAs labelled with MS2-GFP revealed that the elongation rate of RNAPII was approximately 1.9 kb/min.

Alternatively, the MS2 system can be converted from visualization tool to affinity purification coupled with proteomic studies. MS2 fused to the maltose binding protein (MBP) has been used to purify the spliceosome by affinity chromatography of cellular extracts (Zhou et al., 2002). Using this approach 145 distinct spliceosomal proteins were identified, making the spliceosome the most complex cellular machine so far characterized. Furthermore, this tagging system has been also exploited to identify novel host factors associated with HIV-1 RNA. Affinity purification of viral transcripts together with associated proteins via a flag-tagged MS2 protein, coupled to mass spectrometry, led to the identification of Matrin 3 as a cellular cofactor of HIV-1 Rev activity (Kula et al., 2011).

Recently also another method for RNA tagging in living cells has been reported but has not been yet extensively exploited. Similarly to what was done with MS2, an RNA motif derived from the bacteriophage λ (boxB) was coupled to the GFP-tagged 22-amino-acid peptide λ_N that tightly associates with boxB (Daigle and Ellenberg, 2007). By coupling this new approach with the MS2-based tagging system it has been possible to study the mobility of two mRNA species simultaneously in yeast (Lange et al., 2008).

So far, RNA detection either by the MS2 or the boxB system coupled with live-cell imaging technologies represents the most powerful approach for RNA analysis in single cells in real time. Therefore, the possibility to track viral genomes by these methods is of great importance for better understanding virus-host interaction and exploring how RNA dynamics is correlated with protein or organelle dynamics during viral infection.

1.7. Imaging intracellular dynamics in living cells

The discovery and development of fluorescent proteins as molecular tags (Tsien, 1998) combined with technical advances in the field of live-cell imaging has provided profound insight into how molecules are organized in cells and how they interact with each other and the cellular environment (Lippincott-Schwartz and Patterson, 2003). Cells that express proteins or nucleic acids tagged with these fluorescent proteins can be imaged with low light intensity over many hours and can provide useful information about changes in protein localization and steady-state level over time. Time-lapse imaging alone, however, can not reveal the dynamic properties of a molecule, for example, whether the protein is immobilized to a scaffold, free to diffuse, or undergoing constant exchange between compartments. To obtain such information the combination of time-lapse imaging with photobleaching and photoactivation techniques is required. Photobleaching occurs when a fluorophore permanently loses its ability to fluoresce due to photon-induced chemical damage and covalent modification. This can occur through either repeated excitation/emission cycles or by exposure to a high intensity light from a laser beam. Photoactivation, on the other hand, works by converting molecules to a fluorescence state by using a brief pulse of high-intensity irradiation (Lippincott-Schwartz and Patterson, 2003). Both these techniques allow to distinguish a selected pool of fluorescent proteins from other fluorescent proteins in the cells in order to monitor how they re-equilibrate. Results from fluorescence recovery after photobleaching (FRAP) and fluorescence loss in photobleaching (FLIP) experiments can provide important quantitative information about protein diffusion rates, binding kinetics, and movements between cellular compartments.

1.7.1. Fluorescence recovery after photobleaching

Fluorescence recovery after photobleaching (FRAP) is a technique developed in the mid-1970s to study the diffusive properties of molecules in living cells (Axelrod et al., 1976). A defined portion of the cell containing mobile fluorescent molecules is exposed to a brief and intense focused laser beam, thereby causing irreversible, or almost irreversible, photochemical bleaching of the fluorophore in that region. The subsequent kinetics of fluorescence recovery in the bleached region, which results from transport of fluorophores from unirradiated parts of the system into bleached area, provides a quantitative measure of fluorophore mobility (Figure 13). Before the bleaching, the concentration of fluorescent protein should be in equilibrium. At the bleach there is no change in physical or chemical properties of the protein tagged with the fluorophore, but the pool of tagged protein is divided in two families, one that is still fluorescent and the other is not. This artificial gradient of fluorescent protein concentration, that is not a true protein of interest concentration gradient, drives the rescue of the equilibrium by diffusion.

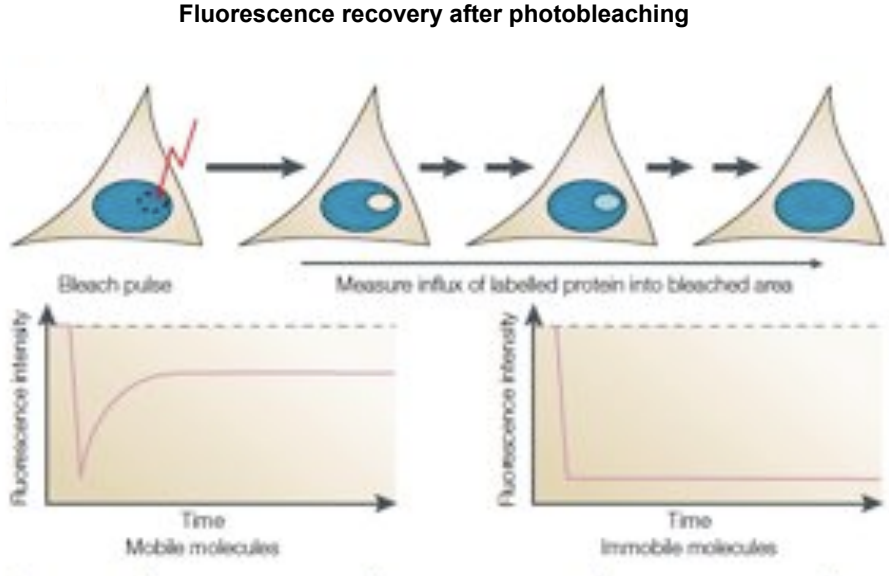

Figure 13 Fluorescence recovery after photobleaching. In a typical FRAP experiment a small area of the region of interest (ROI), in this case the nucleus, is photobleached by a short laser pulse. Recovery of fluorescent molecules from the surrounding area into the photobleached region is monitored over time. Using image analysis of confocal laser scanning microscopy images, the fluorescence intensity within the ROI can be plotted over time (bottom panels). The recovery kinetics of mobile molecules is dependent on the mobility of a protein. Immobile proteins show no recovery. Taken from (Phair and Misteli, 2001).

As already mentioned, analysis of fluorescence recovery can be used to determine the kinetic parameters of a protein, including its diffusion constant, mobile fraction, transport rate or binding/dissociation rate from other proteins (Lippincott-Schwartz et al., 2003). When binding interactions are present, they retard a FRAP recovery in relation to what would be observed if only diffusion occurred. Indeed a bleached protein has to unbind its binding site before to be free to leave the bleached area.

FRAP as now been adopted as a common technique for studying protein dynamics in the cytoplasm, nucleus, organelle lumens and membranes of living cells. Unconjugated GFP is considered a good standard marker of mobility in the absence of binding. It has been calculated that soluble GFP in the cytoplasm and in the nucleoplasm is highly mobile with diffusion rates of about 20 $\mu m^2/s$ (Lippincott-Schwartz et al., 2001; Swaminathan et al., 1997). Diffusion of GFP within the ER lumen appeared instead to be three-to six-fold slower than GFP in the cytoplasm indicating that a greater viscosity characterizes this compartment (Dayel et al., 1999).

FRAP has also unveiled important features of GFP-tagged membrane proteins. Many trans-membrane proteins localized in ER and Golgi compartments appeared to be highly mobile, with diffusion rates ranging from 0.2 to 0.5 $\mu m^2/s$, which is near the theoretical limit for protein diffusion in a lipid bilayer (Cole et al., 1996; Nehls et al., 2000). This suggesting that these proteins are not immobilized but may instead retain lateral mobility in the membrane of these compartments. Consistently, ER associated HCV NS4B and NS5A proteins exhibited a high degree of mobility when expressed alone from a plasmid in the absence of viral replication (Gretton et al., 2005; Jones et al., 2007). However, the mobility of the same proteins expressed from a sub-genomic replicon or analyzed within membrane associated foci (MAFs) appeared dramatically slower. Therefore, most likely, once viral proteins get incorporated into active replication foci they became restricted in their movements by interacting with other viral as well as host factors that are anchored to intracellular membranes. In keeping with these findings, large NS5A-GFP labelled structures, representing HCV-induced membranous webs, showed restricted mobility and displayed a static internal architecture with limited exchange of viral proteins within and between neighbouring RCs (Wolk et al., 2008).

1.7.2. Fluorescence loss in photobleaching

Fluorescence loss in photobleaching (FLIP) is a complementary approach to FRAP most often employed when the continuity of a cell compartment or the mobility of a molecule within the whole compartment is examined. FLIP experiments are similar to FRAP experiments in that a region of the cell is subjected to photobleaching from intense laser light, but in the FLIP approach, the bleaching is repeated in between imaging scans. Over time this will result in the loss of the fluorescent signal in any compartment that is continuous with the bleaching region or in any compartment in which the protein is freely mobile (Lippincott-Schwartz et al., 2001). Therefore, if labelled molecules in certain subcellular compartments are not bleached, the clear implication is that these compartments do not exchange with the compartment being bleached (Figure 14).

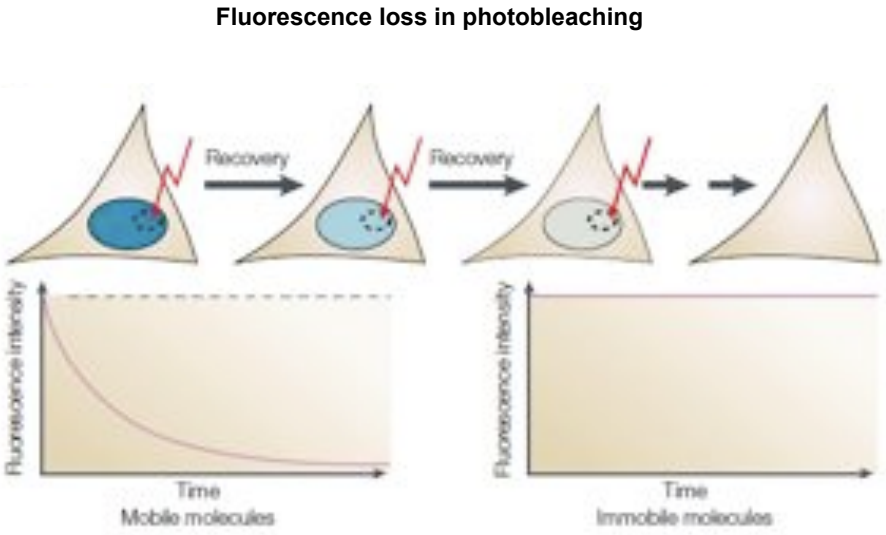

Figure 14 Fluorescence loss in photobleaching. In FLIP experiments the fluorescence intensity is measured in a small area after repeated bleaching of a ROI that is distant from this area. Movement of fluorescent molecules into the region being photobleached results in loss of fluorescence from areas outside the ROI and can be used to access the boundaries for a protein's diffusional movement within a cell. The rate of loss of fluorescence signal is dependent on the mobility of the protein. Immobile proteins show no loss.

1.8. Aim of the thesis

Flaviviruses are a group of emerging arthropod-borne viruses that cause serious diseases both in humans and animals. They replicate in the cytoplasm of the host cell in close association with rearranged membrane. Therefore, in order to generate specialized sites for RNA replication, they must spatially and temporally interact with different intracellular structures, leading to extensive changes in the cellular architecture and physiology. At the beginning of this work, very little was known about the biogenesis, structure and function of flaviviral replication compartments. Therefore we wished to establish a new approach to better understand the interface of flavivirus replication and the host cell machinery.

To this aim, during the part of my PhD, we developed an effective tool to track flaviviral RNA in single living cells by inserting a series of MS2 binding sites within the variable region of the TBEV 3'-UTR. Subsequently, we exploited our system to characterize the dynamic exchange of viral RNA and cellular PRRs between viral replication compartments and the cytosol. Finally, we explored the early innate immune response to TBEV infection and found that a consistent delay of interferon induction correlated with the formation of viral replication compartments.

2. MATERIALS AND METHODS

2.1. Materials

2.1.1. Cells

Bacteria

- **Max Efficiency DH10B Competent Cells** (Invitrogen).
  Genotype: F- *mcr*A Δ(*mrr-hsd*RMS-*mcr*BC) φ80*lac*ZΔM15 Δ*lac*X74 *rec*A1 *end*A1 *ara*D139 Δ (*ara*, *leu*)7697 *gal*U *gal*K λ- *rps*L *nup*G /pMON14272 / pMON7124.
- **XL10-Gold Ultracompetent Cells** (Stratagene).
  Genotype: Tetr Δ(mcrA)183 Δ(mcrCB-hsdSMR-mrr)173 endA1 supE44 thi-1 recA1 gyrA96 relA1 lac Hte [F´ proAB lacIqZΔM15 Tn10 (Tetr) Tn5 (Kanr) Amy].

Mammalian Cells

- **BHK-21 (clone 13):** Baby hamster kidney cell line (ECACC No. 85011433).
- **Hos-143b:** Human bone osteosarcoma cell line (ECACC No. 91112502)
- **U2OS:** Human osteosarcoma cell line (ECACC No. 92022711)
- **Vero:** African green monkey kidney (ECACC No. 84113001)

2.1.2. Media

Bacteria

- **Luria-Bertani (LB) Medium:** 10 g bacto-trypton, 5 g bacto-yeast extract, 10 g NaCl per 1 liter medium. Ampicillin was added at a concentration of 50-100 µg/ml. For hardening 1.5 % agar-agar was added to the liquid medium.
- **SOC Medium:** is identical to Super Optimal Broth (SOB) medium (20 g bacto-trypton, 5 g bacto-yeast extract, 0.5 g NaCl per 1 liter medium), except that it contains 20 mM glucose.

Mammalian Cells

- **DMEM complete medium:** Dulbecco's modified minimal essential medium (Gibco-Invotrogen) supplemented with antibiotic-antimycotic solution (Gibco-Invitrogen) and 10 % fetal calf serum (FCS, Gibco-Invitrogen). For selection G418 (Invitrogen) was added at a concentration of 0,8 mg/ml.
- **OptiMEM:** defined medium formulation with reduced serum (Gibco-Invitrogen)
- **Cryo medium:** for long-term storage, cells were frozen in liquid nitrogen in 90% FCS, 10 % DMSO.

2.1.3. Antibodies and antisera

Primary antibodies:

Table 1. Primary antibodies used in this study.

Reactivity	Species	Subtype	Source	Comments
TBEV-NS1	Mouse	IgG Monoclonal	Dr. Connie Schmaljohn (Iacono-Connors et al., 1996)	1:100, IF
TBEV-polyprotein	Rabbit	Polyclonal	Dr. C.W. Mandl (Orlinger et al., 2006)	1:100, IF
dsRNA J2	Mouse	IgG Monoclonal	English & Scientific Consulting	1:200, IF
Human-EEA1	Mouse	IgG Monoclonal	n. 610456, BD Biosciences	1:200, IF
Human-CD71	Mouse	IgG Monoclonal	clone 10F11, NeoMarkers	1:200, IF
Human-ERGIC-53	Goat	Polyclonal	sc32442, Santa Cruz	1:100, IF
Human-TGN-46	Rabbit	Polyclonal	AB50595, Abcam	1:200, IF
Human-Giantin	Rabbit	Polyclonal	AB24586, Abcam	1:200, IF
Human-PDI	Mouse	IgG Monoclonal	AB2792, Abcam	1:100, IF
Human-IRF-3	Rabbit	Polyclonal	Dr. T. Fujita, Kyoto University	1:50, IF
Human-RIG-I	Goat	Polyclonal	Sc48929, Santa Cruz	1:200,WB
GFP	Rabbit	Polyclonal	Molecular Probes, Invitrogen	1:1000, WB

Secondary antibodies:

- Donkey anti-rabbit IgG, Alexa Fluor 594 (Molecular Probes); 1:1000 for IF.
- Donkey anti-mouse IgG, Alexa Fluor 594 (Molecular Probes); 1:1000 for IF.
- Donkey, anti-rabbit IgG, Alexa Fluor 488 (Molecular Probes); 1:1000 for IF.
- Donkey, anti-goat IgG, Alexa Fluor 594 (Molecular Probes); 1:1000 for IF.
- Goat polyclonal, anti-rabbit immunoglobulins/HRP (DakoCytomation); 1:10000 for WB.
- Rabbit polyclonal, anti-goat immunoglobulins/HRP (DakoCytomation); 1:10000 for WB.

2.1.4. Vectors

Table 2. Cloning and expression vectors used in this study

Plasmid	Relevant characteristics	Reference
pTNd/ΔME-EGFP	Amp^r	(Gehrke et al., 2005)
pSL-MS2-12	Amp^r	(Bertrand et al., 1998)
pSL-MS2-24	Amp^r	(Bertrand et al., 1998)
pcDNA-MS2-EYFPnls	Amp^r	(Boireau et al., 2007)
pEYFP-N1	Kan^r	Clontech
p12xMS2	Amp^r	(Hoenninger et al., 2008)
p24xMS2	Amp^r	(Hoenninger et al., 2008)
phRL-SV40	Amp^r	Promega
pCherry-MS2nls	Amp^r	(Boireau et al., 2007)
pCAGGS-PR8-NS1	It encodes the influenza A H1N1 Puerto Rico strain (A/PR/8/34) NS1 protein; Amp^r	Kindly provided by Adolfo García-Sastre (Talon et al., 2000)
pEGFP-N1	Kan^r	Clontech
p125-Luc	It carries the Firefly Luciferase gene under control of the natural IFNβ promoter Amp^r	Kindly provided by Dr. Takashi Fujita, Kyoto University
pRL-CMV	Amp^r	Promega
pGFP-IRF3	Kan^r	(Basler et al., 2003)
pGFP-RIG-I	Amp^r	Kindly provided by Dr. Takashi Fujita, Kyoto University

2.1.5. Oligonucleotides

Table 3. Sequences of oligonucleotides used in this study. The restriction sites contained in the primer sequence are underlined and the changes in base composition for mutagenesis are shown in bold for ease of comprehension.

Name	Sequence (5' to 3')
TBE-XbaI-fw	GCGCAT***T***CTAG***A***TATAGTTCTAGAGG
TBE-NheI-rv	ACGTCGCTAGCGGGTGTTTTTC
BclI-fw	GGCGTCACTGATCAATGGGG
GAA-rv	CCACACAA***G***CG***G***CACCACTG
GAA-fw	GTCAGTGGTG***C***CG***C***TTGTGTG
BstBI-rv	CCATGGCCATTCGAAATTGG
MS2-XhoI-fw	CCGCTCGAGATGGCTTCTAACTTTAC
MS2-BamHI-rv	GAAGATCTCCGTAGATGCCGGAGTTG
5'NCRA1fw	GCGTTTGCTTCGGA
5'NCRA1rv	CTCTTTCGACACTCGTCGAGG
5'NCRA2fw	CGGATAGCATTAGCAGCG
5'NCRA2rv	CCTTTCAGGATGGCCTT
MS2rv	GGCAATTAGGTACCTTAGGATC
MS2fw	CGTCGACCTGAGGTAATTATAACC
BA1	CATGTGCAAGGCCGGCTTCG
BA4	GAAGGTGTGGTGCCAGATTT
IFNβ-fw	AGGACAGGATGAACTTTGAC
IFNβ-rv	TGATAGACATTAGCCAGGAG
VSV-fw	TGATACAGTACAATTATTTTGGGAC
VSV-rv	GAGACTTTCTGTTACGGGATCTGG

2.2.General Procedures

2.2.1. Cell culture

Monolayers of cells were grown at 37°C, 5 % CO_2 in DMEM complete medium. Cells were passaged after treatment with 0.05 % Trypsin – 0.02 % EDTA and seeded at the appropriate dilution. Upon electroporation cells were washed and seeded in medium without addition of antibiotic-antimycotic solution.

2.2.2. Plasmids construction

All plasmid constructs containing the cDNA of TBE Western subtype prototypic strain Neudoerfl were derived from pTNd/ΔME-EGFP (Gehrke et al., 2005).

The constructs pTNd/ΔME_12xMS2 and pTNd/ΔME_24xMS2 were generated by replacing the variable region of the 3'NCR with 12 or 24 repeats of a stem-loop RNA structure (19 nucleotide each) specifically recognized by the MS2 bacteriophage coat protein. This was achieved by replacing the SacII-NotI fragment of pTNd/ΔME-EGFP with the EcoRI-NotI fragment of pSL-MS2-12 and pSL-MS2-24 (Bertrand et al., 1998). Since these constructs carried an additional NheI site that would cause premature termination of in vitro transcribed RNA, an additional step of mutagenesis by PCR was performed with the primer TBE-XbaI-fw and TBE-NheI-rv. The PCR fragment was digested with XbaI and NheI and used to replace the NheI-NheI fragment to yield the final plasmids pTNd/ΔME_24xMS2 and pTNd/ΔME_12xMS2.

As control we generated pTNd/ΔME_2SMx42, a construct carrying the 24 repeats in the opposite orientation by inverting the NotI-BstBI fragment. The replication-deficient replicon TNd/ΔME_24xMS2_GAA carries the GDD to GAA mutation in the viral NS5 protein that abolishes RdRp activity (Khromykh et al., 1998). Mutagenesis was performed by PCR by generating two overlapping fragments to yield the full-length insert using primers BclI-fw, GAA-rv, GAA-fw and BstBI-rv. The final PCR product was digested with BclI and BstBI and used to replace the corresponding fragment in pTNd/ΔME_24xMS2.

To obtain pMS2-EYFP, the coding sequence of the MS2 protein without the nuclear localization signal was amplified from pcDNA-MS2-EYFPnls (Boireau et al., 2007)

by PCR and cloned into plasmid pEYFP-N1 (Clontech) between restriction sites XhoI and BamHI. The primer sequences for this PCR were MS2-XhoI-fw and MS2-BamHI-rv. A list of the primers used for this study is reported in Table 3. Please note that restriction sites contained in the primer sequence are underlined and changes in base composition for mutagenesis shown in bold for ease of comprehension.

pTNd/ΔME-derivative plasmids were propagated, according to the manufacturer's instructions, in XL10-Gold Ultracompetent cells (Stratagene) that are recombination deficient (*recA*) in order to ensure insert stability. All other plasmids were instead propagated, according to the manufacturer's protocol, in Max Efficiency DH10B competent cells (Invitrogen).

2.2.3. *In vitro* RNA transcription

Template DNA for *in vitro* transcription was prepared from large-scale preparations of plasmid DNA performed using QIAfilter Plasmid Maxi kit (Qiagen) according to the manufacturer's protocol. All the pTNd/ΔME-EGFP derivative plasmids were linearized by digestion with NheI. After phenol-chloroform extraction and ethanol precipitation, the 5'-overhang was partially filled-in using Klenow polymerase (New England Biolabs) in the presence of 12.5 μM dCTP and dTTP at 25°C for 30 minutes. Linearized DNAs were again purified by phenol-chloroform extraction, precipitated with ethanol and washed with 70 % ethanol. The pellet was then resuspended with RNase-free water and 500 ng of template were transcribed using the T7 MEGAscript kit (Ambion). The transcription reaction contained 7.5 mM each of ATP, CTP and UTP, 1.5 mM GTP and 1 mM cap analogue (m^7G(5')ppp(5')G; Ambion). The reaction mixture (20 μl) was incubated for 3 hours at 37°C. At the end of the reaction, 2U of TURBO DNase (Ambion) were added and the mix was incubated for 15 minutes at 37°C to remove the template DNA. RNA was purified using the RNeasy Mini kit (Qiagen). The RNA was eluted in RNase free water and the integrity of the *in vitro* transcripts was confirmed by denaturing agarose gel electrophoresis. The yield of RNA was determined by absorbance at 260 nm.

2.2.4. RNA transfection by electroporation

Single cell suspensions were prepared by trypsinization of monolayers and subsequent resuspension with DMEM complete medium. Cells were then washed in

ice-cold PBS and counted. Aliquots of 5 x 10^6 cells were resuspended in 500 µl ice-cold phosphate buffered saline (PBS) and were mixed in a 0.4 cm Gene Pulser cuvette with 10 µg of RNA and 5-10 µg of plasmid DNA when required. Cells were electroporated with a Bio-Rad Gene Pulser apparatus applying either two subsequent pulses at 0.25 KV, 500 µF (for BHK-21 and Hos-143b cells) or one single pulse at 0.25 KV, 960 µF (for U2OS cells). After electroporation cells were washed three times in DMEM complete without antibiotic-antimycotic solution and seeded in the same medium.

2.2.5. Northern blot analysis

For Northern blot hybridization, total RNA from BHK-21 and BHKA3 cells was extracted at different time points after transfection with the replicon TNd/ΔME_24xMS2 using RNeasy Mini kit (Qiagen) and treated with DNAseI (Invitrogen) according to the manufacturer's protocol. 5 µg of total RNA were separated by agarose-formaldehyde gel electrophoresis. RNA was then transferred to nylon membranes (Hybond-NX; Amersham Biosciences) with 10X SSC and cross-linked by UV irradiation. For prehybridization, the membrane was incubated for 2 hours at 42°C in hybridization solution containing salmon sperm DNA. TBEV RNA was detected by hybridization with a ^{32}P-labeled DNA probe complementary to nucleotides 7768 to 8019 of TBEV strain Neudoerfl in hybridization solution at 42°C overnight. Hybridization with a β-actin-specific DNA probe was used to monitor equal sample loading in each lane of the gel. Membranes were washed twice with SSC 5X, SDS 0.1 % for 30 minutes at 42°C, twice with SSC 2X, SDS 0.1 % for 30 minutes at 42°C and twice with SSC 1X, SDS 0.1 % for 30 minutes at 42°C. Finally, membranes were briefly dried and signals were detected using Cyclon (Perkin Elmer).

As quantity standards for the amount of TBEV RNA into cell extracts, defined numbers of in vitro transcribed RNA molecules (10^9, 10^8 and 10^7) were loaded in parallel.

2.2.6. TBEV RNA amplification by RT-PCR

An RT-PCR assay was performed to monitor viral replication. After electroporation of replicon RNA, cells were harvested by trypsinization at different time points.

RNA was extracted using RNeasy Mini Kit (Qiagen), treated with DNaseI (Invitrogen) and quantified. RT-PCR was performed using the reagents and protocols supplied with ImProm-II Reverse Transcription System (Promega). Primers used in this study were 5'NCRA1rv, to generate the cDNA, and 5'NCR A2fw and 5'NCRA2rv for amplification of the 5'NCR as described by Han and co-workers (Han et al., 2001). To assess maintenance of the repeats during TBEV replication a strategy was developed that takes advantage of the extra DNA that is present every two 19nt stem-loops due to the cloning procedure used to obtain the array (Bertrand et al., 1998). cDNA was synthesized with the MS2rv primer, mapping every two repeats, and amplified with the same together with MS2fw primer. This strategy allowed the counting of two repeats at a time in replicated TBEV RNA. cDNA for the β-actin was generated using random primers and amplified with the primers BA1 and BA4.

2.2.7. dsRNA-immunoblotting

Total RNA extracted from U2OS mock transfected or electroporated with the TNd/ΔME_24×MS2 replicon RNA (10µg) was spotted onto a nylon membrane (Hybond N+), UV cross-linked and then blotted with the J2 mouse monoclonal anti-dsRNA antibody (1:2000).

2.2.8. Indirect Immunofluorescence analysis

Expression of viral proteins was determined by immunofluorescence (IF) staining with a mouse anti-protein NS1 monoclonal antibody generously provided by Connie Schmaljohn (Iacono-Connors et al., 1996) and a polyclonal rabbit anti-TBEV serum that can be used for both structural and non-structural protein detection (Orlinger et al., 2006). The J2 mouse monoclonal anti-dsRNA antibody (English & Scientific Consulting, Szirak, Hungary) was used to detect the replication complexes.

In general, cells were seeded into 6-wells plates containing microscope coverslips and supplied with complete growth medium to be confluent at the time of fixation. For IF analysis cells were washed three times with PBS and fixed in 3.7 % paraformaldehyde (PFA) solution for 15 minutes at room temperature (RT). Thereafter, cells were again washed three times with PBS and incubated 5 minutes with 100 mM glycine in order to saturate excesses of PFA and to stop the fixation

reaction. For permeabilization, cells were incubated for 5 minutes with 0.1 % Triton X-100 in PBS and washed three time. Before incubation with antibodies, a blocking step was performed at 37°C for 30 minutes with PBS, 1 % bovine serum albumine (BSA) and 0.1 % Tween 20 (blocking solution). Primary antibodies were diluted to the desired concentration in blocking solution to prevent aspecific binding of the antibodies. After one hour incubation at 37°C, or overnight (O/N) incubation at 4°C, coverslips were rinsed three times with PBS 0.1 % Tween 20 (washing solution) and incubated with secondary antibodies for 45 minutes at 37°C. Coverslips were finally washed three times with washing solution and mounted on slides using Vectashield mounting medium with or without addition of DAPI (Vector Laboratories).
In order to detect endogenous IRF-3 intracellular localization, U2OS cells were fixed and permeabilized as previously described. The blocking was instead performed at 37°C for 1 hour with PBS, 0.5 % BSA and 0.04 % Tween 20 following Dr. Takashi Fujita protocol. Cells were next incubated O/N at 4°C with the anti IRF-3 antibody diluted in the blocking solution described above, washed twice for 20 minutes at RT with PBS 0.04 % Tween 20 and finally incubated with the secondary antibody for 45 minutes at 37°C with the same blocking solution used before. After two washes at RT for 20 minutes, coverslips were mounted on slides as already described.

2.2.9. Plasma membrane permeabilization

Selective permeabilization of the plasma membrane was achieved by treatment with digitonin (Sigma) 24 hours after BHK-21 co-transfection with the replicon RNAs and the EYFP-MS2 plasmid. After three washes with cold KHM buffer (110 mM potassium acetate, 20 mM HEPES and 2mM $MgCl_2$), cells were permeabilized by incubation in KHM buffer containing 20 μM digitonin for 6' at 4°C and then extensively washed with cold KHM buffer to allow diffusion of the free cytoplasmic proteins. Cells were then fixed with 3.7% paraformaldehyde (PFA) and incubated 5' at room temperature in the presence or in the absence of 0.1% Triton X-100. For the treatment with nucleases, digitonin-permeabilized cells were incubated with 1 μg/ml RNaseA (Roche) for 15' at 37°C. Cells were then fixed in PFA 3.7%, permeabilized with 0.1% Triton X-100 for 5' at room temperature and processed for dsRNA staining as already described.

2.2.10. RNA *in situ* hybridization

For RNA *in situ* hybridization, 24 hours post-transfection, BHK-21 cells were fixed for 30 minutes at RT in 3.7 % PFA. After three washes in PBS, cells were permeabilized by treatment with 70 % ethanol at 4°C O/N. Next day coverslips were rehydrated in 1xSSC, 20 % formamide and hybridized O/N at 37°C in 20 µl of a mixture containing 10 % dextran sulphate, 2 mM vanadyl-ribonucleoside complex, 0.02 % RNase free BSA, 10 µg yeast tRNA, 1xSSC, 20 % formamide and 10 ng of Cy3-conjugated oligonucleotide probe against the MS2 binding sites. Cells were then washed three times for 30 minutes at RT in 20 % formamide, 1xSSC, rinsed in PBS and mounted on slides using Vectashield mounting medium (Vector Laboratories).
The amino-allyl thymidine modified oligonucleotide probe for RNA FISH listed below was generously provided by E. Bertrand (IGMM, Montpellier, France). The probe was Cy3-labelled as previously described (Boireau et al., 2007).

Sequence of the probe used for RNA *in situ* hybridization:
AxGTCGACCTGCAGACAxGGGTGATCCTCAxGTTTTCTAGGCAATxA

2.2.11. Flow cytometry analysis

For the analysis of MS2-EYFP expression, 24 hours after transfection, cell monolayers were treated with 0.05 % Trypsin – 0.02 % EDTA to prepare single cells suspensions. Cells were then washed twice with PBS, were resuspended with 300 - 500 µl PBS and analyzed immediately by flow cytometry using a FACSCalibur apparatus (Becton Dickinson) and the Cell Quest Pro software.

2.2.12. Transfection of U2OS cells with Lipofectamine LTX

Plasmid DNAs, Poly(I:C) (InvivoGen) and total RNA extracts were delivered into U2OS cells using Lipofectamine LTX (Invitrogen) according to the manufacturer's instructions.

2.2.13. Luciferase assay

In order to assess the effect of the insertion of MS2 binding sites on TBEV translation and replication, a Dual-Glo Luciferase Assay System (Promega) was used

according to the manufacturer's instructions to simultaneously measure both firefly and Renilla luciferase activity. After electroporation of BHK-21 cells with RNA and/or DNA, cells were washed once with growth medium without phenol red and counted. A maximum of 60,000 cells were seeded onto 96-well plates (Perkin Elmer), and triplicate wells were lysed at individual time points, followed by measurement with a Victor Light Luminometer (Perkin Elmer). The primary data are given in relative light units (RLUs). For normalization of the firefly luciferase values, replicon RNA (1.9×10^{12} copies) containing the firefly luciferase gene was cotransfected with either 6 µg of RNA that had been transcribed in vitro from phRL-SV40 (encoding Renilla luciferase) as a standard for the early time points (3 hours), or 6 µg of phRL-SV40 DNA for later time points (13–96 hours). In addition, a separate "control standard" consisting of BHK-21 cells transfected with the control nucleic acid alone was included in each experiment, and the mean value of the Renilla luciferase activity of these cells was determined at each time point. The ratio of the uncorrected luciferase activity measured for the RNA versus the DNA controls differed less than two-fold between individual transfection experiments indicating that only little variability was introduced due to the usage of two different controls within a single time course experiment. The same electroporation conditions were used for DNA and RNA samples and yielded consistently high efficiencies between 50 and almost 100 % of the transfected cells as determined by immunofluorescence or flow cytometry. To calculate the normalized firefly luciferase activity, the measured Renilla luciferase activity from each cotransfected sample was divided by the corresponding control standard value to obtain a normalization factor by which the measured firefly luciferase value of that well was divided. To correct for variability between different plates, the control standards from each plate were normalized to a single standard to obtain a factor by which the firefly luciferase values for that plate were then multiplied. In this way, corrections could be made for differences in transfection efficiency as well as total cell count at different time points. The corrected data are presented as "normalized RLUs" (Hoenninger et al., 2008).

To monitor IFN-β promoter activity, 2.5×10^5 U2OS were seeded on 6-well plates and grown until the next day to a density of around 70-80 %. Cells were then transfected using Lipofectamine LTX, according to the manufacturer's instructions, with the p125-luc plasmid, kindly provided by Dr. T. Fujita, and with the pRL-CMV

construct for normalization. After 24 hours cells were either mock or Poly(I:C) (InvivoGen) stimulated for 1 hour again using Lipofectamine LTX. 12 hours upon stimulation cells were lysed and processed for the luciferase assay using protocol and reagents provided by the Dual-Luciferase Reporter Assay System (Promega). Measurements of luciferase activities in cell lysates were performed using the Envision Multimode Plate Reader **(**Perkin Elmer).

2.2.14. Real-time quantitative reverse transcription PCR (qRT-PCR)

Total cellular RNA was extracted at the indicated time points after transfection or infection by using Trizol (Invitrogen) according to the manufacturer's instructions, treated with DNase I (Invitrogen) and then quantified. Aliquots of 600 ng were used as a template to synthesize cDNA using random primers (Invitrogen) and M-MLV Reverse Transcriptase (Invitrogen) according to manufacturer's protocol. Viral RNAs (TBEV, VSV) and mRNA levels of human β-actin and IFN-β were detected by real-time quantitative PCR using iQ SYBR Green Supermix (Bio-Rad). Signals of inducible cellular mRNAs or viral RNAs were normalized to the β-actin mRNA signal.

The sequences of oligonucleotides used for this analysis are reported in table 3. For TBEV RNA detection we used primers 5'NCRA1fw and 5'NCRA1rv whereas for VSV amplification VSV-fw and VSV-rv. IFNβ-fw and IFNβ-rv oligonucleotides were used for IFN-β mRNA amplification and BA1 and BA4 for β-actin mRNA quantification. Amplification and detection were carried out on a CFX96 Real Time System (Bio-Rad).

2.2.15. Western blot analysis

Whole cell lysates were resolved by 4–15% or 6% SDS–polyacrylamide gel electrophoresis (SDS-PAGE). For Western blotting, nitrocellulose membrane (Reinforced NC, Whatman) was used and membranes were blocked for 1 hour in 5% milk followed by incubation with the appropriate primary antibodies diluted in 3% milk / 0,5% Tween-20 at 4°C O/N. After three washing with TBS 0.5% Tween-20 secondary antibodies conjugated with HRP (DakoCytomation) were diluted in 3% milk / 0,5% Tween-20 and incubated for 1 hour. Blots were developed using

Immobilon Western Chemiluminescent HRP Substrate (Millipore) according to manufacturer's instructions.

2.3. Working with viruses

2.3.1. Preparation of TBEV and VSV stocks

Viral stocks were prepared by infection of Vero cells at a low multiplicity. The TBEV strain Hypr and vesicular stomatitis virus Indiana serotype (VSV-IN) (ATCC VR-1238) were used for these studies. After cytopathic effect (CPE) was observed, cell culture supernatant was collected, clarified by centrifugation, supplemented with 20 % FBS, and stored in aliquots at -80°C. Viral titres were determined by using a plaque-forming assay. Vero cells were seeded into 24-well dishes till monolayer was formed and infected with a 10-fold serial dilution of TBEV in a total volume of 200 µl of serum-free medium. After 1 hour incubation at 37°C with 5 % CO_2, the inoculum was removed and a 500 µl overlay containing 1 volume of 6% carboxymethyl cellulose (CMC) to 1 volume of maintenance medium (DMEM supplemented with 4 % FCS) was added. The plates were incubated for 72 hours before fixation with 4 % PFA dissolved in PBS. Infected cells were stained adding 300 µl of crystal violet solution in 80 % methanol / 20 % PBS. After 30 minutes the staining solution was removed and cells were washed 3-4 times with water. The titre of the virus was determined by counting the number of plaques produced at each dilution.

2.3.2. TBEV and VSV infection of cells

For standard infection assays, U2OS cells were seeded at a density of 1.3 x 10^5 per well of a 12-well plate. 24 hours after, cells were infected at the appropriate MOI by adding 500 µl of virus stock properly diluted in serum-free medium. After 1 hour incubation at 37°C with 5 % CO_2, the inoculum was replaced with maintenance medium (DMEM supplemented with 4 % FCS). Cells were then harvested at the appropriate time point.

2.4. Microscopy and image acquisition.

2.4.1. Imaging of fixed cells

Fluorescent images of fixed cells were captured with different microscopes, either the DMRI wide-field (Leica), and the LSM 510 META confocal microscope (Carl Zeiss Microimaging, Inc.).

The LSM 510 META confocal microscope was equipped with a 63× NA 1.4 Plan-Apochromat oil objective. The pinhole of the microscope was adjusted to get an optical slice of less than 1.0 µm for any wavelength acquired. MS2-EYFP was excited with the 488 nm line of the Ar laser and its emission was monitored using a custom-made Meta band pass filter between 510 and 563 nm. The Alexa594 (Molecular Probes) and Cy3 (Molecular Probes) fluorophores as well as the Cherry variant of the MS2 tagged protein were excited with the 543 nm HeNe laser and their emission collected using a custom-made Meta band pass filter between 552 and 670 nm. Online emission fingerprinting was performed for the simultaneous acquisition of MS2-EYFP and EGFP. Previously acquired emission spectra of cells transfected only with EGFP or MS2-EYFP, both excited with the 488 nm laser line, were used as standards for the linear unmixing algoritm of the LSM510 META software.

The DMRI wide-field inverted microscope was equipped with a 63× NA 1.3 objective and was controlled by Metamorph (Universal Imaging). Digital images were collected using a CoolSnap K4 CCD camera (Roper scientific). Data in figure 13 were obtained from stacks of 21 planes acquired at bin = 1 with steps of 0.5 µm in the z-axis. Three dimensional deconvolution and reconstruction was performed with the ImageJ plug-in “Iterative Deconvolve 3D” (http://rsb.info.nih.gov/ij/).

2.4.2. Quantification of IRF-3 activation

Quantification of IRF-3 nuclear translocation was performed at the ICGEB High-Throughput Screening Facility (http://www.icgeb.org/high-throughput-screening.html). In these experiments, images were acquired using an ImageXpress Micro automated high-content screening microscope (Molecular Devices) equipped with a 20× objective; a total of 24 fields were acquired from each coverslip, which corresponds to an average of 2000-3000 cells imaged and analysed per experimental

condition and replicate. Automated image analysis of IRF-3 translocation was performed in MetaXpress software (Molecular Devices) using the "Multi Wavelength Cell Scoring" application module that identifies cell nuclei (blue channel) and subsequently quantifies the average nuclear fluorescence of IRF-3 (green channel). Cells were scored as positive for IRF-3 translocation when the average nuclear intensity of the green channel was at least twice that of mock treated cells.

2.4.3. Live imaging acquisition

BHK-21 or U2OS cells were electroporated with the TBEV replicons' RNA and plated on glass-bottom plates (MatTek, Ashland, MA, USA). For the visualization of the viral RNA cells were co-transfected either with CherryMS2nls, expressing a hybrid protein composed by the core protein of the MS2 bacteriophage fused to Cherry and to a nuclear localization signal (nls), or with the MS2-EYFP construct with and without the nls. At the appropriate time point post-transfection, cells were transferred on a humidified and CO2-controlled on-stage incubator (PeCon GmbH, Erbach, Germany) at 37°C in complete DMEM medium without phenol red for live cell imaging.

FRAP and FLIP analysis were performed by using the inverted META LSM510 confocal microscope (Zeiss, Jena, Germany) with an oil immersion 63× objective (NA 1.4, Zeiss). For FRAP experiments images of 512 × 512 pixels (29.25 × 29.25 µm for BHK-21 cells; 48.75 × 48.75 µm for U2OS cells) and optical thickness of 1 µm were acquired using 1 % or less of the power of the 514 nm laser line. EYFP and GFP were bleached at 514 nm and 488 nm respectively (Argon laser, maximum output 500 MilliWatt) in a circle of 30 pixels of diameter, at full laser power, for 10 passages. For FLIP measurements images were acquired as described above and bleaching was performed at every acquisition.

Images were analyzed with ImageJ (Rasband, W.S., ImageJ, National Institutes of Health, Bethesda, Maryland, USA, http://rsb.info.nih.gov/ij/). For the mathematical analysis of the data experimental normalized recovery curves (for FRAP) or loss of fluorescence curves (for FLIP) from at least 10 cells were averaged

Videos of the live imaging acquisitions are available upon request.

3. RESULTS

3.1. Development of the Flavivirus MS2-based replicon system

The MS2-based tagging system is a well-established method for RNA labelling in living cells. This technique was pioneered by Singer and co-workers in yeast in order to track the movement of *ASH1* mRNA into the daughter cell or bud during cell division (Beach et al., 1999; Bertrand et al., 1998). Two elements are required for the labelling: a tag protein or peptide fused to the MS2 phage coat protein and a reporter RNA containing MS2 binding sites repeated in tandem. MS2 binds specifically and avidly to a 19-nucleotide RNA stem loop structure allowing the detection of a specific RNA. This method has been extensively used for the detection of mRNA and genomic retroviral RNA in living cells (Basyuk et al., 2003; Boireau et al., 2007; Darzacq et al., 2007; Fusco et al., 2003; Shav-Tal et al., 2004). However, MS2 tagging has never been applied for the study of positive sense RNA viruses in mammalian cells. To track flaviviral RNA in living cells through the MS2 based system we took advantage of a well-characterized TBEV subgenomic replicon previously established by Mandl and co-workers (Gehrke et al., 2005) (Figure 15).

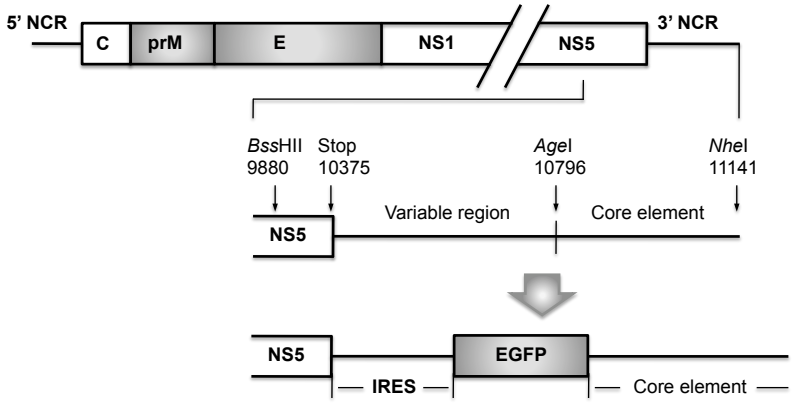

Figure 15 Schematic drawing of the TBEV-based pTNd/ΔME-EGFP expression vector. The diagram at the top shows the structure of the full length TBEV genome, containing the long ORF encoding the structural proteins C, prM and E and the non-structural proteins NS1-NS5, flanked by short non-coding regions (NCRs). Below a detailed view of the 3'-NCR is reported. The 3'-end of the genome is composed by a variable region and a more conserved core element. The positions of the stop codon and restriction sites used during the construction of the pTNd/ΔME-EGFP vector are also shown (nucleotide numbers refer to the wild-type TBEV-genome, GeneBank accession number U27495). In the pTNd/ΔME-EGFP replicon vector the prM and E genes were deleted (shaded) and the variable region of the 3'-NCR was replaced by an IRES-EGFP cassette as indicated in the diagram shown at the bottom. The figure is not drawn to scale. Modified from (Gehrke et al., 2005)

The replicon is based on the Neudoerfl strain and carries a deletion of the envelope proteins (ΔME) that does not allow viral propagation. However, all the elements required for RNA replication are maintained: the 5'-NCR, the capsid protein followed directly by the non-structural proteins and a modified 3'-NCR in which the variable region was replaced by an IRES-EGFP expression cassette.

It is well known that highly conserved secondary and tertiary RNA structures present in the genome of flaviviruses play essential regulatory roles during viral translation, RNA replication and assembly (Alvarez et al., 2005b; Brinton and Dispoto, 1988; Lindenbach et al., 2007; Lo et al., 2003; Markoff, 2003; Rice et al., 1985; Wallner et al., 1995). Moreover, long-range RNA-RNA interactions between sequences at the 5' and 3' ends of the viral genome are also required for RNA cyclization during TBEV replication (Kofler et al., 2006). Therefore, in order to preserve these essential genome structures and cyclization sequences (CS), we decided to clone the MS2 binding sites within the variable region at the 3'-end of the genome (Figure 16).

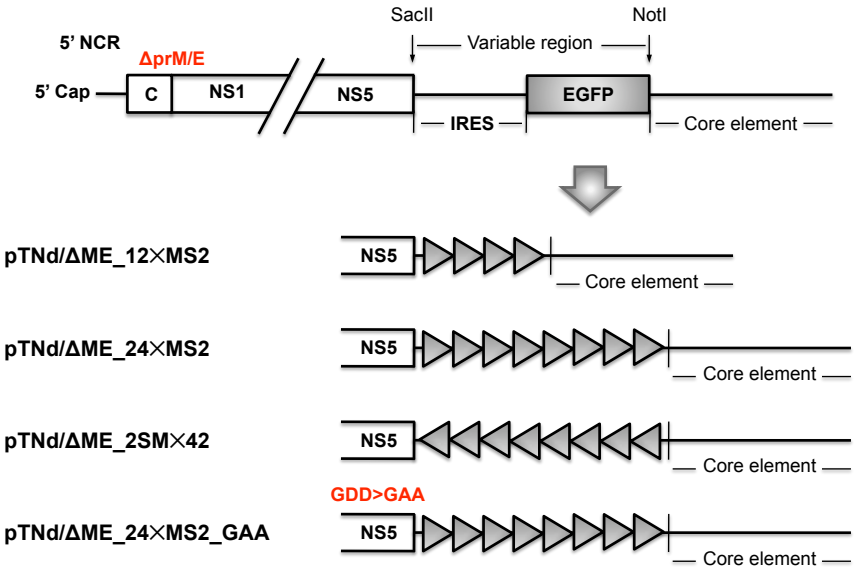

Figure 16 Structure of the MS2-tagged flaviviral replicons. The parental pTNd/ΔME-EGFP vector used for the generation of the MS2-tagged replicons is shown at the top of the figure. It contains the capped 5'NCR, the long ORF carrying a deletion of the prM and E proteins (ΔprM/E) and the IRES-EGFP cassette replacing the variable region at the 3'-end of the TBEV genome. The SacII and NotI restriction sites used for the insertion of the MS2 binding sites are also shown. Below, the constructs carrying the insertion of 12 (pTNd/ΔME_12×MS2) or 24 (pTNd/ΔME_24×MS2) binding sites for the phage MS2 core protein in the 3'-NCR are reported. In the pTNd/ΔME_2SM×42 construct the 24 MS2 binding sites were cloned in the opposite orientation. The pTNd/ΔME_24×MS2_GAA construct at the bottom contains the 24 MS2 binding sites and carries a GDD>GAA mutation in NS5 that disrupt RdRp activity. The diagram is not drawn to scale.

By replacing the IRES-EGFP cassette in the pTNd/ΔME-EGFP replicon we could generate sub-genomic replicons carrying arrays of 12 (pTNd/ΔME_12XMS2) or 24 (pTNd/ΔME_24XMS2) MS2 binding sites and two control replicons. One carries the array of 24 MS2 binding sites in the opposite orientation (pTNd/ΔME_2SMX42) while the other one contains the GDD to GAA mutation in the catalytic domain of the NS5 protein that does not allow viral replication. *In vitro* transcription from a T7 promoter upstream of the viral genome allowed the production of the full length sub-genomic RNAs that could be transfected into cells.

The second element required to establish the MS2-based system is the autofluorescent protein fused to the MS2 protein. In order to allow cytoplasmic detection of TBEV replicating RNAs by fluorescence microscopy we engineered a fusion protein between the MS2 core protein and the enhanced yellow fluorescent protein (EYFP). By removing the nuclear localization signal from a previously well-characterized EYFP-MS2nls fusion protein (Boireau et al., 2007) we could obtain a diffused nucleus-cytoplasmic localization of the signal at steady state, without further compartmentalization.

3.2. Characterization of the TBEV-based replicons

3.2.1. TBEV replicons carrying MS2 binding sites are competent for replication.

Upon infection, cytoplasmic flaviviral RNA is immediately translated by the host cell machinery into a single polyprotein, that is then cleaved by a combination of host and viral proteases, to yield three structural and seven non-structural proteins. Following the formation of replication complexes tightly associated with cytoplasmic membranes, the RNA-dependent RNA polymerase NS5 copies complementary minus strand RNA from genomic input RNA. This negative sense genome-length RNA serves as a template for the synthesis of new positive-strand viral genomes that are subsequently used for translation of further viral proteins and for additional replication cycles (Lindenbach et al., 2007). In order to test whether the engineered replicons were competent for replication we monitored positive-strand RNA levels over time by Northern hybridization (Figure 17).

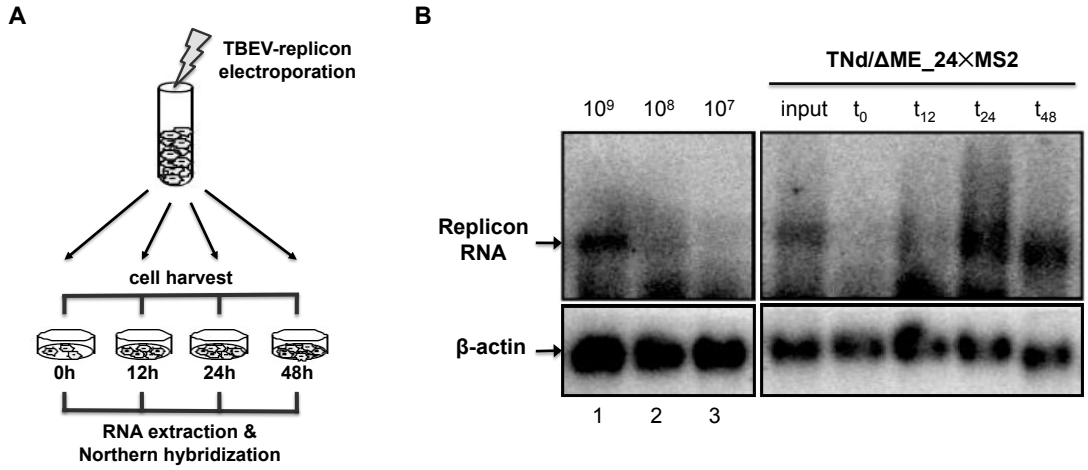

Figure 17 Time course of TBEV RNA replication. (A) Schematic drawing of the experimental approach. After electroporation of BHK-21 cells with 10µg of the TNd/ΔME_24XMS2 replicon RNA, equal amounts of cells were seeded into dishes. Transfected cells were harvested either immediately after transfection (0h) or at 12, 24 and 48 hours after transfection to perform total RNA extraction and Northern hybridization. **(B)** *In vitro* transcribed TNd/ΔME_24×MS2 RNA was transfected into BHK-21 cells. At the time points indicated above the panel total RNA was extracted from transfected cells and processed for northern hybridization using a TBEV-specific probe. Equal sample loading was monitored by detection of β-actin RNA (bottom). As controls, serial dilutions of known amounts of *in vitro* transcribed RNA spiked into total RNA of naïve cells were loaded in parallel (lanes 1 to 3). Input: BHK-21 cells incubated with RNA but not yet electroporated.

BHK-21 cells were electroporated with *in vitro* transcribed TNd/ΔME_24XMS2 replicon RNA and seeded in aliquots. At the indicated time points thereafter, total RNA was extracted and analyzed. Figure 17 shows a typical Northern blot analysis where known concentrations of the TNd/ΔME_24XMS2 *in vitro* transcript are loaded as a reference. The appearance of a signal of the size of the replicated RNA demonstrates that TBEV replication had already started 12 hours upon transfection and peaked at 24 hours yielding approximately 5 X 10^8 copies of replicon RNA / μg of total RNA.

3.2.2. MS2-EYFP co-expression does not inhibit viral replication

Next, we analyzed the effect of the MS2 protein expression on TBEV replication by RT-PCR. As in the previous experiment, capped sub-genomic RNAs were produced *in vitro* and used for the electroporation of BHK-21 cells. In addition, some of the cells were also simultaneously transfected with the plasmid pEYFP-MS2, which contains the gene for the bacteriophage MS2 core protein fused to EYFP, driven by the CMV promoter. Viral RNA replication was then monitored with a primer set within the 5'-NCR. As shown in Figure 18, co-expression of the MS2-EYFP protein did not significantly inhibit TNd/ΔME_24XMS2 replication (compare left and right middle panels) although flow cytometry analysis performed 24 hours upon transfection demonstrated that al least 60% of the cells expressed this protein. Immediately after electroporation (t_0) we could detect intracellular input RNA, then, after 8 hours the signal decreased, most likely because of RNA degradation, to increase again after 20 hours as newly synthesized viral RNA. The same did not happen with a cellular β-actin control RNA (Figure 18, bottom panels). However, the possibility exists that the replication process selects for variants that delete out the MS2 repeats. To rule out this possibility, the same cDNA was amplified with primers that map uniquely in the 5' end of the repeats, and every two repeats, thus allowing the counting of the number of repeats present. Clearly, both in the absence and in the presence of MS2-EYFP the repeats were maintained at the various time points after transfection (Figure 18A, top panels).

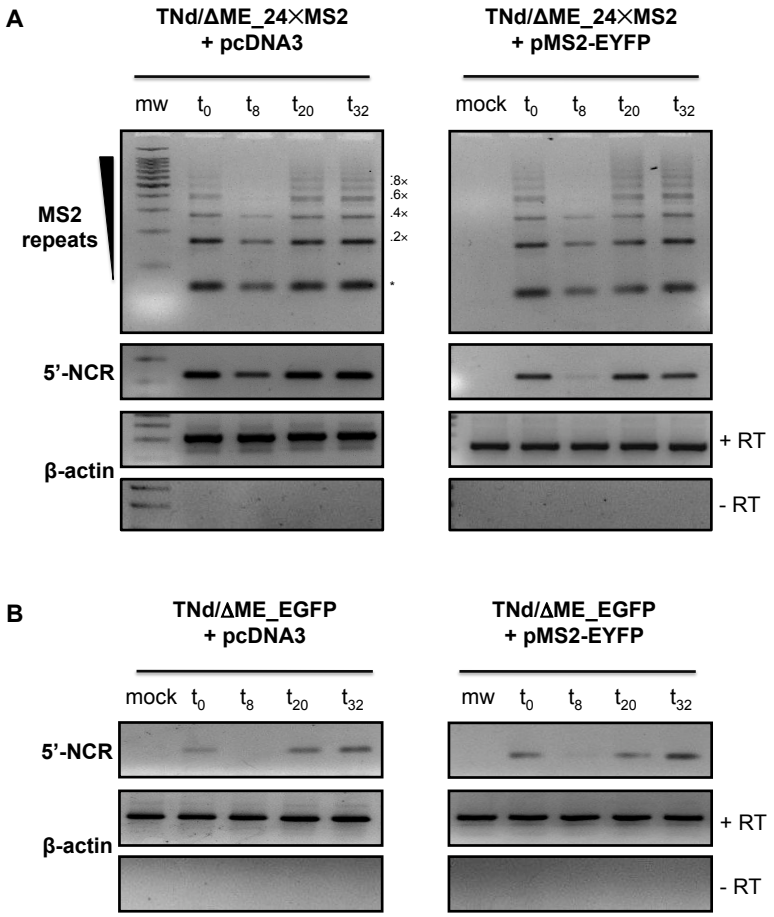

Figure 18 MS2-EYFP expression does not inhibit TBEV replication (I). (A) BHK-21 cells were electroporated with the TNd/ΔME_24×MS2 replicon RNA together with pcDNA3 (left panels) or together with a plasmid for MS2-EYFP expression (right panels). RNA was extracted at the indicated time points and RT-PCR was performed with primers specific for the MS2 repeats (top panels), the 5'-NCR (middle panels) and the cellular RNA for β-actin (lower panels). Controls for DNA contamination (no RT) for the β-actin samples are also included. The asterisk indicates the first amplification product of 60 bp corresponding to a fragment that does not contain any repeat. Mock corresponds to cells incubated with the replicon RNA but not electroporated and washed extensively. **(B)** BHK-21 cells were electroporated with the parental TNd/ΔME_EGFP replicon RNA as already described for panel A. At the indicated time points, total RNA was extracted and RT-PCR performed with primers specific for the 5'-NCR (top panels) and the cellular RNA for β-actin (lower panels).

The replication profile of the parental TNd/ΔME_EGFP replicon was also monitored by RT-PCR (Figure 18B) and appeared comparable to that of its derivative tagged TNd/ΔME_24XMS2 replicon. Finally, to conclude this analysis, we tested also the two control replicons previously generated. The TNd/ΔME_2SMX42 construct, carrying the MS2 repeats in the opposite orientation, which showed normal kinetics

of RNA replication (Figure 19A) both in the presence and in absence of MS2-EYFP, and the TNd/ΔME_24XMS2_GAA replication deficient control. As shown in Figure 19B, the TNd/ΔME_24XMS2_GAA replicon did not replicate the input RNA as its wild-type counterpart (compare t_{20} and t_{32} time points), despite similar levels of input RNA (compare t_0 time points), clearly demonstrating that the RNA was indeed generated by the viral RdRp.

Altogether these data prove that TBEV replicons retain heterologous repetitive sequences that allow tight binding of the MS2 core protein within the variable 3'-NCR and are able to replicate full-length RNA. Furthermore, the replication of none of the tested constructs was inhibited by transient MS2-EYFP co-expression.

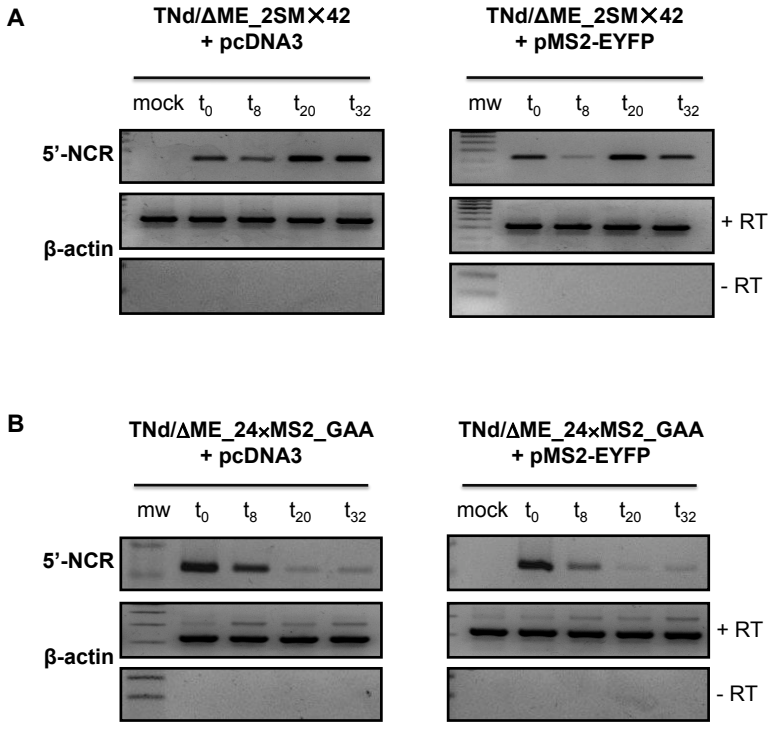

Figure 19 MS2-EYFP expression does not inhibit TBEV replication (II). (A) BHK-21 cells were electroporated with the replicon TNd/ΔME_2SM×42 RNA together with pcDNA3 (left panels) or together with a plasmid for MS2-EYFP expression (right panels). Also in this case RNA was extracted at the indicated time points and RT-PCR was performed with primers specific for the 5'-NCR (top panels) and the cellular RNA for β-actin (lower panels). **(B)** BHK-21 cells were electroporated with the mutant replicon TNd/ΔME_24×MS2_GAA RNA as described for the previous panel. RNA was extracted at the same time points and RT-PCR was performed with primers specific for the 5'-NCR (top panels) and the cellular RNA for β-actin (lower panels).

3.2.3. The TBEV replicons efficiently replicate in a cell clone constitutively expressing the MS2-EYFP protein

In order to analyze whether the engineered replicons were able to efficiently replicate also in cells constitutively expressing MS2-EYFP, we established a stable BHK-21 cell line for MS2-EYFP expression. Upon transfection of BHK-21 cells with the selectable MS2-EYFP plasmid, we were able to isolate and grow G418-resistant colonies. The different clones were then further characterized in order to select the more homogeneously MS2-EYFP expressing populations. Also in this case we monitored TNd/ΔME_24XMS2 replication by Northern hybridization (Figure 20B) and RT-PCR (Figure 20C). For this experiment we chose the BHK-A3 cell clone that showed a high percentage of EYFP positive cells both by flow cytometry (Figure 20A) and by fluorescence microscopy analysis.

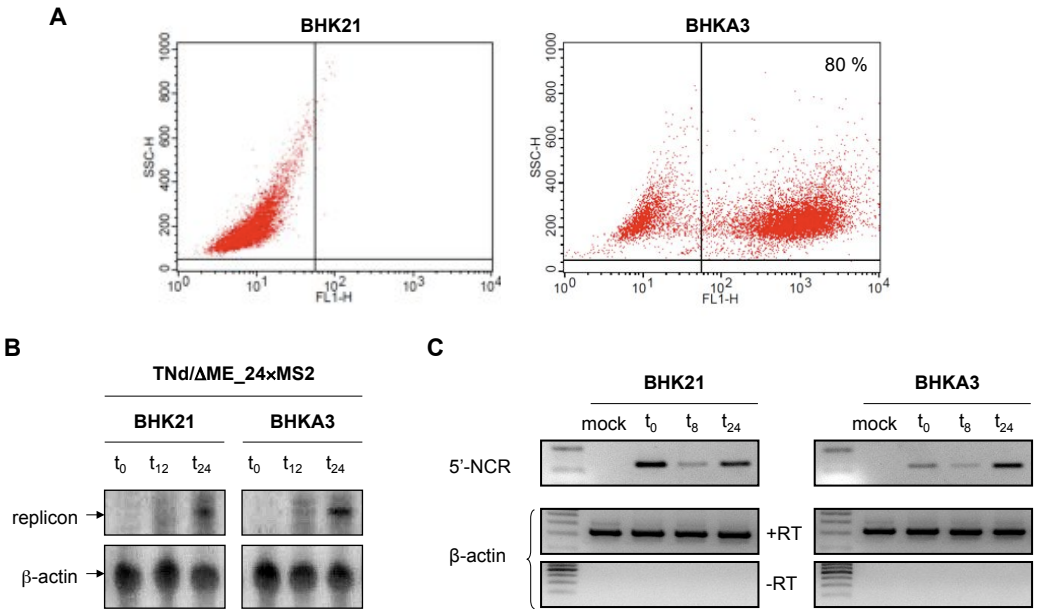

Figure 20 Characterization of the BHKA3 cell clone expressing MS2-EYFP. (A) Cytofluorimetric analysis was conducted both in wild type BHK21 cells (left) and in the BHKA3 cell clone (right). As shown in the graph, 80% of BHKA3 cells were expressing MS2-EYFP. **(B)** In vitro transcribed RNA of TNd/ΔME_24×MS2 was transfected into BHK21 or BHKA3 cells that were harvested at the time points indicated above the panel. Total RNA was prepared and analyzed with a TBEV-specific probe. Equal sample loading was monitored by detection of β-actin RNA (bottom). **(C)** BHK21 or BHKA3 cells were electroporated with the replicon TNd/ΔME_24×MS2 RNA. RNA was extracted at the indicated time points and RT PCR was performed with primers specific for the 5'-NCR (upper panels) and the cellular RNA for β-actin (middle panels). Controls for DNA contamination (no RT) for the β-actin samples are also included (lower panels).

Again, we could not observe significant differences in TNd/ΔME_24XMS2 replication related to MS2-EYFP over-expression (compare BHK21 and BHKA3 panels in Figure 20B and Figure 20C). Therefore, we could conclude that MS2-EYFP co-expression does not inhibit replication of the tagged sub-genomic replicon.

3.2.4. Development of a sensitive TBEV-based luciferase reporter system

To allow a more quantitative analysis of translation and replication efficiencies of the engineered TBEV replicons, we established a sensitive luciferase-based reporter system in collaboration with Prof. Christian Mandl's Laboratory in Vienna (Hoenninger et al., 2008). We generated plasmid constructs in which most of the region of the TBEV genome encoding the structural proteins C, prM and E was replaced in-frame by a luciferase reporter gene. In these constructs, the natural translation initiation site of the viral polyprotein was retained together with the first 17 amino acids of the capsid protein fused to the reporter (Figure 21A). The rest of the C gene, the entire prM gene, and the entire E gene except for the second transmenbrane region (TM2) were deleted. The TM2 portion of E was retained because it also serves as an internal signal sequence for establishing the proper topology of the polyprotein in the ER membrane and targeting the non-structural protein NS1 to the secretory pathway (Lindenbach et al., 2007). The sequence was preceded by a 2A sequence from the Thosea asigna virus to allow the luciferase to be liberated post-translationally from the polyprotein precursor. Finally, the variable region of the TBEV reporter construct was replaced, like in the tagged replicons TNd/ΔME_12XMS2 and TNd/ΔME_24XMS2 previously described, by 12 or 24 copies of the stem loop structure required for MS2-tagging. When we transfected BHK-21 cells with these reporter replicons we could confirm that neither the 12- nor the 24- repeats insertion had significant effect on translation of the input RNA. Normalized luciferase levels at 3 hours after transfection were indeed similar for these constructs and the control replicon C17fluc-TaV2A that does not contains heterologous sequences at the 3' variable region (Figure 21B). At later time points, however, luciferase levels remained about ten-fold lower in cells transfected with RNAs carrying the repeats than in cells transfected with the parental construct (Figure 21B), suggesting a modest effect of these elements on viral RNA replication.

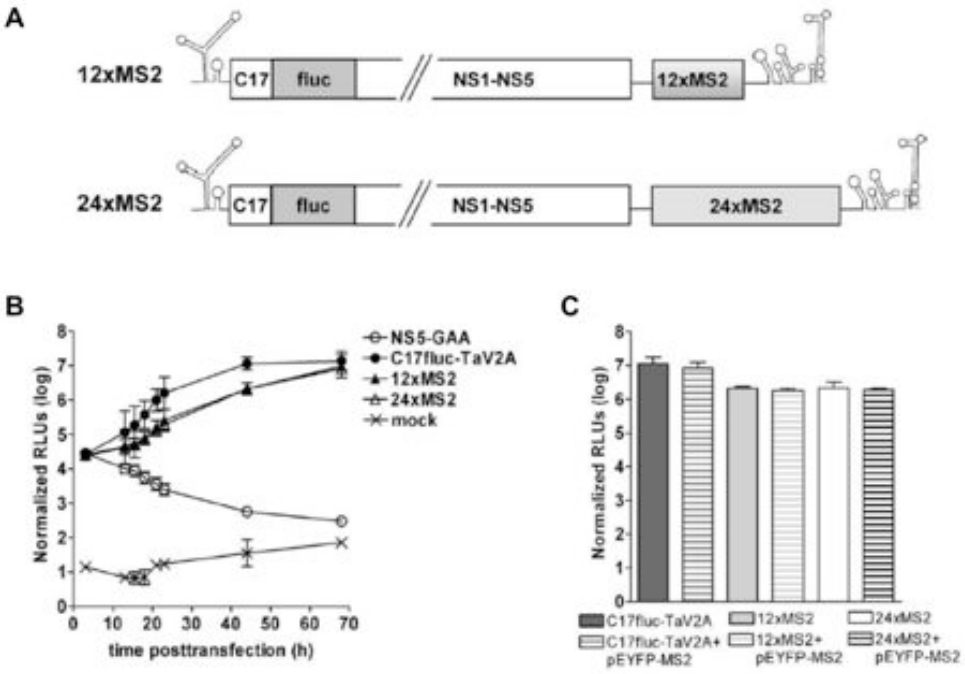

Figure 21 Effect of the insertion of MS2 binding sites on TBEV translation and replication. (A) Schematic diagram of the TBEV replicons generated. In these constructs the region of the genome encoding the structural proteins, except for the first 17 codons (C17) of the capsid, has been replaced by the firefly luciferase reporter gene (fluc). 12 (12xMS2) or 24 (24xMS2) MS2 binding sites were cloned in the same genomic position than in the previously described pTNd/ΔME_12×MS2 and pTNd/ΔME_24×MS2 replicons. **(B)** Kinetics of reporter expression in BHK-21 cells transfected with 12xMS2 and 24xMS2 replicon RNAs, shown on a logarithmic scale. As a control cells were also transfected with the C17fluc-TaV2A replicon which does not contains MS2 binding sites and with the replication deficient NS5-GAA mutant. Mock, mock-transfected cells; RLUs relative light units. **(C)** BHK-21 cells were either transfected with 12xMS2, 24xMS2 or C17fluc-TaV2A reporters alone or co-transfected with both the replicon RNA and the pMS2-EYFP plasmid, as indicated below the figure. The data, shown on a logarithmic scale, are normalized luciferase values measured 44 hours upon transfection. A similar lack of interference of MS2-EYFP co-expression was also observed at 13, 15, 18, 21, 23 and 68 hours post-transfection (data not shown). Error bars represent the standard deviation from a minimum of three independent experiments. From (Hoenninger et al., 2008).

However, this effect does not appear to be proportional to the number of the inserted sequences since 12XMS2 and 24XMS2 yielded essentially identical curves. Furthermore, cells in which 12XMS2, 24XMS2 or the parental control were co-transfected with the MS2-EYFP plasmid, did not manifest any additional effect on luciferase activity at any of the time points analyzed (Figure 21C). Therefore, it is possible to definitely exclude that MS2-EYFP could interfere not only with viral replication but also with replicon translation.

All together these results supported the use of the MS2-tagged TBEV replicons as a tool to track viral RNA in living cells.

3.3. Visualization of TBEV replicated RNA in living cells

3.3.1. MS2-EYFP localization upon TBEV replicon transfection

The results described so far clearly demonstrated that the engineered constructs are able to efficiently replicate in BHK-21 cells co-expressing the MS2-EYFP phage protein required for RNA tagging *in vivo*. Therefore, we hypothesized that the production of novel MS2 binding sites would allow detection of the viral RNA by fluorescence microscopy. Indeed, when we co-transfect cells with both the TNd/ΔME_24XMS2 *in vitro* transcribed replicon RNA and its EYFP-tagged cognate protein, a dramatic change in the MS2 localization occurred (Figure 22A). Compatible with the formation of newly replicated viral RNAs, evident clustering of the EYFP signal was observed in the cytoplasm. The same pattern was observed also with the TNd/ΔME_12XMS2 replicon (Figure 22B). The nucleus of the cell appeared "empty" in agreement with the accumulation of novel high-affinity binding sites in the cytoplasm that would shift the equilibrium between the two compartments at steady state. A time course is shown in Figure 22B. The analysis started 8 hours after transfection, in the "eclipse" phase when the input transfected RNA has been degraded and the synthesis of novel RNA has just been initiated, thus allowing the visualization of truly replicated viral RNA with little input RNA as well as allowing cells to recover after electroporation. After 12 hours no obvious changes were noticed. However after 24 hours, cells carrying the replicon with the MS2 binding sites showed a marked increase in signal in the cytoplasm with loss of signal in the nucleus (Figure 22B, top panels). When the experiment was repeated with the TNd/ΔME_24XMS2_GAA mutant that is unable to replicate, no clustering of the signal in the cytoplasm was observed at 24 hours, consistently with the lack of binding sites for the MS2 protein that could not be produced by the defective replicon (Figure 22B, bottom panels).

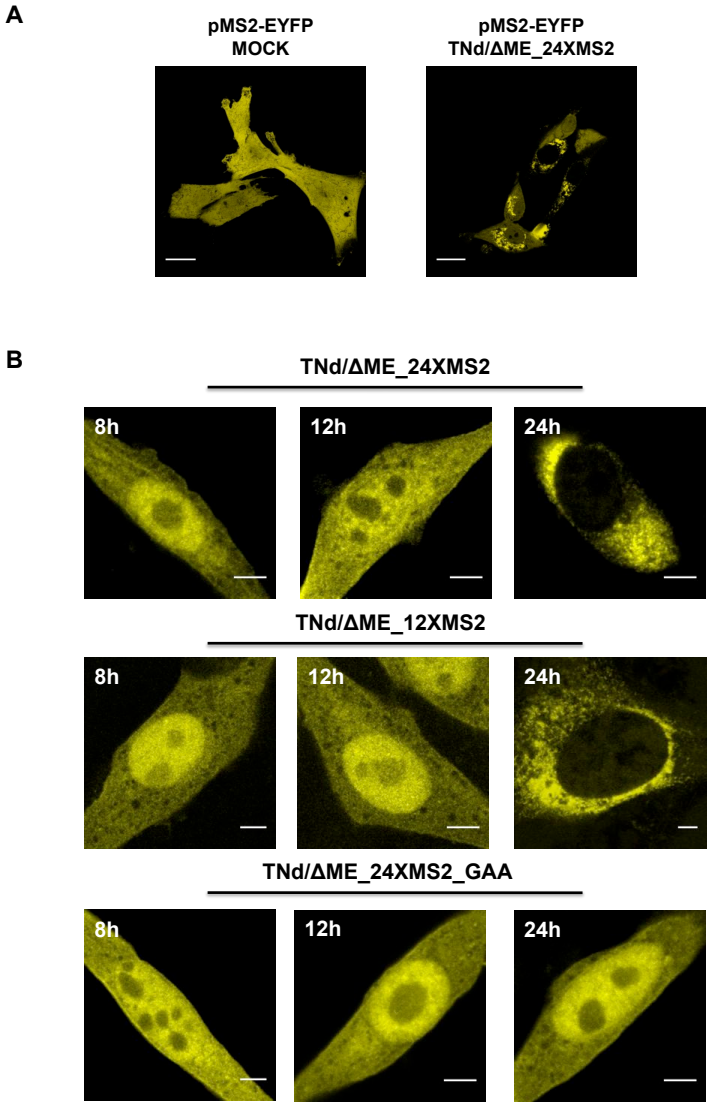

Figure 22 TBEV replicon transfection induces MS2-EYFP clustering in the cytoplasm. (A) BHK-21 cells were electroporated with the pMS2-EYFP plasmid alone (left) or together with the replicon TNd/ΔME_24×MS2 RNA (right). Cells were fixed after 48 hours and analyzed by confocal microscopy. Bars, 20μm. **(B)** BHK-21 cells were co-transfected with the pMS2-EYFP plasmid together with the TNd/ΔME_24×MS2 replicon RNA (top), the TNd/ΔME_12×MS2 (middle) or with the TNd/ΔME_24×MS2_GAA control replicon (bottom). At the indicated times after electroporation cells were fixed and analyzed by confocal microscopy. Bars, 5μm.

To get a better appreciation of the early time points we also performed a time-lapse analysis of the BHK-A3 cell clone, constitutively expressing MS2-EYFP, upon TNd/ΔME_24XMS2 replicon transfection. A blow-up of the movie is shown in Figure 23 were a single cell starts showing clusters of signal in the perinuclear region 14h after transfection.

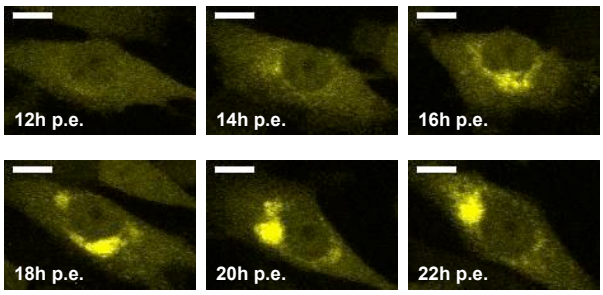

Figure 23 Time-lapse analysis of the BHKA3 clone upon TBEV replicon transfection. The cell clone BHKA3 constitutively expressing MS2-EYFP was electroporated with the TNd/ΔME_24×MS2 replicon RNA and a time lapse analysis was conducted on living cells for 24 hours. Bars, 10μm.

3.3.2. MS2 specifically binds TBEV RNA

To demonstrate that MS2-EYFP clustering in the cytoplasm was indeed due to viral RNA, an RNA *in situ* hybridization was performed with a probe specific for the MS2 repeats present in the TBEV sub-genomic replicon. Again, BHK-21 cells were co-transfected with the *in vitro* transcribed TNd/ΔME_24XMS2 RNA and with the MS2-EYFP plasmid. After 24h, cells were fixed with 4% PFA and processed for *in situ* hybridization. As shown in Figure 24A (top panels), the staining of the newly replicated replicon RNA perfectly co-localized with the MS2-EYFP cytoplasmic cluster confirming that both RNA and MS2 are present in the same compartments. However, as expected, at the same time upon transfection, neither MS2-EYFP clustering, nor viral RNA accumulation was observed in cells transfected with the replication deficient TNd/ΔME_24XMS2_GAA control replicon (Figure 24A, bottom panels). This observation is consistent with the substantial input RNA degradation already observed by RT-PCR (Figure 19B).

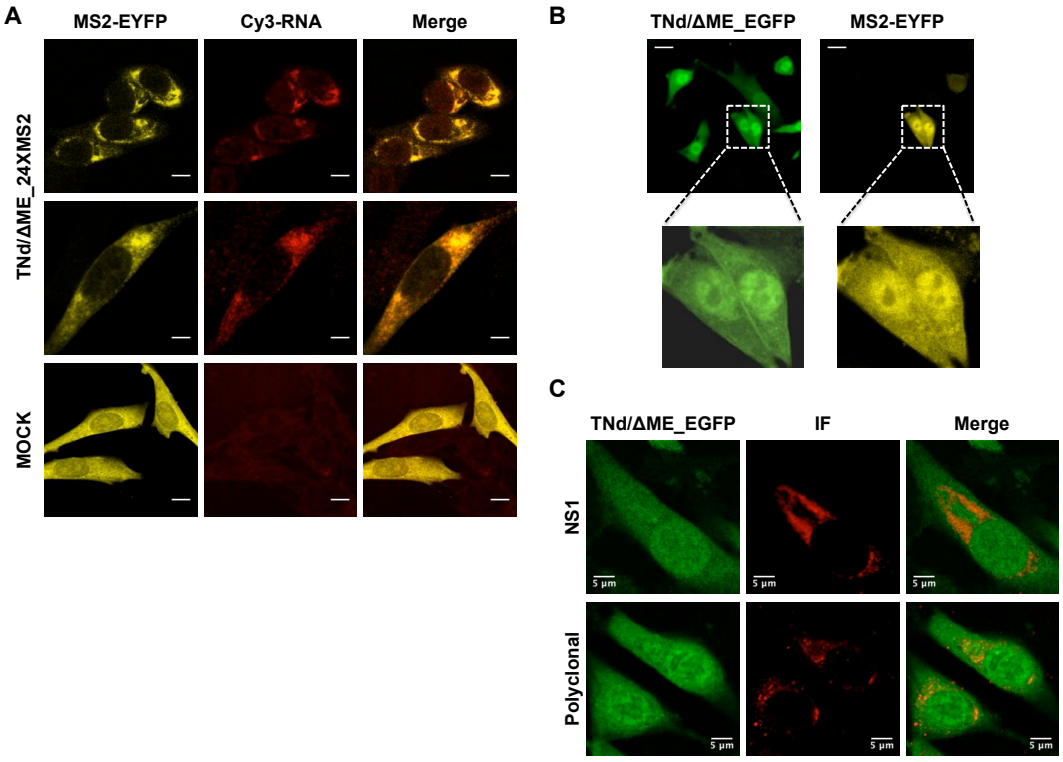

Figure 24 MS2 is specifically bound to viral RNA. (A) BHK-21 cells were electroporated with the TNd/ΔME_24×MS2 replicon RNA together with the pMS2-EYFP plasmid. After 24 hours, cells were fixed and processed for MS2 repeats specific RNA FISH as described. A control for mock-transfected cells is also shown (bottom panels). Bars, 20µm. **(B)** BHK-21 cells were electroporated with the TNd/ΔME_EGFP parental replicon and with the MS2-EYFP expressing plasmid. Overlap of EGFP and EYFP emission signals were resolved by a spectral unmixing. Bars, 20µm. **(C)** BHK-21 cells were transfected with the TNd/ΔME_EGFP RNA. After 24 hours, cells were fixed and incubated with a monoclonal antibody against the NS1 viral protein (upper panels) or an antiserum that can be used for both structural and non-structural protein detection (lower panels).

Although both RNA and MS2 are present in the same compartment, yet we did not directly demonstrated that the MS2-EYFP protein is clustered there because specifically bound to viral RNA. Therefore, to address this point and to rule out the possibility that MS2-EYFP could be trapped into replication compartments independently of its binding to the viral RNA, we analyzed MS2-EYFP localization in cells transfected with the TNd/ΔME_EGFP parental replicon that does not carry any MS2 binding sites (Gehrke et al., 2005). Cells that are replicating the virus in this case would produce EGFP as well as induce membrane compartmentalisation characteristic of Flaviridae replication. Therefore, if the clustering of MS2-EYFP would depend on these membrane rearrangements, then it would be observed also in these cells. BHK-21 cells co-transfected with the MS2-EYFP plasmid and the

parental replicon RNA were analyzed 48hpe (Figure 24B). As shown in Figure 18B and Figure 24C, replication levels of the TNd/ΔME_EGFP construct were comparable to those of the TNd/ΔME_24XMS2 and viral proteins were produced in the cytoplasm as expected. However, no MS2-EYFP clustering in the perinuclear region was observed (Figure 24B). The protein indeed was evenly diffused all over the cell clearly demonstrating that TBEV replicons carrying the binding sites for the MS2 core protein specifically associate MS2-EYFP on newly replicated RNA in the cytoplasm of the cell.

3.4. Characterization of the clustered TBEV RNA compartments

3.4.1. Replicated RNA clusters mark TBEV replication compartments

It has been known for many years that positive-strand RNA viruses replicate their genomes in association with cytoplasmic virus-induced membranes that enhance replication efficiency and most likely protection from host defences. Ultrastructural analysis of flavivirus-infected cells showed that these induced membranes include convoluted membranes (CM), paracrystalline structures (PC), proliferating endoplasmic reticulum (ER), and clusters of vesicles of about 100 nm in diameter also called vesicle packets (VP) (Mackenzie et al., 1999; Mackenzie et al., 1996; Mackenzie et al., 1998; Westaway et al., 1997). However, the cellular origins of these membrane structures, their detailed organization and functions are still poorly understood. In order to assess whether the viral RNA-enriched compartments we observed are also sites of TBEV replication and to characterize the composition of the TBEV-induced membranes associated with the newly replicated RNA we performed an extensive immunofluorescence analysis.

In view of previous reports showing that NS1 is associated with RNA replication (Mackenzie et al., 1996; Westaway et al., 1997) within virus-induced VPs, we used a monoclonal antibody against NS1 (Iacono-Connors et al., 1996) (Figure 25A) and a polyclonal raised against the TBEV proteins (Orlinger et al., 2006) (Figure 25B) to mark the sub-cellular sites of viral replication. As shown in Figure 25, MS2-EYFP clustering is perfectly co-localized with the viral proteins. Hence, viral RNA tagged with the MS2-EYFP protein appeared to be localized within compartments enriched in proteins of the viral replication complex. As expected the replicon with the GAA mutation in RdRp did not show any signal for replicated RNA neither for TBEV proteins. Transfection of the TBEV replicon carrying the 24X repeats in the opposite orientation (pTNd/ΔME_2SMX42) was also performed (Figure 25B, bottom panels). In this case the model would predict that binding sites of the MS2-EYFP protein would form only in the negative strand RNA that is produced in small amounts from the input RNA and serves as template for the synthesis of novel positive-strand RNA. Hence, since the negative-strand RNA template is believed to be 1/100th of the replicated positive-strand RNA (Lindenbach et al., 2007), the MS2-EYFP signal

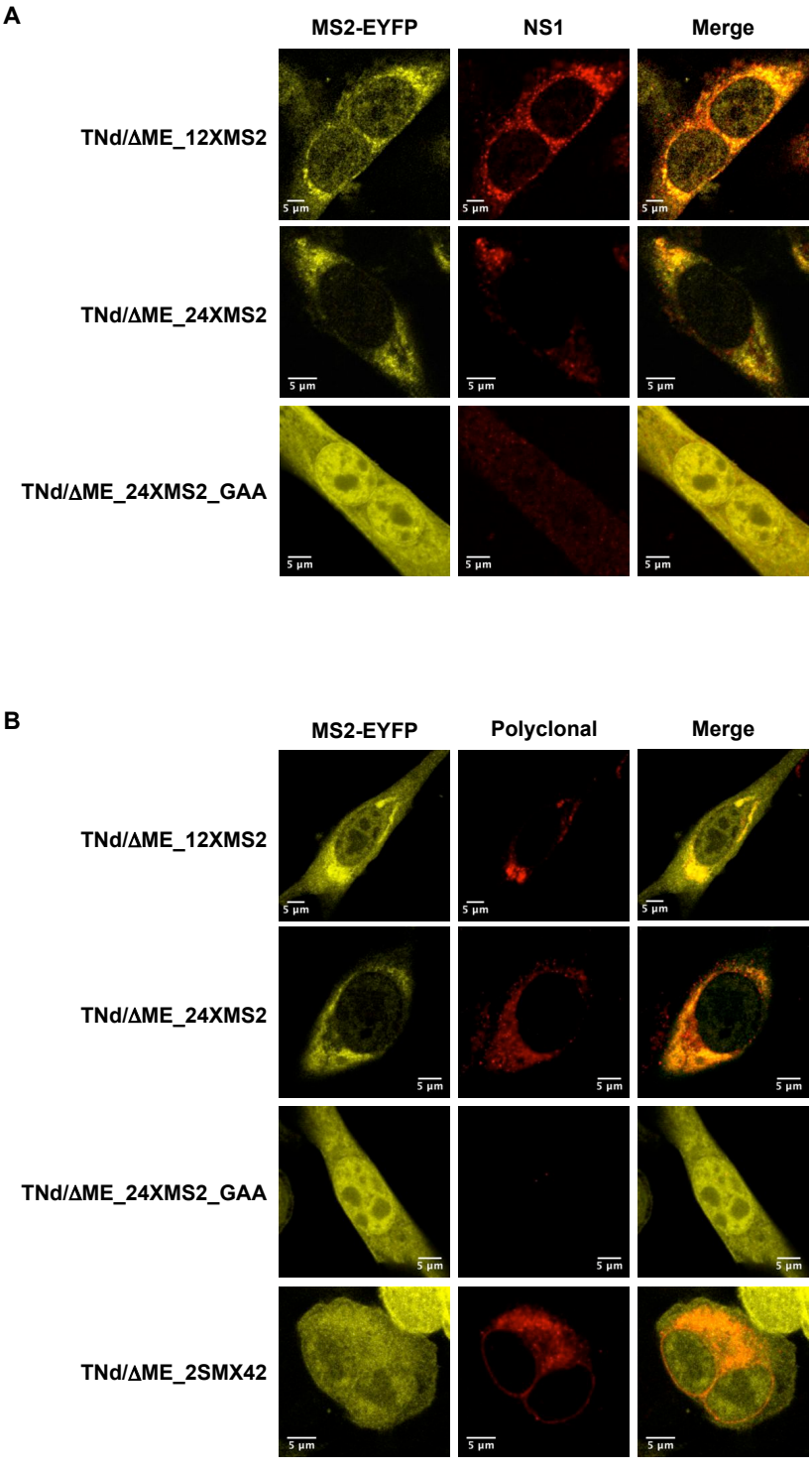

Figure 25 Co-localization of TBEV RNA with viral markers. BHK-21 cells were electroporated with replicon RNA together with a plasmid expressing for MS2-EYFP as indicated. After 24 hours, cells were fixed and incubated with a monoclonal antibody against the NS1 viral protein **(A)** or an antiserum that can be used for both structural and non-structural protein detection **(B).** As control cells were electroporated with TNd/ΔME_24×MS2_GAA that is unable to replicate input RNA and with the TNd/ΔME_2SM×42 replicon carrying the repeats in the opposite orientation.

would be either too small to be visible above background or would mark the sites of negative-strand RNA production. The former hypothesis appears to be correct since cells transfected with TNd/ΔME_2SMX42 showed a diffused EYFP signal although viral proteins were produced as expected. An alternative explanation would be that the minus strand is not accessible to MS2, either being protected by a secluded replication complex or being in a double-stranded conformation.

Flaviviruses, like most of the positive-strand RNA viruses, are also known to produce substantial amounts of dsRNA during the course of replication (Targett-Adams et al., 2008; Westaway et al., 1999; Westaway et al., 1997). For this reason, dsRNA staining in virus-infected cells has been effectively used as a tool to characterize viral RCs and to investigate their properties and interactions with cell-derived factors or organelles. As shown in Figure 26 we could demonstrate that also TBEV generates dsRNA in the cytoplasm of transfected cells.

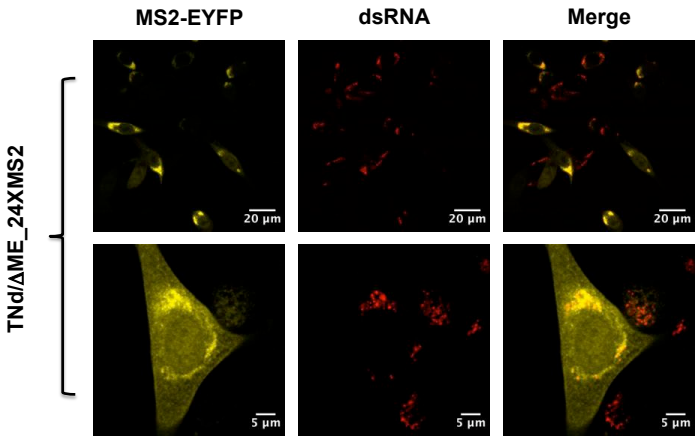

Figure 26 Co-localization of the MS2-tagged TBEV RNA with dsRNA. BHK-21 cells were electroporated with the TNd/ΔME_24×MS2 replicon RNA together with a plasmid expressing for MS2-EYFP as indicated. After 24 hours, cells were fixed and incubated with a monoclonal antibody against dsRNA. A low magnification field (upper panel) and a single cell (lower panel) are shown.

Moreover, we could observe that the signal for MS2-EYFP was including that of dsRNA and extended beyond. These observations are in agreement with the fact that MS2-EYFP stains positive-strand replicon RNAs emanating from replication complex and clearly demonstrate that this MS2 enriched perinuclear region can be exploited as marker of TBEV replication compartments intracellular localization.

3.4.2. TBEV dsRNA is protected by intracellular membranes

To further characterize the RCs we applied a differential permeabilization protocol coupled to immunofluorescence analysis to simultaneously detect MS2-tagged viral RNA and dsRNA. BHK-21 cells transfected with TNd/ΔME_24×MS2_GAA and EYFP-MS2 were grown on coverslips, treated or not with Digitonin to selectively permeabilize the plasma membrane, washed to remove soluble MS2-EYFP, and then fixed with paraformaldehyde. This treatment resulted in the removal of soluble MS2-EYFP from the cytoplasm but not from the nucleus that is protected by the nuclear membrane (compare Figure 27A to Figure 27B). Cells transfected with TNd/ΔME_24×MS2 and MS2-EYFP were processed with the same protocol. After fixation, cells were treated with Triton X-100 to gain access to dsRNA with a specific antibody. As shown in Figure 27C, co-localization of viral RNA and dsRNA was detected in cytoplasmic perinuclear compartments. A control experiment, where cells were not permeabilized with Triton X-100 after fixation, detects only MS2-EYFP but not dsRNA (Figure 27D). Therefore, dsRNA is retained into a compartment that is not accessible to antibodies unless intracellular membranes are permeabilized by Triton-X100. Next, cells permeabilized with Digitonin were treated with RNAse before fixation to remove accessible viral RNAs and washed to remove EYFP-MS2 bound to it. After fixation, cells were permealized with Triton X-100 and stained with anti dsRNA antibodies. As shown in Figure 27E, residual MS2-EYFP staining is detected in a punctuate perinuclear patterns co-localizing with dsRNA. Finally, we took advantage of the EYFP-MS2nls reporter that accumulates efficiently in the nucleus (Figure 28). We noticed that MS2-carrying replicons that are actively replicating in the cytoplasm are able to associate with tagged MS2nls that becomes trapped before reaching the nucleus. This is particularly useful when doing IF studies because viral RNA remains tagged against a dark background.

As shown in Figure 28A, co-localization between EYFP-MS2nls and dsRNA was observed in the perinuclear compartment only in cells transfected with the TNd/ΔME_24×MS2 replicon. Control cells transfected with the GAA mutant replicon show only nuclear localization of EYFP-MS2nls (Figure 28B). We conclude, at the resolution limit of the optical technique exploited, that MS2-EYFP tagged viral RNA is found also within perinuclear compartments that resist RNAse treatment and are enriched in dsRNA.

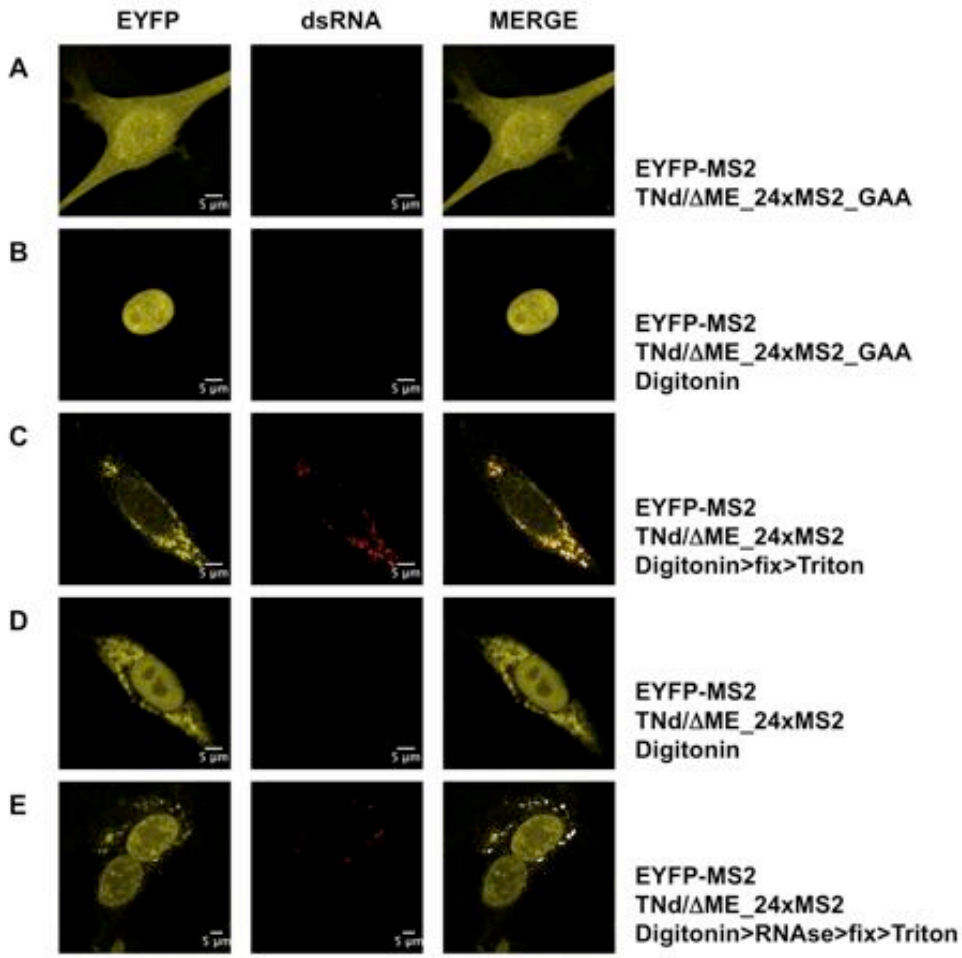

Figure 27 Co-localization of MS2-tagged viral RNA and dsRNA within intracellular membrane compartments. (A) BHK-21 cells were electroporated with the TNd/ΔME_24xMS2_GAA replicon RNA together with a vector expressing MS2-EYFP. 24 hours after transfection cells were fixed, permealized with Triton X-100 and incubated with an antibody against dsRNA that was then revealed by a secondary antibody conjugated with Alexa-594. The EYFP channel is shown in the left panel, dsRNA in the middle panel and the merge in the right panel. The merge panel shows in white the co-localization obtained with the quantitative co-localization tool of Zeiss LSM510 META (R is the Pearson's correlation coefficient). **(B)** BHK-21 cells, treated as in Figure 28 A, where incubated with Digitonin and washed extensively before fixation. **(C)** BHK-21 cells were electroporated with the TNd/ΔME_24xMS2 replicon RNA together with a vector expressing MS2-EYFP. Cells where incubated with Digitonin and processed as in Figure 28 B (R = 0.4). **(D)** BHK-21 cells were treated as in Figure 28 C, but the post-fixation permeabilization step before incubation with the antibody against dsRNA was omitted. **(E)** BHK-21 cells were electroporated with the TNd/ΔME_24xMS2 replicon RNA together with a vector expressing MS2-EYFP. After Digitonin treatment, cells were incubated with RNAse and processed as in Figure 28 C (R = 0.5).

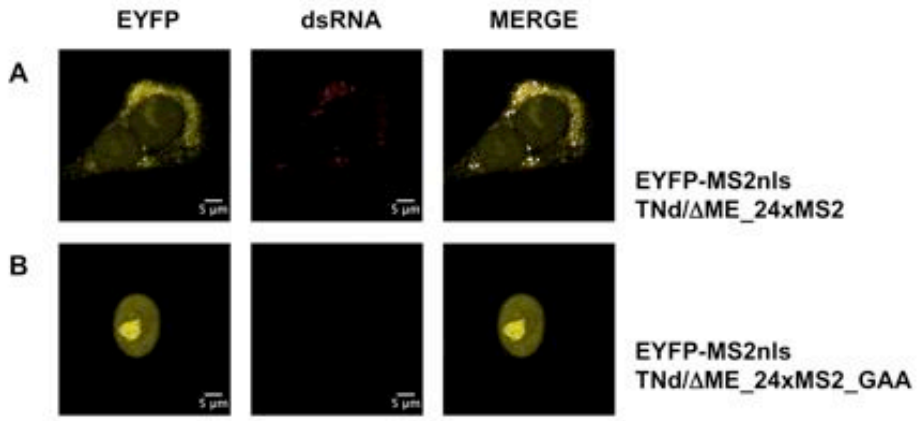

Figure 28 Co-localization EYFP-MS2nls with dsRNA in the cytoplasm of TBEV transfected cells. (A) BHK-21 cells were electroporated with the TNd/ΔME_24xMS2 replicon RNA together with a vector expressing EYFP-MS2nls. 24 hours after transfection cells were fixed, permealized with Triton X-100 and incubated with an antibody against dsRNA that was then revealed by a secondary antibody conjugated with Alexa-594. The EYFP channel is shown in the left panel, dsRNA in the middle panel and the merge in the right panel. The merge panel shows in white the co-localization obtained with the quantitative co-localization tool of Zeiss LSM510 META (R is the Pearson's correlation coefficient). (R = 0.2). **(B)** BHK-21 cells were electroporated with the TNd/ΔME_24xMS2_GAA replicon RNA together with a vector expressing MS2-EYFPnls. Cells were then treated as in Figure A.

3.4.3. TBEV replicates its genome within the ER compartment

Next, in order to define the cellular origins of the membranes associated with newly replicated TBEV-RNA we performed an IF analysis using antibodies to various cellular compartments (Figure 29). BHK-21 cells were transfected with pTNd/ΔME_MS2X24 and EYFP-MS2, fixed after 24 hours and incubated with the indicated antibodies. Sites of replicated viral RNA where clearly distinct from vesicles stained with the transferrin receptor (CD-71) and the early endosome antigen 1 (EEA-1) demonstrating that surface recycling vesicles are not sites of replicated TBEV RNA deposition. Instead, clear co-localization was obtained with the protein disulphide-isomerase (PDI), a marker for endoplasmic reticulum, consistent with earlier studies on the localization of the RNA of the similar Kunjin Flavivirus (Mackenzie et al., 1999) (Mackenzie and Westaway, 2001). However, no co-localization was observed neither with the ER-Golgi intermediate compartment (ERGIC-53) nor with Giantin, a marker for Golgi (Figure 29).

The work of Mackenzie et al. (Mackenzie et al., 1999) showed that Kunjin dsRNA localizes in the trans-Golgi network in African green-monkey Vero cells. Unfortunately, the antibody for the trans-Golgi network protein TGN-46 gave a nuclear stain in BHK-21 cell indicating a possible artefact of an antibody raised against a human antigen used to probe a cell line derived from rodents. Hence, we repeated the analysis in human osteosarcoma HOS cells. As shown in Figure 30, co-localization was evident for the RER as for the BHK-21 cells, but not for trans-Golgi.

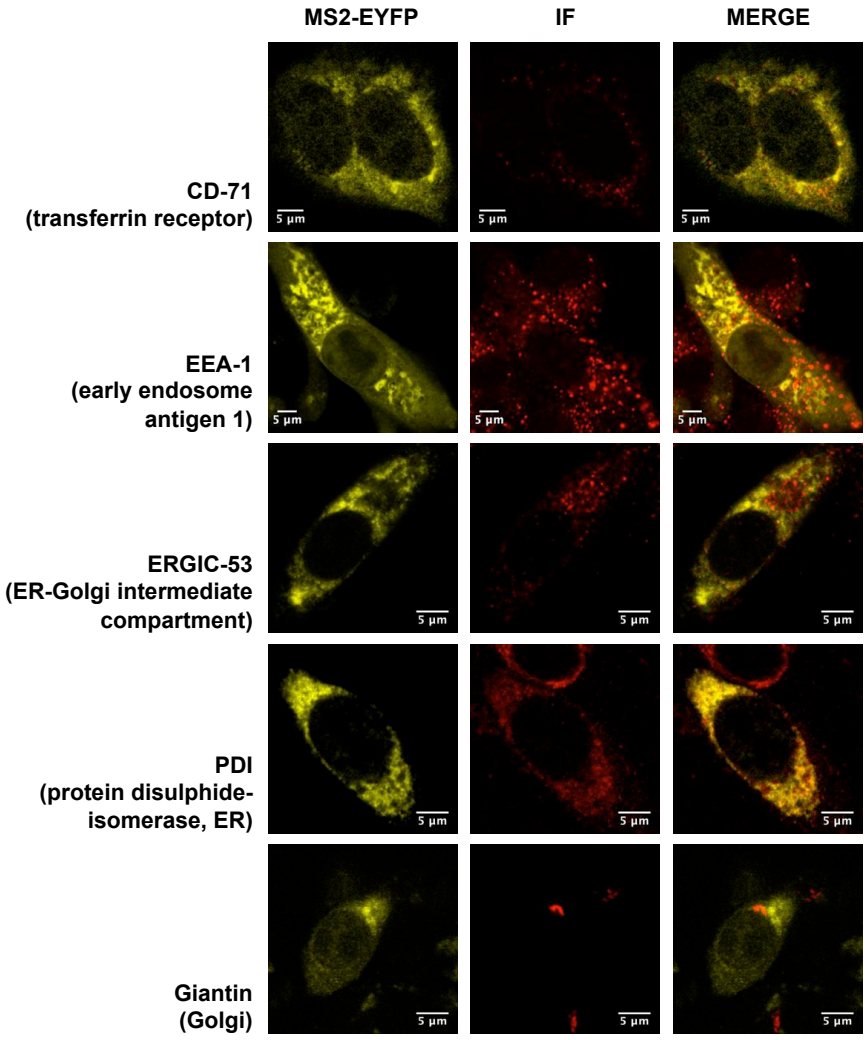

Figure 29 Association of TBEV RNA to selected sub-cellular cytoplasmic markers. BHK-21 hamster cells transfected with replicon TNd/ΔME_24×MS2 RNA and MS2-EYFP were fixed and incubated with antibodies to the transferrin receptor (CD-71), the early endosome antigen 1 (EEA-1), the endoplasmic-reticulum/Golgi intermediate compartment marker ERGIC-53, the protein disulphide-isomerase (PDI) marker of the endoplasmic reticulum and Giantin, a marker for Golgi membranes. Co-localization was observed only between MS2-EYFP clusters of TBEV RNA and the ER marker PDI.

Interestingly, partial co-localization was obtained with Giantin in HOS cells, indicating that some replicated TBEV RNA might be present also in this compartment, or that membranes induced by replicon transfection contain also markers for the Golgi.

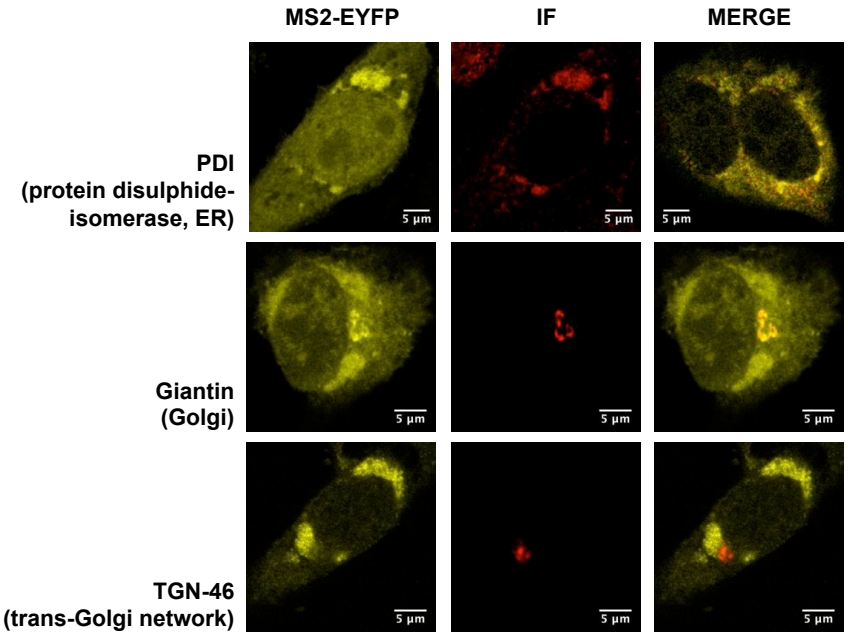

Figure 30 Association of TBEV RNA to selected sub-cellular cytoplasmic markers in a human cell line. HOS human cells transfected with replicon TNd/ΔME_24×MS2 RNA and MS2-EYFP were fixed and incubated with antibodies to the protein disulphide-isomerase (PDI), a marker of the endoplasmic reticulum, Giantin, a marker for Golgi membranes and TGN-46 that is a marker for the *trans*-Golgi network. In human cells co-localization was observed between MS2-EYFP clusters of TBEV RNA and PDI, but also partially with the Golgi marker Giantin.

3.5. TBEV induced innate immunity activation

By exploiting our engineered sub-genomic replicons we could clearly demonstrate that TBEV, like other positive-strand RNA viruses, manipulates host cell ER membranes to provide a scaffold for the replication complex. Importantly, we also showed that, during the course of replication, TBEV generates long dsRNA intermediates that are potentially strong innate immunity agonists. Recently, many speculations have been made about the possible role of such organized replication complexes in shielding viral stimulatory RNAs from host defences. However, accessibility of PRRs to replication intermediates located within RCs and their signalling through adaptor molecules are still unresolved issues that have never been addressed so far.

Therefore, during the final part of my PhD program we wished to exploit the tick-borne encephalitis flavivirus replicon system we have developed in order to provide deeper insight in Flavivirus induced innate immunity activation and to address the dynamics of virus-induced vesicle formation with respect to interferon induction.

3.5.1. U2OS cells: a good cellular model to study TBEV innate immunity

As mentioned in the introduction, a key mediator of host defence against pathogens is the interferon response. During viral infection this response is triggered by recognition of cytoplasmic viral stimulatory products by PRRs (Akira et al., 2006; Fredericksen et al., 2008; Kato et al., 2006; Saito et al., 2008; Yoneyama et al., 2004). This recognition leads to a cascade of signalling events, including the activation of the IRF-3 transcription factor, that are involved in induction of IFNβ expression. So far, we mostly relied on the BHK-21 cell line to perform our experiments. BHK-21 is a hamster cell line convenient to study virus infection because is defective for interferon production. However, in order to investigate TBEV-induced innate immune responses we wished to move on a human cell model able to support viral replication and, at the same time, to properly sense and counteract TBEV infection. We chose the human osteosarcoma (U2OS) cell line since it has been shown to support HCV replication (Jones et al., 2010; Targett-

Adams and McLauchlan, 2005) and has been used to characterize the host response to WNV infection (Fredericksen et al., 2004).

Upon U2OS transfection with the TNd/ΔME_24XMS2 replicon, newly synthesized MS2-EYFP tagged viral RNA formed a defined peri-nuclear compartment in the cytoplasm (Figure 31, right panels), suggesting that U2OS cells represent another cell line in which TBEV replication could be examined. As expected, this compartment was also enriched in viral proteins (TBEV) and dsRNA intermediates indicative of active replication (dsRNA). Moreover, as already shown for BHK-21 (Figure 29) and for HOS (Figure 30) cells, co-localization between viral RNA and ER derived membranes (PDI) was observed also in this cell line.

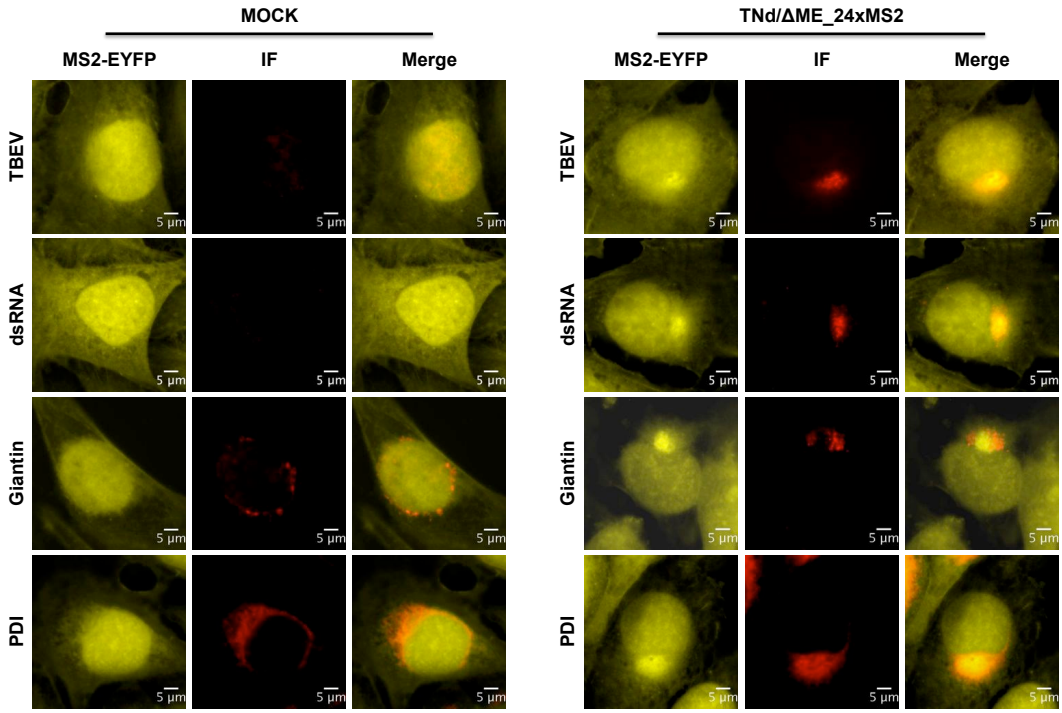

Figure 31 Immunofluorescence analysis of TBEV-transfected U2OS cells. U2OS cells were both mock transfected or transfected with the TNd/ΔME_24×MS2 replicon RNA and MS2-EYFP. After 24h, cells were fixed and incubated with antibodies for the staining of TBEV proteins (TBEV) and dsRNA to mark RCs. Association of the MS2-EYFP-tagged RNA with Golgi (Giantin) and endoplasmic reticulum (PDI) derived membranes was also analysed. Co-localization was observed only between MS2-EYFP clusters of TBEV RNA and the ER marker PDI. (Alexa Fluor 594; red).

Then, in order to ascertain whether the PRRs signalling pathway was functional we monitored IRF-3 nuclear translocation and IFNβ promoter activity in our U2OS cells. To this end, we artificially stimulated innate immune response by transfecting

cells with Poly(I:C), a synthetic dsRNA molecule. As shown in Figure 32, both the GFP-tagged (Figure 32A) and the endogenous (Figure 32B) IRF-3 transcription factor were efficiently translocated into the nucleus of transfected cells already 2 hours upon stimulation. To monitor IFNβ promoter activity, U2OS were instead transfected with a plasmid carrying the Firefly luciferase reporter gene under control of the natural IFNβ promoter (p125-Luc) and with a Renilla expressing construct for normalization. 24 hours upon plasmids transfection, U2OS were either mock or Poly(I:C) stimulated.

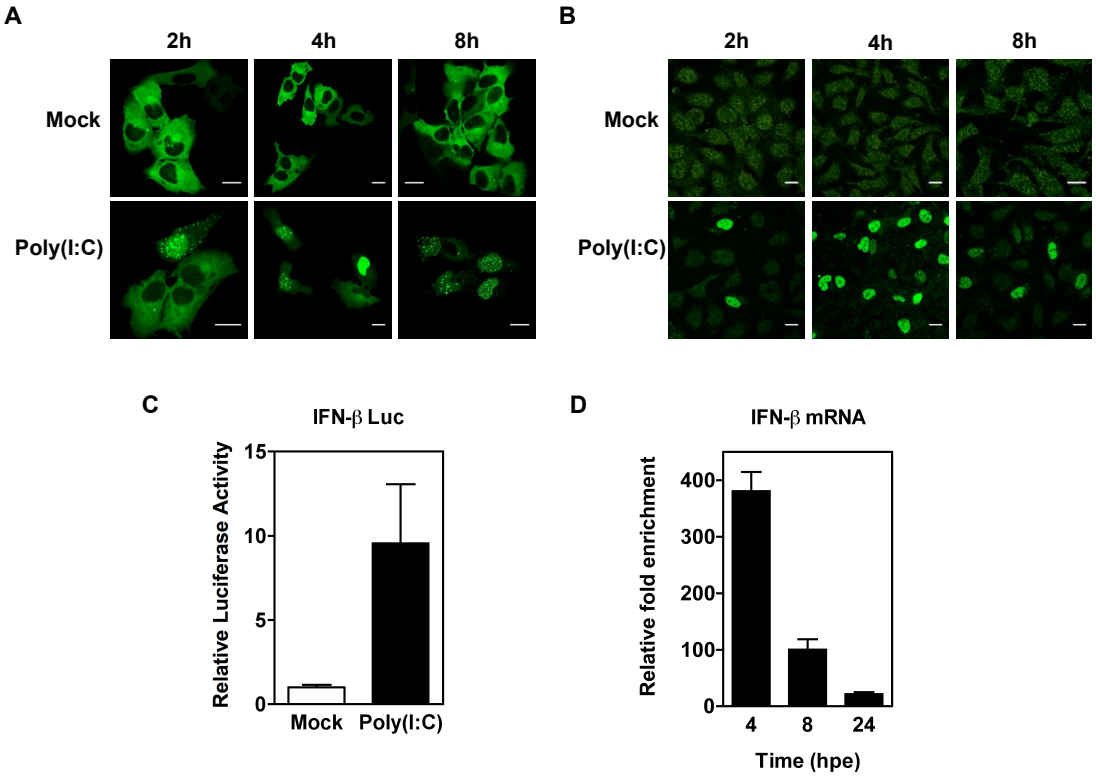

Figure 32 The PRR signalling pathway is efficiently activated by Poly(I:C) in U2OS cells. (A) U2OS cells were transfected with a plasmid for the expression of the GFP-tagged IRF-3 transcription factor. After 24 hours, transfected cell where either mock or Poly(I:C) stimulated in order to monitor IRF-3 nuclear localization by fluorescence microscopy. Images from samples fixed 2, 4 and 8 hours (h) upon stimulation are shown. Bars, 20μm. **(B)** U2OS cells where either mock or Poly(I:C) stimulated. 2, 4 and 8 h after stimulation cells were fixed and endogenous IRF-3 (Alexa Fluor 488, green) was stained in order to monitor nuclear translocation. Bars, 20μm. **(C)** U2OS were transfected with the p125-Luc reporter plasmid and with a pRL-CMV construct for normalization. After 24 hours cell were either mock or Poly(I:C) stimulated for 12 hours and were subjected to the Dual-Luciferase assay. Data represent firefly luciferase activity relative to mock stimulated cells. Error bars show standard deviation from three independent biological replicates (n=3). **(D)** U2OS cells were either mock electroporated or electroporated with 10μg of poly(I:C). At the indicated hours post-electroporation (hpe) total RNA was isolated from transfected cells and the intracellular IFNβ mRNA levels were quantified by RT-qPCR. β-actin mRNA quantification from the same samples was used for normalization. Results are expressed as fold induction relative to IFNβ mRNA levels in mock-transfected U2OS cells. Data are represented as mean ± standard deviation (n=3).

Consistently, Poly(I:C) treated cells could induce higher levels of IRF-3 dependent IFNβ promoter activity compared to mock-stimulated cells at 12 hours post-treatment (Figure 32C), indicating that U2OS can rapidly and efficiently induce IFNβ expression in response to cytoplasmic non-self RNAs.

Finally, to further confirm that U2OS cells are fully competent for IFNβ expression we wished to monitor IFNβ mRNA levels upon Poly(I:C) electroporation. As shown in Figure 32D, IFNβ mRNAs were induced within few hours following dsRNA agonist transfection, definitely ruling out any cell-dependent defect in the pathway.

3.5.2. Delayed induction of interferon following TBEV infection

In order to investigate the interferon response triggered by TBEV RNA, we then infected U2OS cells with the Western TBEV strain Hypr at a multiplicity of infection (MOI) of 1. The Vesicular stomatitis virus (VSV), a well-established inducer of IFN, was used as positive control. Cells were harvested every 4 hours post infection (hpi) and total RNA extracts were analyzed for viral RNA and IFNβ expression by RT-qPCR. As shown in Figure 33A and B, viral RNA levels increase between 4 and 8 hours after infection. In contrast, induction of IFNβ mRNA differed between the viruses. Real-time RT-PCR analyses showed that the increase of IFNβ mRNA induced by TBEV infection started after 12 hours. VSV instead induced IFNβ from 4 hours after infection (compare red lines of Figure 33A and 33B). Thus, although TBEV RNA levels increased at early time points, PAMP sensing and subsequent IFNβ induction showed a delayed kinetic.

These results are in keeping with similar observations obtained for WNV (Fredericksen et al., 2004) and recently also for TBEV by Overby and co-workers (Overby et al., 2010).

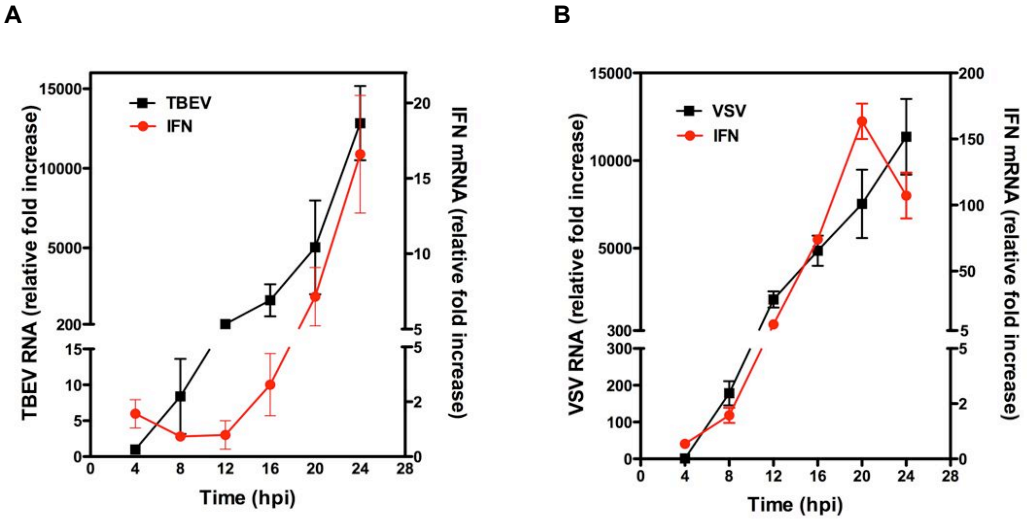

Figure 33 Delayed induction of IFNβ by TBEV. (A) U2OS cells were either mock infected or infected with TBEV strain Hypr at MOI = 1. At various times thereafter, total RNA was isolated from TBEV-infected or uninfected cells and the intracellular TBEV RNA and IFNβ mRNA levels were quantified by RT-qPCR. β-actin mRNA quantification from the same samples was used for normalization. Results are expressed as fold increase relative to time 4 hpi TBEV RNA (black line, squares) or to IFNβ mRNA levels in uninfected U2OS cells (red line, circles). **(B)** A control infection was performed with VSV at MOI = 0.1. The experiment was conducted as described above. Results are expressed as fold increase relative to time 4 hpi VSV RNA (black line, squares) or to IFNβ mRNA levels in uninfected U2OS cells (red line, circles). Data are represented as mean ± standard deviation from three independent biological replicates (n = 3).

3.5.3. Interferon induction depends on TBEV replication

To better dissect the mechanisms behind the TBEV-induced interferon expression we took advantage of the well-characterized sub-genomic replicons established during the first part of the PhD program (Hoenninger et al., 2008; Miorin et al., 2008). U2OS cells were transfected with *in vitro* transcribed TNd/ΔME_24XMS2 and TNd/ΔME_24XMS2_GAA sub-genomic RNAs. As in the previous experiment, at the indicated time points after transfection, cellular extracts were analyzed for TBEV RNA and IFNβ expression. Similar kinetic of viral replication and IFNβ induction were observed. Again, viral replication started between 4 and 8 hours after transfection (Figure 34A) whereas IFNβ mRNA expression was strongly induced only after 24 hours (Figure 34B). Additionally, we could also observe that the triggering of innate immunity was dependent on the amplification of viral RNA since the replicon carrying the GAA mutation in NS5, the viral RNA-dependent RNA polymerase, was unable to induce IFNβ.

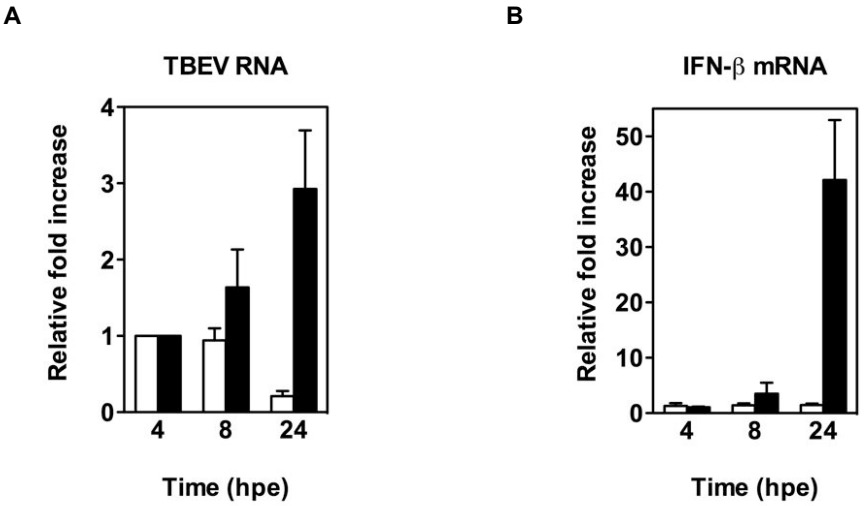

Figure 34 TBEV replication is required for interferon induction. U2OS cells were either mock electroporated or electroporated with TNd/ΔME_24xMS2 (black bars) and TNd/ΔME_24xMS2_GAA (white bars) replicon RNAs (10μg each). At the indicated hours post-electroporation (hpe) total RNA was isolated from transfected cells and the intracellular TBEV RNA **(A)** and IFNβ mRNA **(B)** levels were quantified by RT-qPCR over β-actin as described previously. Results are expressed as fold increase relative to time 4 hpe TBEV RNA **(A)** or to IFNβ mRNA levels in mock-transfected U2OS cells **(B)**. Data are represented as mean ± standard deviation from three independent biological replicates (n = 3).

3.5.4. Delayed interferon induction correlates with delayed IRF-3 nuclear translocation

Next, we analyzed the activation state of the constitutively expressed IRF-3 transcription factor in response to TBEV. To monitor IRF-3 sub-cellular localization, U2OS cells were electroporated with both the TNd/ΔME_24XMS2 and the TNd/ΔME_24XMS2_GAA sub-genomic RNAs and stained with specific antibodies. As shown in Figure 35A, the time course of IRF-3 nuclear translocation was similar to that of IFNβ mRNA induction with the appearance of IRF-3 in the nucleus after 24 hours. Again, the poly(I:C) control triggered an earlier IRF-3 activation (Figure 35C and 35D), whereas no nuclear translocation was detected after transfection of the replication deficient sub-genomic RNA (representative pictures are shown in Figure 35A, and quantification is shown in Figure 35B). These results further confirmed that viral replication is required for TBEV-induced innate immunity activation.

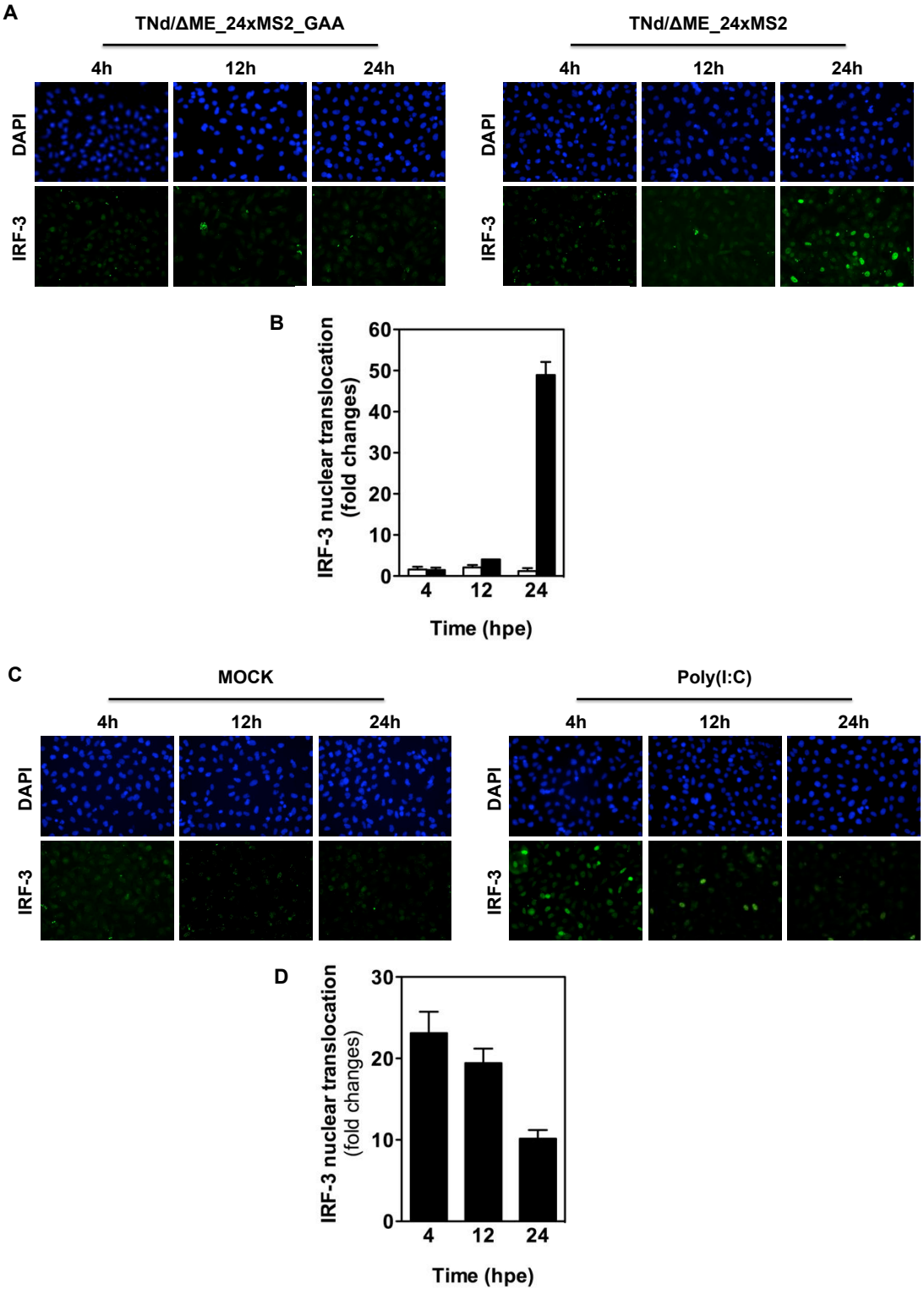

Figure 35 TBEV replication is required for IRF-3 activation. (A) U2OS cells were either mock transfected or transfected with TNd/ΔME_24xMS2_GAA and TNd/ΔME_24xMS2 replicon RNAs (10μg each). At 4, 12 or 24 hours post-electroporation (hpe) cells were fixed and immunostained for the detection of IRF-3 intracellular localization (green). Nuclei were visualized by staining with DAPI (blue). **(B)** Quantification of TBEV induced IRF-3 nuclear translocation. Cells were scored as positive for IRF-3 translocation when the average nuclear intensity of the green channel was at least twice that of mock treated cells. Values are expressed as fold changes of the percentage of positive cells over mock-transfected cells. **(C)** U2OS cells were either mock electroporated or electroporated with 10μg of poly(I:C). At the indicated time points cells were fixed and immunostained for the detection of

IRF-3 intracellular localization as described above. **(D)** Quantification of poly(I:C) induced IRF-3 nuclear translocation. Cells were scored as positive for IRF-3 translocation like in B.

Furthermore, we could also observe a strong correlation between interferon induction and IRF-3 activation that clearly points towards a defect in the pattern recognition receptor's signaling.

3.5.5. Naked PRRs TBEV RNA agonists are immediately recognized

In order to gain insight into the mechanism behind the delay of IRF-3 activation we wished to assess whether the replication intermediates responsible for IFNβ induction were generated early upon TBEV transfection. To this end, we extracted total RNA from cells carrying the TNd/ΔME_24XMS2 replicon, or the GAA mutant replicon, both at 8 hours after transfection, when viral replication is already taking place but IFNβ has not yet been induced, and at 24 hours after transfection, when IFNβ has been instead already greatly induced by replication intermediates (Figure 34B). Extracted RNA was then re-transfected into U2OS cells and IFNβ mRNA induction monitored at 4 hours post-induction.

As shown in Figure 36, in line with our previous observations, only re-transfection of extracts from cells carrying the replication-competent sub-genomic RNA could trigger IFNβ induction. Strikingly, also RNA extracted as early as 8 hours post-transfection was significantly stimulating IFNβ expression suggesting that the viral RNA agonists are generated early during replication. However, thanks to a still unrevealed viral strategy, they cannot be properly sensed by the innate immunity surveillance in the context of active TBEV replication.

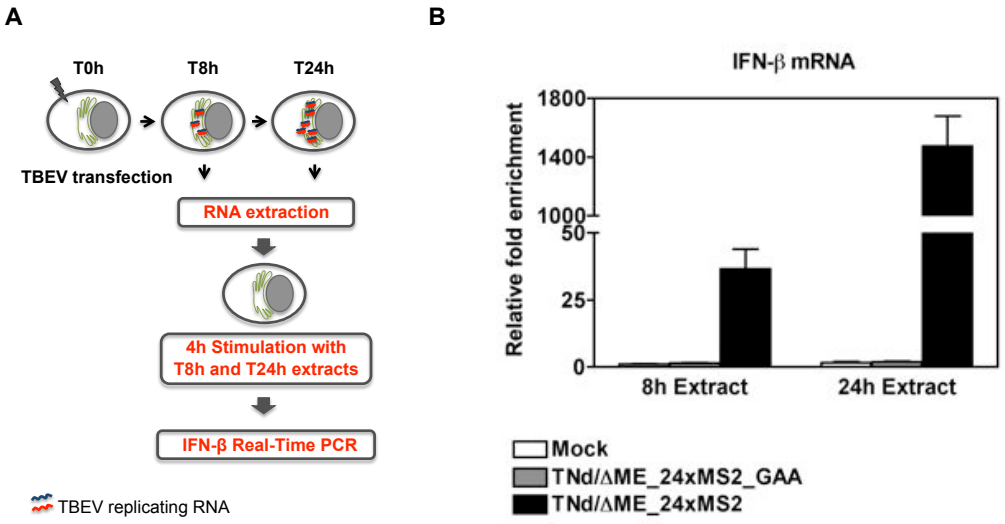

Figure 36 Naked TBEV replication intermediates trigger fast IFNβ induction. (A) Schematic drawing of the experimental approach. At 8 and 24 hours upon U2OS electroporation cells were collected and total RNA isolated. U2OS cells were then stimulated for 4 hours with the extracts previously isolated and the intracellular IFNβ mRNA levels were quantified by RT-qPCR. **(B)** U2OS were either mock electroporated or electroporated with TNd/ΔME_24xMS2_GAA and TNd/ΔME_24xMS2 replicon RNAs (10μg each). Total RNA extracts isolated from cells at 8 and 24 hours post-electroporation were then treated with DNase I and re-transfected into U2OS cells as described in (A). Intracellular IFNβ mRNA levels quantified by RT-qPCR and normalized with that of β-actin are shown in the graph. Results are expressed as fold enrichment relative to IFNβ mRNA levels of cells treated with transfection reagent only. Data are represented as mean ± standard deviation (n = 3).

3.5.6. TBEV proteins do not subvert PRR signalling pathways

We next investigated whether also TBEV, like many other viruses (Garcia-Sastre et al., 1998; Li et al., 2005; Meylan et al., 2005; Rodriguez-Madoz et al., 2010a), expresses IFN-antagonistic proteins able to impose a direct block to this signaling pathway. To this end, U2OS cells were either mock-treated (pGFP) or electroporated with the TNd/ΔME_24XMS2 replicon RNA or with the plasmid expressing the NS1 protein from the influenza PR8 strain, that functions as an inhibitor of IFNβ induction (Gack et al., 2009; Guo et al., 2007; Mibayashi et al., 2007; Opitz et al., 2007; Pichlmair et al., 2006; Rehwinkel et al., 2010). After 8 hours, to allow proteins expression, transfected cells were stimulated for 4 hours with poly (I:C) and their ability to efficiently trigger IFNβ induction was monitored by quantitative RT-PCR (in Figure 37A a scheme of the experiment is reported).

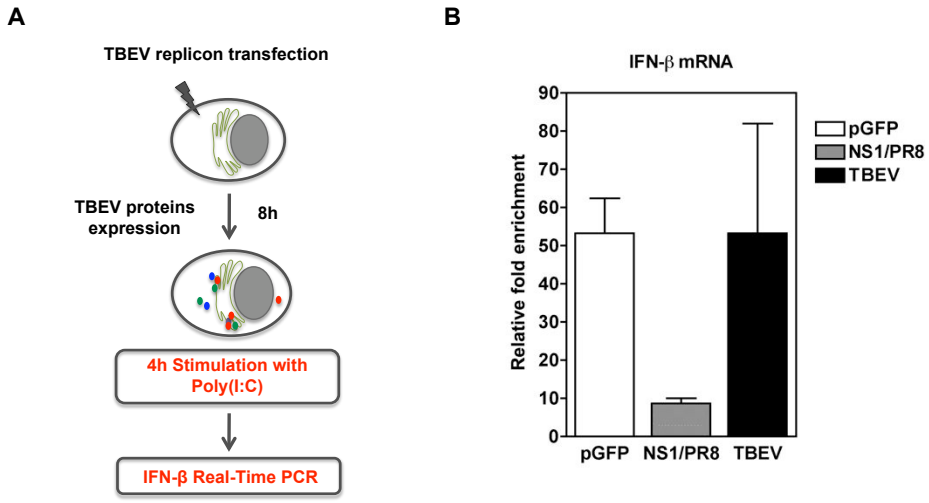

Figure 37 IFNβ induction is not affected by TBEV replicon expression. (A) Schematic drawing of the experimental approach. At 8 hours upon TBEV replicon transfection cells were stimulated with Poly(I:C) for 4 hours. Total RNA was then extracted and the levels of IFNβ transcripts quantified by RT-qPCR. **(B)** U2OS cells were electroporated with the TBEV replicon RNA (10μg) or with a plasmid expressing GFP (pEGFP-N1) or with pCAGGS-NS1 (10μg each) as controls. After 8 hours cells were Poly(I:C) stimulated and processed as described in (A). The IFNβ mRNA expression levels, normalized with that of β-actin and expressed as fold-enrichment over respective mocks (cells electroporated but not stimulated), are shown in the graph. Data where averaged from four independent experiments and are represented as mean ± standard deviation.

As shown in Figure 37B, while NS1 overexpression efficiently inhibited the signaling, as expected, induction of IFNβ transcripts remained unaffected by the presence of TBEV proteins.

To ensure a specific TBEV replication-dependent PRRs signaling activation, total RNA extracted at 24 hours upon TNd/ΔME_24×MS2 replicon transfection was used to stimulate mock and TBEV infected cells (Figure 38A). Consistently with Figure 37B, we did not detect impaired IFNβ induction in cells stimulated at 8 hours after infection as well as at later time points after infection (24 hpi). The dsRNA immunoblot in Figure 38B shows that the RNA extracts used for the re-tranfection were enriched in dsRNA generated during viral replication in agreement with dsRNA detection in the cytoplasm (Figure 31). All together these data strongly indicate that the delay of IFNβ induction is neither mediated by a direct effect of a viral protein on the signalling (Figures 37 and 38) nor by the lack of PRRs agonists (Figure 36).

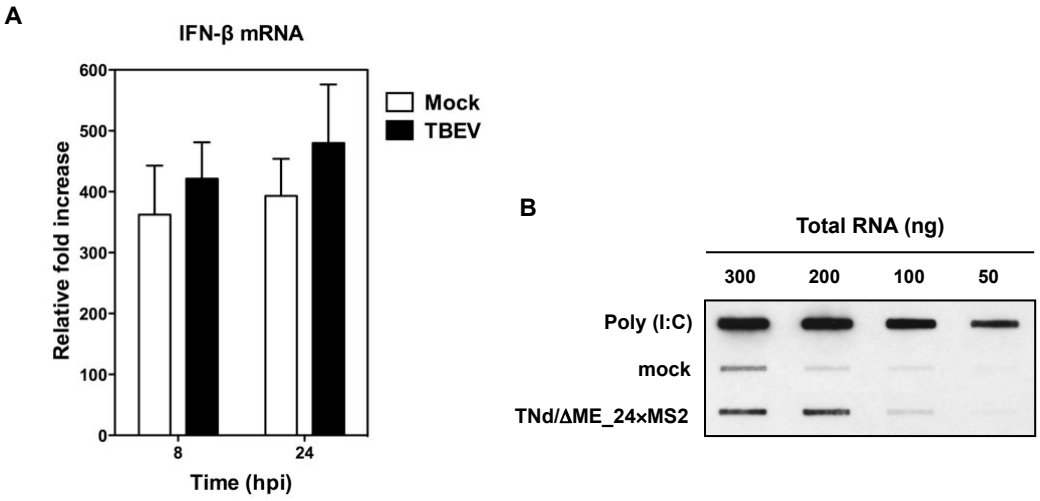

Figure 38 IFNβ induction is not affected by TBEV infection. (A) U2OS cells were either mock infected or infected with TBEV strain Hypr at MOI = 1. 8 and 24 hours after infection, cells were stimulated for 4 hours with total RNA extracted from mock-transfected cells or from cells collected at 24 hours upon TNd/ΔME_24xMS2 replicon transfection. Intracellular IFNβ mRNA levels were then quantified by RT-qPCR. The expression level of IFNβ was normalized with that of β-actin. Results are expressed as fold increase relative to IFNβ mRNA levels of mock-infected cells stimulated with RNA extracts from mock-transfected cells. Data are represented as mean ± standard deviation (n = 3). **(B)** dsRNA-immunoblotting of total RNAs harvested from mock-transfected cells (mock) or from cells collected at 24 hours upon TNd/ΔME_24xMS2 replicon transfection (TNd/ΔME_24xMS2). The commercial dsRNA analogue poly(I:C) was spotted as a positive control. The indicated amount of total RNA was spotted on the membrane and then blotted with the anti dsRNA antibody.

Therefore, we were intrigued by the fact that this delay could be due to an indirect mechanism connected with the arrangement of secluded environments for replication that may affect agonist availability to PRRs signalling (den Boon et al., 2010; Gillespie et al., 2010; Overby et al., 2010).

3.5.7. Replicated viral RNA is not freely diffusible in the cytoplasm

In order to better elucidate agonist availability by PRRs we next analyzed the dynamic exchange of proteins and TBEV replicated RNA between RCs and the cytoplasm. To this end we took advantage of the fluorescence recovery after photobleaching (FRAP) technique. FRAP is a method for measuring the mobility of fluorescent particles in living cells (Axelrod et al., 1976; Maiuri et al., 2010). A defined portion of the system containing mobile fluorescent molecules is exposed to a brief and intense focused laser beam, thereby causing irreversible photochemical

bleaching of the fluorophore in that region. The subsequent kinetics of fluorescence recovery in the bleached region, which results from transport of fluorescent molecules into the bleached area from non-irradiated parts of the cells, as well as transport of dark fluorophores out of the bleached area, provides a quantitative measure of the mobility of the fluorophore. If the tagged protein does not move, or is bound to an immobile substrate, the recovery cannot reach the pre-bleach values showing an immobile fraction. In our case the viral RNA substrate, which binds avidly MS2-EYFP, is continuously synthesized by the viral polymerase and should be able to diffuse in the cytoplasm unless a membranous compartment impairs its mobility. BHK-21 cells were chosen for this experiment because they show a larger and more experimentally treatable MS2-defined compartment (compare Figures 39 and 40).

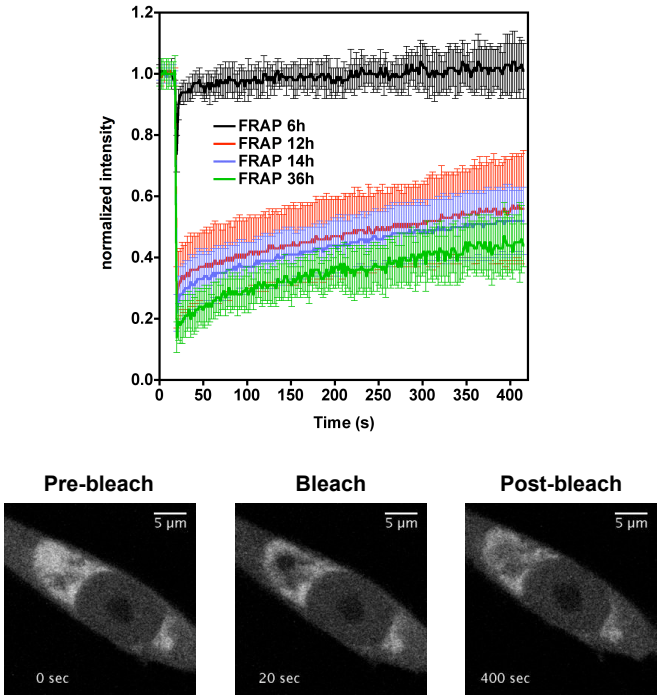

Figure 39 TBEV replicated RNA is not freely diffusible in the cytoplasm. Analysis of TBEV RNA dynamics by FRAP time course. BHK-21 cells were electroporated with the TNd/ΔME_24xMS2 replicon RNA together with a vector expressing MS2-EYFP. At the indicated time points post-electroporation the fluorescence recovery of the MS2-EYFP protein in the area of bleaching was analyzed. The graph shows values of fluorescence intensity normalized to the pre-bleach values and corrected for the loss of fluorescence due to the imaging procedure (Phair and Misteli, 2000) (Maiuri et al., 2010). Data represent the average of acquisitions from at least 10 cells ± standard deviation. An image sequence from a FRAP experiment performed in BHK-21 cells 14 hours upon electroporation is shown at the bottom of the graph (29,25 × 29,25 µm). The bright perinuclear region represents the subcellular compartment into which replicated viral RNA is clustered and where ROIs were drawn. Times were collected before bleaching (pre-bleach, 0 sec.), immediately after the bleaching (bleach, 20 sec.) and at 400 sec. after the bleaching event (post-bleach).

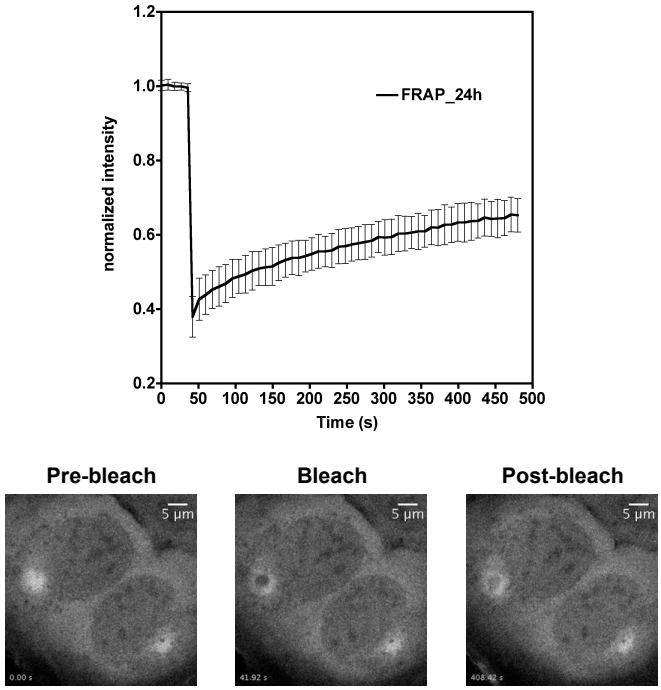

Figure 40 Analysis of TBEV RNA dynamics on U2OS cells. U2OS cells were electroporated with the TNd/ΔME_24xMS2 replicon RNA together with a vector expressing MS2-EYFP. After 24 hours the fluorescence recovery of the MS2-EYFP protein in the area of bleaching was analyzed. The graph shows values of fluorescence intensity normalized to the pre-bleach values and corrected for the loss of fluorescence due to the imaging procedure. Data represent the average of acquisitions from 10 cells ± standard deviation. An image sequence from the FRAP experiment is shown at the bottom of the graph (48,75 × 48,75 µm). Times were collected before bleaching (pre-bleach, 0 sec.), immediately after the bleaching (bleach, 42 sec.) and at 408 sec. after the bleaching event (post-bleach).

However, the conclusions are essentially valid also for U2OS cells (Figure 40). BHK-21 cells expressing the TNd/ΔME_24XMS2 replicon RNA and MS2-EYFP were subjected to FRAP analysis at different time points (Figure 39). Full recovery of the signal in few seconds was observed 6 hours after electroporation indicating free mobility of MS2-EYFP. Instead, recovery was severely impaired after 12 hours. Subsequent time points up to 36 hours showed similar recovery profiles indicating that the vesicles are established early and maintained thereafter. These results can be interpreted in different ways.

One possibility is that the replicated viral RNA is secluded into compartments that are not accessible by the MS2-EYFP. To address this point we exploited the red-shifted variant Cherry-MS2nls to mark viral RNA while the mobility of free GFP was monitored by FRAP as previously described (Boireau et al., 2007; Molle et al.,

2007). As shown in Figure 41, mobility of GFP within the compartment did not differ significantly from the free mobility of the protein in the cytoplasm. GFP is a small protein and it is not surprising that it is able to access the compartment where TBEV replicated RNA accumulates.

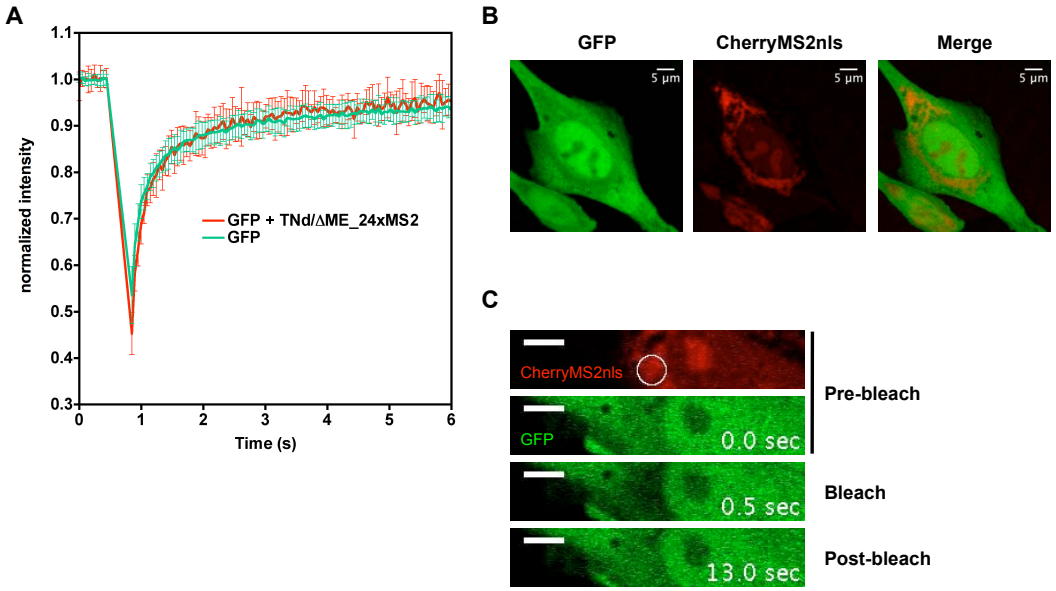

Figure 41 Analysis of GFP mobility within the MS2 enriched compartment. BHK-21 cells were electroporated with a vector expressing CherryMS2nls, to mark sites of RNA accumulation, and with a GFP expressing plasmid (pEGFP-N1) both in the presence (red line, GFP + TNd/ΔME_24×MS2) and in the absence (green line, GFP) of the TBEV replicon RNA. After 24 hours GFP kinetics was investigated by FRAP. **(A)** In the graph the recovery curves of the GFP protein in the two different experimental conditions are compared. The values of fluorescence intensity are normalized to the pre-bleach values and corrected for the loss of fluorescence due to the imaging procedure as already described. Data represent the average of acquisitions from 10 cells ± standard deviation. **(B)** Representative image of BHK-21 cells transfected with GFP and CherryMS2nls in the presence of the TBEV replicating RNA. A z-projection of 41 images 0,5 µm apart is shown. **(C)** Image sequence from the FRAP experiment described in (A) (36,56 × 7,14 µm). Top, pre-bleach stacks in both channels (0 sec.). The circle indicates the area of bleach chosen in the region marked by CherryMS2nls. Middle, time point immediately after the bleaching event (0,5 sec.); bottom, post-bleach stack (13 sec.).

We were intrigued by the accessibility of this compartment of a PRR like RIG-I. Therefore we repeated the experiment using RIG-I fused to GFP. To be sure that we were tracking the full-length fusion protein, and not only GFP from a degradation product, we immunoblotted extracts from cells with antibodies against GFP or RIG-I. As shown in Figure 42D, GFP-RIG-I is expressed as a full-length protein product. Again, mobility of GFP-RIG-I within the compartment defined by Cherry-MS2nls in

TNd/ΔME_24×MS2 transfected BHK21 cells, did not differ significantly from the free mobility of the protein in the cytoplasm of mock-transfected cells (Figure 42). Interestingly, we also could not observe any increase of the immobile fraction in the recovery of GFP-RIG-I in cells transfected with TNd/ΔME_24×MS2 at 24 hpe. At this time point IRF3 is already being translocated to the nucleus (Figure 35), IFNβ is activated (Figure 34B) and from preliminary data also endogenous RIG-I appears activated. Therefore, either the fraction of GFP-RIG-I activated is too low to be significantly detected in the FRAP experiment, or activation does not affect mobility of the protein.

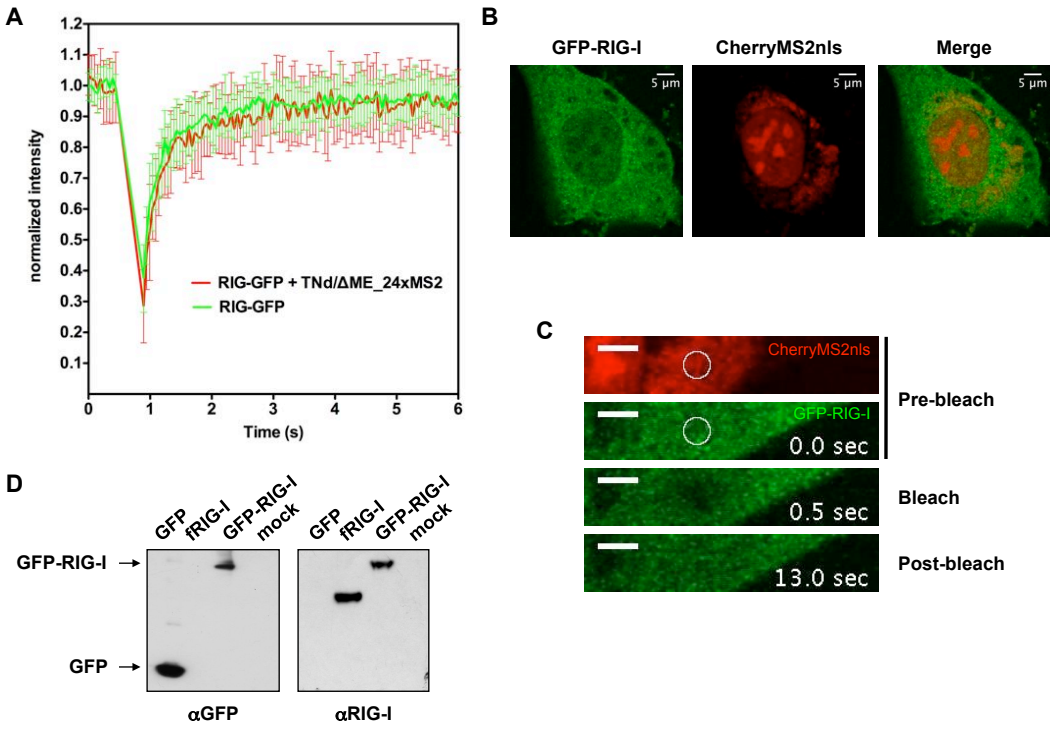

Figure 42 Analysis of RIG-I mobility within the MS2 enriched compartment. BHK-21 cells were electroporated with CherryMS2nls and with a GFP-RIG-I expressing plasmid both in the presence (red line, GFP-RIG-I + TNd/ΔME_24×MS2) and in the absence (green line, GFP-RIG-I) of the TBEV replicon RNA. **(A)** After 24 hours GFP kinetics was investigated by FRAP as described in Figure 42. **(B)** Representative image of BHK-21 cells transfected with GFP-RIG-I and CherryMS2nls in the presence of the TBEV replicating RNA **. (C)** Image sequence from the FRAP experiment described (36,56 × 7,14 µm). Top, pre-bleach stacks in both channels (0 sec.). The circle indicates the area of bleach chosen in the region marked by CherryMS2nls. Middle, time point immediately after the bleaching event (0,5 sec.); bottom, post-bleach stack (13 sec.). **(D)** Immunoblot of whole cell extracts expressing GFP-RIG-I. Antibodies where against GFP (left panel) or RIG-I (right panel). position of full-length GFP-RIG-I and GFP are indicated. Flag-tagged RIG-I was used as control (fRIG-I) because endogenous RIG-I is not sufficiently expressed in non-induced cells.

All together these experiments show that proteins are free to move in and out of the MS2 enriched compartments.

Another possibility is that the viral RNA is only slowly or even not replicated at all, resulting in little or no substrate available to free MS2-EYFP. We know that replicated viral RNA accumulates continuously up to 72 hours post-transfection (Figures 18 and 21). Therefore we can exclude that the RCs are dead with respect to replication. However, it has been shown that Kunjin virus replicates its genome in about 15 minutes (Westaway et al., 1999) and considering that viral RNA biogenesis can affect the recovery curve, this possibility cannot be completely ruled out.

Finally, a slow release of replicated viral RNA bound to bleached MS2-EYFP from the compartments may also result in an increase of the immobile fraction of the FRAP experiment.

3.5.8. Impaired release of replicated flaviviral RNA from the replication compartments

To address the release of replicated, MS2-tagged, viral RNA from the RCs we set to deplete fluorescent MS2-EYFP from the cytoplasm and measure loss of florescence at the compartment. This approach is called fluorescent loss in photobleaching (FLIP) and is complementary to FRAP (Dundr and Misteli, 2003; Lippincott-Schwartz et al., 2001). As shown in Figure 43, we chose a region for bleaching in the cytoplasm away from the perinuclear compartment and then we measured loss of fluorescence at a site in the cytoplasm as well as within the compartment in order to assess vesicle-to-cytoplasm RNA exchange. Both sites were chosen approximately at the same distance from the bleaching area. After each bleaching the intensity of fluorescence was measured in every region of interest (ROI). In principle each mobile fluorescent molecule that diffuses at the bleaching site will be irreversibly bleached. Hence, regions of freely mobile proteins will be loosing fluorescence quickly, whether regions where the proteins are immobile or secluded into vesicles will resist bleaching. This kind of measurements clearly showed that fluorescent TBEV RNA-bound MS2-EYFP (blue line) is depleted less efficiently than freely diffusible MS2-EYFP (green line).

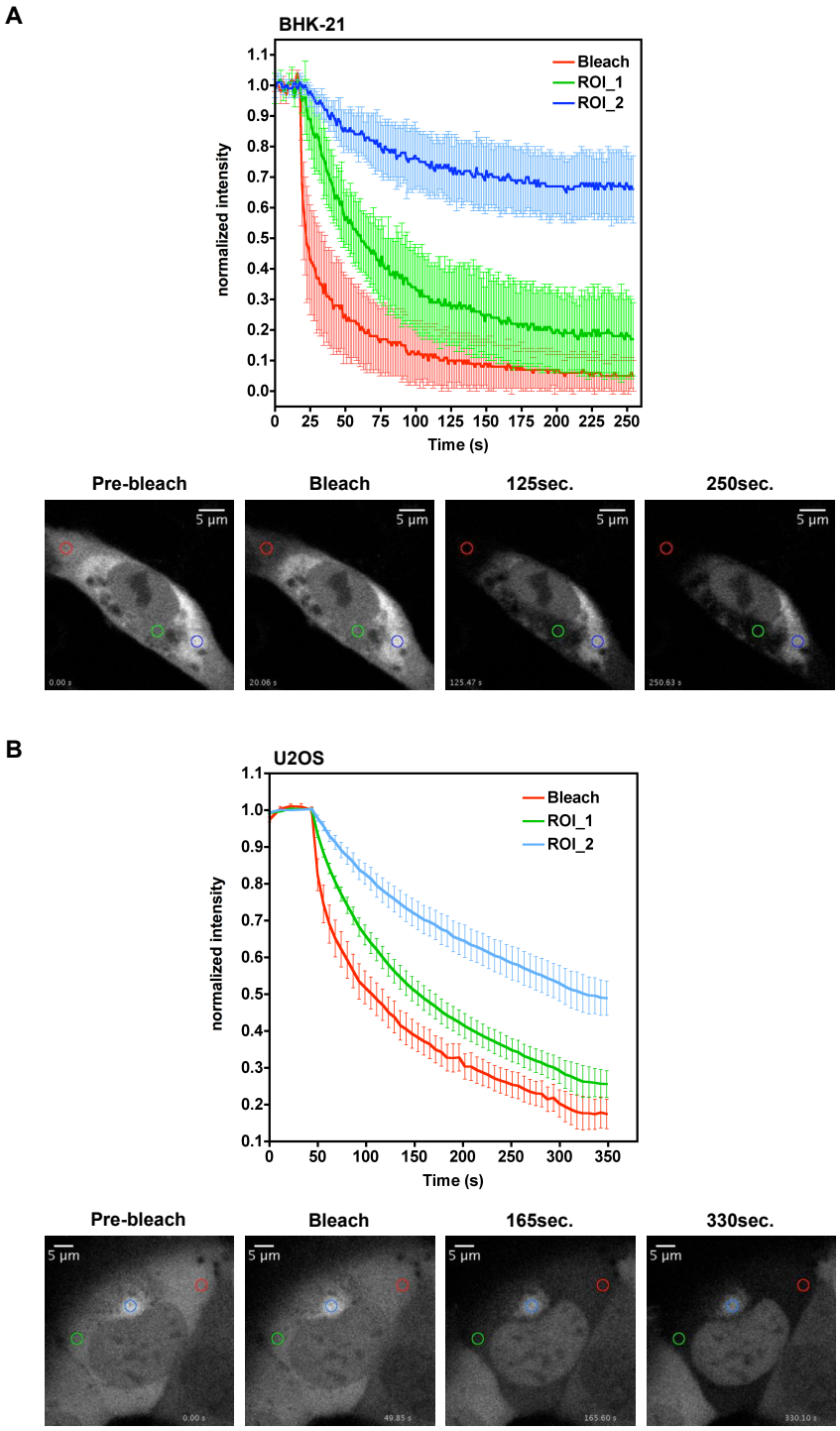

Figure 43 TBEV replication compartments allow slow release of viral RNA to the cytoplasm. BHK-21 **(A)** and U2OS **(B)** cells were electroporated with the TNd/ΔME_24×MS2 replicon RNA together with a vector expressing MS2-EYFP. After 24 hours viral RNA release from the RC was monitored by FLIP. At the bottom of the graphs, selected images from a FLIP experiment are shown (36,56 × 36,56 µm). The region for bleaching (red circle in the bottom panels) was chosen in the cytoplasm away from the clustered TBEV RNA. Loss of fluorescence was then measured in the cytoplasm both within (blue circle, ROI_1) and outside (green circle, ROI_2) the RC. In the graphs the loss in fluorescence intensity within the three different ROIs (Bleach; ROI_1 and ROI_2) is compared. Data are normalized as described in Figure 43 and represent the average of acquisitions from 10 cells ± standard deviation.

To note however that, as it was observed for the FRAP experiments (Figure 39), where the immobile fraction decreased at later time points, immobilization of trapped TBEV RNA within compartment is not complete since 30% depletion is observed after 4 minutes of FLIP. This clearly points towards a certain degree of TBEV RNA exchange between the compartments and the cytoplasm.

3.5.9. Free diffusion of replicated viral RNA within defined regions of the replication compartments

Finally, we wanted to investigate the dynamic interchange of TBEV RNA within the compartment itself. For this purpose we took advantage of the EYFP-MS2nls reporter that accumulates efficiently in the nucleus (Boireau et al., 2007). We observed that, in the presence of replicating TNd/ΔME_24XMS2, EYFP-MS2nls accumulates in the cytoplasm against a dark background greatly enhancing the signal-to-noise ratio (Figure 28). This configuration was useful to study diffusion of the viral ribonucleotide particle (vRNP), composed of viral replicated RNA and associated proteins, within the replication vesicles. For this purpose a FLIP experiment was designed where the bleached area is located within the compartment (Figure 44). If replication vesicles were all interconnected, continuous bleaching would have resulted in depletion of fluorescence from the entire compartment. Conversely, as shown in Figure 44, depletion of fluorescence was restricted to a portion of the compartment, leaving the rest unaffected. This experiment demonstrates that the perinuclear region evidenced by EYFP tagging of the vRNP is not a unique environment but is rather composed of physically separated sub-compartments. Within a sub-compartment the viral RNA is able to freely diffuse indicating that the RNA is probably not associated with membranes. This finding, together with the observation that the viral RNA is unable to leave these compartments (Figure 43) fits with the definition of a replication compartment separated from the cytoplasm.

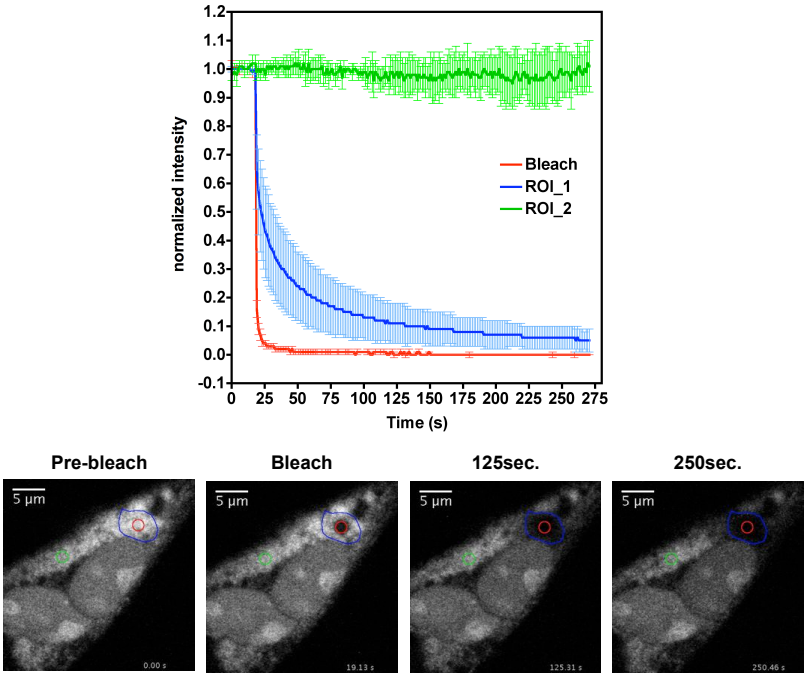

Figure 44 TBEV replication compartments are organized in discrete clusters. BHK-21 cells were electroporated with the TNd/ΔME_24×MS2 replicon RNA and with the EYFP-MS2nls reporter. At 24 hours upon transfection viral RNA trafficking within the RC was analyzed by FLIP. For this purpose, as shown in the bottom images (29,25 × 29,25 µm), the area of bleaching (red circle) was located inside the compartment. Loss of fluorescence was then measured in two different regions, one surrounding the bleaching area (blue region; ROI_1) and the other one more distant (green circle; ROI_2). The top panel compares the loss of fluorescence curves of the three selected ROIs. Data are normalized as already described and represent the average of acquisitions from 10 cells ± standard deviation.

4. DISCUSSION

4.1. Main scope of this work

Viruses depend entirely on the host cell machinery to complete their life cycle and establish a productive infection. The host cell not only provides building blocks such as nucleotides and amino acids for viral metabolism but also structural platforms for viral replication and assembly. Therefore, during their journey into the host, viruses spatially and temporally interact with different cellular structures, leading to extensive changes in the cellular architecture and physiology. In particular, positive-sense RNA viruses are known to usurp and rearrange cytoplasmic membranes to generate specialized sites for RNA replication. These sites are enriched in specific intracellular membranes, viral RNA as well as viral and host proteins that altogether participate in coordinating different steps of the virus life cycle and in subverting antiviral responses (den Boon et al., 2010; Miller and Krijnse-Locker, 2008; Novoa et al., 2005). Over the past several years, studies based on immunofluorescence and electron microscopic imaging have begun to address the structure and composition of these compartments. In the case of flaviviruses, subcellular sites of viral RNA replication have been probed by metabolic labelling of nascent RNAs (Westaway et al., 1999), by immune-labelling with sera reactive to dsRNA (Mackenzie et al., 1998) and by *in situ* hybridization (Grief et al., 1997). However, many critical aspects about their formation and function are still poorly understood.

Recently, methods based on bacterial operator/repressor systems allowed the intracellular detection of the genomes of various DNA viruses (Fraefel et al., 2004; Sourvinos and Everett, 2002). Furthermore, a method based on the binding of the MS2 phage core protein to a series of RNA aptamers has been proposed for the detection of viral RNA genomes (Basyuk et al., 2003; Beckham et al., 2007; Boireau et al., 2007). These new tools are important not only for the qualitative analysis of the subcellular localization of viral genomes, but also they can provide quantitative information such as the rate of RNA biogenesis in living cells (Boireau et al., 2007) or the kinetic of RNA trafficking (Basyuk et al., 2003; Fusco et al., 2003). Furthermore, the possibility of detecting the viral RNA in the living cell allows the analysis of the dynamic recruitment of host and viral factors to the viral genome to be measured in real time in order to build a kinetic model of the process (Dundr et al., 2002; Molle et al., 2007).

In this study we developed a method to track flaviviral RNA in real time in living cells in order to dissect the dynamic interaction between newly replicated viral genomes and the host cell machinery. Since all flaviviruses share similar intracellular life cycles (Lindenbach et al., 2007), we chose the well-described TBEV replicon system (Gehrke et al., 2005; Mandl et al., 1997) as a model to study the behaviour of replicated RNA in living cells.

4.2. Construction and characterization of the TBEV-based replicons

Previous work has shown that it is possible to insert heterologous RNA sequences in the variable region of the 3'-UTR of a TBEV replicon and maintain self-replication of the transfected RNA (Gehrke et al., 2005). Here, we inserted at that location a series of 24 repeats of the 19 nucleotides RNA loop that is recognized by the MS2 core protein (Figure 16). Previously it has been shown that this is the optimal length for the visualization of single mRNA ribonucleoparticles in the cytoplasm of living cells (Fusco et al., 2003). However, in order to minimize the possible impact of these highly structured RNA sequence on viral translation and/or replication, we also attempted to generate clones carrying 12 MS2 binding sites (Figure 16). The replication ability of the engineered subgenomic replicons carrying the repeats was then deeply characterized in BHK-21 cells by different approaches, as described below.

Flavivirus replication requires a relatively long lag phase of about 10 - 15 hours (Lindenbach et al., 2007). During this time, both viral RNA and protein synthesis occurs at a low but detectable level. Consistently, Northern blot hybridization clearly showed that the TNd/ΔME_24XMS2 subgenomic replicon was already replicating 12 hours upon transfection (Figure 17). However, since the system for the tracking of the viral RNA in living cells requires the specific interaction of the target RNA with the MS2 protein (Bertrand et al., 1998), the effect of the MS2-EYFP co-expression on viral replication was also addressed. RT-PCR analysis performed at different time points upon transfection not only confirmed that the replicons retain the heterologous sequences and are able to replicate full-length RNA, but also revealed that both transient and constitutive MS2-EYFP co-expression do not abolish replication of

none of the tested constructs (Figure 18 – 20). Altogether these experiments represented the first indication that the MS2-based approach might be exploited to dissect the dynamic interaction between the TBEV RNA and the host cell machinery. However, in order to allow a more quantitative analysis of translation and replication efficiencies of the engineered replicons, we also established a luciferase-based reporter system in collaboration with Prof. Christian Mandl. Strikingly, by this approach we could clearly demonstrate that both the 12 - and the 24 - repeat insertions do not affect translation of the input RNA and have only a modest effect on viral RNA replication (Figure 21). These results differ from recent findings obtained with closely related mosquito-borne flaviviruses and with the blood-borne HCV (Alvarez et al., 2005a; Friebe and Bartenschlager, 2002; Tajima et al., 2007). Deletion of the variable region of these viruses was indeed shown to significantly impair viral growth. However, what we observed is in agreement with the fact that in the case of TBEV this region is extremely variable, both in sequence and length, and appeared to be dispensable to maintain viral viability in cell culture and virulence in mice (Mandl et al., 1998; Mandl et al., 1991).

4.3. Visualization of newly replicated TBEV RNA in living cells

Excluding few reports of nuclear replication (Brawner et al., 1979; Uchil et al., 2006), all researchers agree on the fact that flaviviral RNAs is synthesized in association with cytoplasmic membranes in the perinuclear region of the mammalian cells (den Boon et al., 2010; Gillespie et al., 2010; Welsch et al., 2009). Consistently, by exploiting our cytoplasmic variant of the EYFP-MS2nls protein, we could appreciate that the EYFP signal was no longer diffused all over the cells but instead specifically clusterized in the cytoplasm of the cells transfected with the replicons carrying the MS2 binding sites (Figure 22). This dramatic change in the MS2 localization was observed starting from 14 hours upon transfection (Figure 23) and was compatible with the formation of newly synthesized viral RNA. Indeed, when we repeated the experiment with the replication deficient TNd/ΔME_24XMS2_GAA mutant we could not observe any clustering of the signal in the cytoplasm (Figure 22B, bottom panels). Interestingly, the same was true also upon transfection of the

TNd/ΔME_EGFP parental replicon that does not contain any MS2 binding sites (Figure 24B). This observation, together with the co-localization of the viral RNA with the perinuclear EYFP cluster, as shown by *in situ* hybridization (Figure 24A), prompted us to conclude that the MS2 protein is not just trapped within rearranged cytoplasmic compartments induced upon TBEV transfection but is specifically bound to the newly replicated genomes. Therefore, we exploited our system in order to define and deeply characterize the sub-cellular sites of TBEV replication.

4.4. Characterization of the clustered TBEV RNA compartments

The Kunjin virus has been a useful model to investigate the membrane sites of flavivirus replication. In Kunjin virus infected Vero cells, dsRNA corresponding to the recycling minus strand template for genomic RNA synthesis was shown to co-localize with NS1, NS2A, NS3, NS4A and NS5 within an ER-derived compartment termed vesicle packets (VP), which appears to be also enriched in the *trans*-Golgi marker β-1,4-galactosyltransferase (GalT) (Gillespie et al., 2010; Mackenzie et al., 1996, Mackenzie, 1999 #113; Westaway et al., 1999). VPs were shown to be connected through the ER to other membranes, the convoluted membrane/paracrystalline (CM/PC) structures that are believed to be sites of viral translation and proteolytic cleavage. CM and PC originate from the intermediate compartment (IC) and the ER as well (Mackenzie et al., 1999). Most importantly, for direct comparison with TBEV replicons used in our studies, Kunjin replicon sites of replication appeared to recruit the same cell membrane markers as those associated with Kunjin virus replication upon infection (Mackenzie et al., 2001). However, the perinuclear pattern of dsRNA staining was more diffused as compared with the large perinuclear inclusion characteristic of Kunjin virus infection, with no accumulation of VPs. This may reflect the inefficient replication of the replicon RNA that does not allow extensive accumulation of non-structural proteins and dsRNA to induce the formation of VPs or by the requirement of structural proteins (M and E) for their formation. This scenario applies also to the TBEV replicon shown in this study, although no direct comparison with virus infection has been performed. Large foci of TBEV replicon RNA and protein accumulation were not observed, instead a diffuse

pattern with a strong perinuclear component was constantly present (Figure 25). Furthermore, when we analyzed dsRNA localization, we could show that the MS2-EYFP signal was including that of the dsRNA, clearly demonstrating that the cytoplasmic sites of MS2-tagged TBEV RNA accumulation can be exploited as a marker of TBEV replication compartments localization (Figure 26). We also found that the TBEV induced membrane compartments protect viral dsRNA from being detected by antibodies and digested by RNase treatment (Figure 27). Because of the intrinsic limit of resolution of optical microscopy we could only provide evidence of co-localization between dsRNA and tagged viral RNA. Also resistance to treatment with RNase only provides indication of their association in a membrane compartment. However, we cannot tell whether within these compartments other physical barriers exist. Indeed, they may correspond to the extremely organized RCs found in electron microscopy or there might be more secluded vesicles dedicated to viral replication that release the RNA in a larger compartment connecting replication vesicles and virion assembly sites.

During the present study, we also analyzed the composition of the membrane structures hijacked by TBEV in order to generate functional replication compartments. Consistently with what has been described also for other members of the family (Gillespie et al., 2010; Overby et al., 2010; Targett-Adams et al., 2008; Welsch et al., 2009), we showed that actively replicating TBEV RNA accumulates in compartments mostly enriched in the RER marker PDI (Figure 29; Figure 31). These compartments do not contain either the *trans*-Golgi network TGN-46 marker or the intermediate compartment ERGIC marker, but may contain the Golgi marker Giantin (in human HOS cells) (Figure 30). Hence, it appears that TBEV newly replicated ssRNA accumulates in the ER, the site of RNA translation but also the site of virus particle formation (Welsch et al., 2009). Some replicated RNA is found also associated with Golgi membranes in HOS cells indicating a possible transport along the cellular secretion pathway compatible with later stages of virus assembly, although subgenomic replicons as those used in this work lack structural proteins and are not likely to follow this pathway. Alternatively, replicated TBEV RNA localization may engage different cytoplasmic structures depending on the cell type used. These membrane wrapped compartments provide a convenient environment for efficient replication and have been also involved in protection from host surveillance (Hoenen et al., 2007). Interestingly, recent EM tomography studies of flavivirus

infected cells, clearly showed interconnections between replication vesicles and between RCs and the cytoplasm (Gillespie et al., 2010; Welsch et al., 2009). These connections, more than likely allow the recruitment of cytoplasmic factors into the vesicles and the release of the newly synthesized viral RNA to the cytosol for translation and packaging. These new findings are in contrast with the model previously proposed by Uchil and Satchidanandam who suggested closed double-layered vesicles housing the viral RNA (Uchil and Satchidanandam, 2003). However, they revealed shared features in the architecture of the replication factories with other positive-sense RNA viruses (Knoops et al., 2008; Kopek et al., 2007).

4.5. TBEV induced innate immunity activation

Although EM tomography studies revealed important information about the organization and three-dimensional structure of the flaviviral replication compartments, many critical aspects still need to be elucidated. A key unresolved question concerns the dynamic trafficking of proteins and viral RNA within the replication compartment and from/to the cytosol. This is critical since on one side cellular co-factors of virus replication need to access the replication factory, but on the other side RNA intermediates of viral replication are strong inducers of innate immunity. Signaling to interferon induction requires physical association of PRRs with viral RNA intermediates and its spatial association with the mitochondria (Onoguchi et al., 2010). Therefore a mechanism must exist that allows activation of PRRs by a viral replication RNA intermediate, that is found within cytoplasmic vesicles. Having established an effective tool to follow TBEV RNA through its intracellular trafficking, during the second part of this study we exploited the MS2 system in order to address these issues and to advance our understanding of the crucial relationship between the formation of membrane wrapped RCs and the subversion of the innate immune response.

Several groups had shown that Flaviviruses, in order to establish a productive infection have evolved different strategies against innate immunity surveillance (Fredericksen et al., 2004; Keller et al., 2007; Lin et al., 2006b; Mackenzie et al., 2007; Munoz-Jordan et al., 2005; Rodriguez-Madoz et al., 2010a). However, very

little was known about the interaction of TBEV and the type I interferon system. We have chosen U2OS cells to perform our studies since they appeared to be permissive to TBEV replication (Figure 31), as well as entirely competent for IFNβ expression (Figure 32). In agreement with what was previously proposed for WNV (Fredericksen and Gale, 2006; Fredericksen et al., 2004) and more recently also for TBEV (Overby et al., 2010), we observed that TBEV infection induces a delayed IFNβ mRNA expression (Figure 33). The same was true also when we repeated the experiment by transfecting our replicon RNAs that recapitulate all the events required for viral replication, namely: translation of the polyprotein, induction of a RC and viral RNA amplification. Indeed, despite efficient TBEV replication, induction of IFNβ expression and IRF3 translocation were delayed (Figure 34 and Figure 35) pointing towards a defect in pattern recognition receptor's signaling. This delay is not imputable to lack of PRR agonists since re-transfection of RNA extracted as early as 8 hours post replicon transfection was highly efficient in triggering the signaling (Figure 36). The nature of the agonists was not addressed, but certainly these RNAs are derived from, or induced by, viral replication since the replication-incompetent GAA construct was unable to trigger the response also upon re-transfection (Figure 36).

Typically, evasion of the innate immune response is accomplished by viral proteins that directly target IFN induction and/or signalling (Garcia-Sastre et al., 1998; Li et al., 2005; Meylan et al., 2005; Munoz-Jordan et al., 2003; Rodriguez-Madoz et al., 2010a). However, in the case of TBEV only the NS5-mediated inhibition of the interferon activated JAK/STAT pathway was previously demonstrated (Best et al., 2005; Werme et al., 2008). Therefore, we wished to investigate whether it also encodes factors that are able to antagonize the initial response, the one involved in the first induction of interferon. Interestingly, PRRs signaling stimulation either by poly (I:C) transfection or by extracts from cells electroporated with the TBEV replicon was not impaired in TBEV infected or TNd/ΔME_24×MS2 expressing cells ruling out a direct targeting of the pathway by viral proteins (Figures 37 and 38).

If the delay in PRR activation is not related to the expression of a particular viral factor able to block IRF3 nuclear translocation, then the mechanism exploited by the virus to escape IFNβ induction must be different. For example, it is possible that the establishment of a sheltered replication environment in the cytoplasm (Figure 27) is

affecting innate immunity activation by decreasing agonist availability for PRRs as well as by interfering with its signaling to the nucleus through adaptor proteins.

4.6.Dynamic trafficking of proteins and viral RNA in the cytoplasm

In order to address agonist availability by PRRs we then analyzed the dynamic exchange of protein and viral RNA between the MS2-tagged sites of replication and the cytoplasm. As already discussed, these compartments most likely represent large vesicles, connected with the cytoplasm, and full of viral RNA that travels from replication factories to virus translation and/or assembly sites. Therefore, in order to avoid confusion with the well described RCs, we would like to call these regions, defined by the mobility of viral RNA and proteins, 'dynamic' replication compartments (dRCs).

By performing FRAP analysis at different time points upon transfection we could observe a consistent delay of the recovery of fluorescence within these perinuclear regions of viral replicated RNA accumulation (Figure 39). However, free GFP showed no significant differences in its mobility within the cytosol compared to that within dRCs (Figure 41). This is a strong indication that these vesicles are open to the cytosol and allow exchange of proteins. Therefore, free accessibility of the fluorescent MS2, associated with a slow recovery after photobleaching indicates an impaired movement of the viral genomic RNA out of the dRCs. This is possibly coupled with the association of a fraction of the viral RNA with polysomes on ER membranes. Interestingly, like the GFP protein, also cytoplasmic PRRs such as RIG-I showed a similar behaviour (Figure 42). This experiment was performed 24 hours upon transfection, when signalling to interferon has been already activated. Hence, either RIG-I is not the PRR responsible for IFN induction or activation does not affect the mobility of the protein. Alternatively, the fraction of GFP-RIG-I activated is too low to be significantly detected in the FRAP experiment.

Furthermore, from the FRAP time course we could also demonstrate that the fluorescence recovery after 36 hours did not differ significantly from that at 12 hours after replicon transfection. Hence, although we cannot formally exclude that replication rates slow down at late time points, thus masking an increase of recovery

in the FRAP curve due to an increased permeability of the dRCs, we can assume that the mobility of viral RNA is similar at early time points, when triggering of the interferon response is inactive, and at late time points when IFNβ is activated. In other terms, at later time points there is not a massive disruption of replication vesicles compatible with the liberation of viral RNA and PRR agonists. To confirm this hypothesis we performed a FLIP experiment that allow to directly measure trafficking of viral RNA between the cytosol and the dRCs (Figure 43). Also this experiment was conducted at 24 hours post transfection, when the interferon response is already activated. Again, we could observe a slow release of replicated RNA from the compartment. Unfortunately, we could only confirm the presence of dsRNA replication intermediates and potential PRR agonists within dRCs by immunostaining of fixed cells (Figure 31), but we could not really address dsRNA exchange with the cytoplasm because our method monitors only replicated RNA mobility. However, from dynamic studies previously performed with components of the HCV replication complex NS4B and NS5A, which were shown to be relatively immobile when associated with active replication foci (Gretton et al., 2005; Jones et al., 2007), we can assume that also dsRNA intermediates remain confined within replicative vesicles by interacting with viral as well as host factors that are anchored to intracellular membranes.

Another important observation relates to the mobility of the tagged viral RNA within the dRCs. Previous FRAP studies performed with the HCV NS5A protein showed that the internal architecture of the membranous web is relatively static, with limited exchange of viral nonstructural proteins between neighbouring factories (Wolk et al., 2008). Here instead, for the first time, we monitored viral replicated RNA dynamics within the dRC. By continuously bleaching MS2 fluorescence in the region where the RNA is clustered, we could observe a fast depletion of fluorescence, consistent with a high mobility of the viral RNA (Figure 44). Mobility within dRCs was indeed higher than mobility between the dRC and the cytosol, confirming that a physical impediment restrict viral RNA egress from dRCs rather than an intrinsic slow mobility of the viral RNP (compare the blue line in Figure 43 and 44). However, depletion of fluorescence was clearly restricted only to a discrete region in the cluster. Therefore, the dRC is partitioned with respect to viral RNA mobility. According to these observations we can conclude that, while viral proteins represent the scaffold required for efficient replication, newly transcribed genomic RNAs can

be easily exchanged between neighboring vesicles, presumably *via* the open necks described for DENV and WNV (Gillespie et al., 2010; Welsch et al., 2009). An organized network of vesicles would certainly help in regulating genomic RNA recruitment for translation and/or packaging. Clusters of interconnected vesicles are likely originated from a single genomic RNA at the ER membrane translating the viral polyprotein that induces vesicles formation. In keeping with this interpretation, TBEV genomes show a low propensity for intermolecular recombination pointing to a physical separation of incoming viral genomes (Taucher et al., 2010).

4.7. Conclusions

In summary, we developed a powerful tool for live cell imaging studies of TBEV RNA intracellular trafficking that might also be exploited for other flaviviruses and positive strand RNA viruses. The strategy of viral RNA tagging described here complements similar approaches where a viral protein like the NS5A protein of HCV has been tagged within a replicon to visualize viral replication (Moradpour et al., 2004). This innovative method, allowed us to provide a dynamic framework of viral RNA and protein trafficking within dRCs. Consistently with the model recently proposed by Gillespie and colleagues (Gillespie et al., 2010), we showed that replicative compartments are organized in a network of interconnected vesicles that is open to the cytosol. Furthermore, we observed that in the context of a delayed innate immune response, dRCs are accessible to proteins from the cytosol but rather impermeable to replicated viral RNA egress (Figure 45). We did not address the nature of the agonist responsible for the observed delayed IFN induction, whether it is the more secluded dsRNA or some other RNA produced during virus replication. However, from our data, it is unlikely that PRR signaling is delayed by a physical barrier that undergo lysis at late time points allowing PRR agonists to become available, as recently proposed (Overby et al., 2010). Due to the limits of the technique exploited, we could not address whether the establishment of membrane wrapped replication compartments prevents the direct interaction between PRRs and their agonists or impairs the release of the PRR-RNP therefore delaying signalling to

downstream adaptors. Further studies are certainly required to answer these questions.

Nevertheless, a more detailed picture of the mechanisms exploited by TBEV to escape innate immune surveillance is emerging. At the early stages of infection viral replication within cytoplasmic compartments most likely allows the generation of sufficient viral genomes to sustain the infection before the first wave of interferon induction. Then, at later stages newly infected cells became resistant to the IFN antiviral activity by blocking the JAK-STAT signaling pathway (Werme et al., 2008).

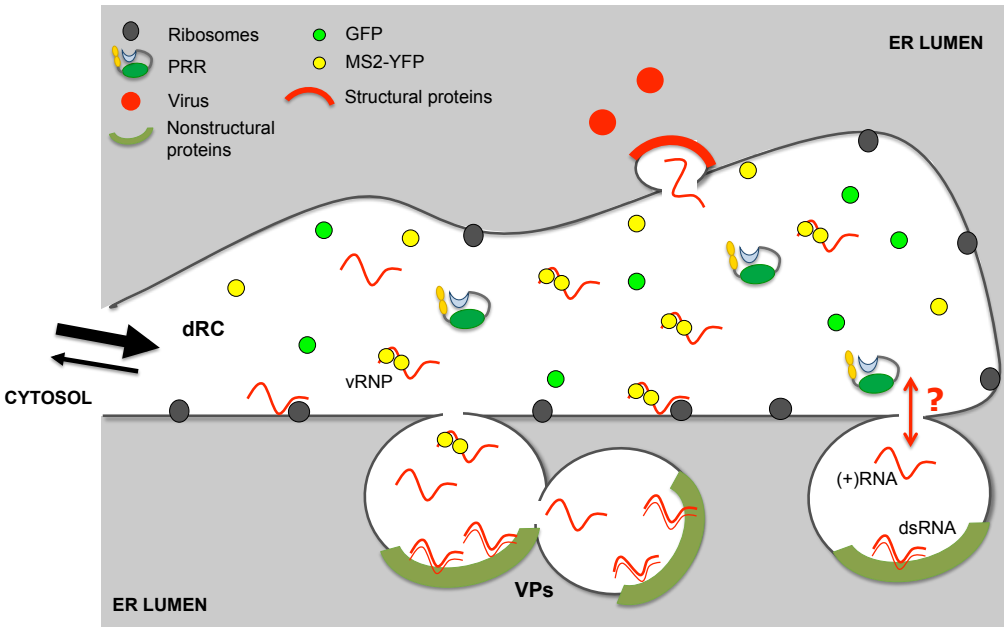

Figure 45 Schematic model of the dynamic exchange of proteins and viral RNA between the dRC and the cytoplasm. Upon infection, the viral genome, indicated as (+)RNA, associates with the rough ER (ribosomes are indicated in dark grey) and the viral polyprotein, composed by the structural (red) and non-structural (green) proteins, is synthesized. Invaginations of the ER membrane are induced, leading to the formation of vesicles packets (VPs) that are connected to the cytosol via a pore. Inside these invaginations, RNA replication occurs and the dsRNA is generated. Viral capsid protein associates with progeny RNA genomes liberated through the pore-like structure into a membrane-defined compartment connected to the cytosol. Virus budding occurs through the ER membrane of this compartment that appears located in close proximity to the replication vesicles (Welsch et al., 2009). The dRC that we describe is the compartment that connects replication vesicles and virion assembly sites. This large vesicle is full of viral RNA that travels from replication vesicles to virus translation and assembly sites and is connected to the cytoplasm. Viral RNA is unable to exit this compartment (small arrow) that is instead accessible to proteins (MS2-YFP, GFP and PRRs) and other cofactors (big arrow). The diagram is not drawn to scale.

5. REFERENCES

Ahlquist, P. (2006). Parallels among positive-strand RNA viruses, reverse-transcribing viruses and double-stranded RNA viruses. Nat Rev Microbiol *4*, 371-382.

Ainger, K., Avossa, D., Morgan, F., Hill, S.J., Barry, C., Barbarese, E., and Carson, J.H. (1993). Transport and localization of exogenous myelin basic protein mRNA microinjected into oligodendrocytes. J Cell Biol *123*, 431-441.

Akira, S., and Takeda, K. (2004). Toll-like receptor signalling. Nat Rev Immunol *4*, 499-511.

Akira, S., Uematsu, S., and Takeuchi, O. (2006). Pathogen recognition and innate immunity. Cell *124*, 783-801.

Alexopoulou, L., Holt, A.C., Medzhitov, R., and Flavell, R.A. (2001). Recognition of double-stranded RNA and activation of NF-kappaB by Toll-like receptor 3. Nature *413*, 732-738.

Alvarez, D.E., De Lella Ezcurra, A.L., Fucito, S., and Gamarnik, A.V. (2005a). Role of RNA structures present at the 3'UTR of dengue virus on translation, RNA synthesis, and viral replication. Virology *339*, 200-212.

Alvarez, D.E., Lodeiro, M.F., Luduena, S.J., Pietrasanta, L.I., and Gamarnik, A.V. (2005b). Long-range RNA-RNA interactions circularize the dengue virus genome. J Virol *79*, 6631-6643.

Ashour, J., Laurent-Rolle, M., Shi, P.Y., and Garcia-Sastre, A. (2009). NS5 of dengue virus mediates STAT2 binding and degradation. J Virol *83*, 5408-5418.

Avirutnan, P., Fuchs, A., Hauhart, R.E., Somnuke, P., Youn, S., Diamond, M.S., and Atkinson, J.P. (2010). Antagonism of the complement component C4 by flavivirus nonstructural protein NS1. J Exp Med *207*, 793-806.

Avirutnan, P., Punyadee, N., Noisakran, S., Komoltri, C., Thiemmeca, S., Auethavornanan, K., Jairungsri, A., Kanlaya, R., Tangthawornchaikul, N., Puttikhunt, C*., et al.* (2006). Vascular leakage in severe dengue virus infections: a potential role for the nonstructural viral protein NS1 and complement. J Infect Dis *193*, 1078-1088.

Axelrod, D., Koppel, D.E., Schlessinger, J., Elson, E., and Webb, W.W. (1976). Mobility measurement by analysis of fluorescence photobleaching recovery kinetics. Biophys J *16*, 1055-1069.

Baronti, C., Sire, J., de Lamballerie, X., and Querat, G. (2010). Nonstructural NS1 proteins of several mosquito-borne Flavivirus do not inhibit TLR3 signaling. Virology *404*, 319-330.

Barton, G.M., and Kagan, J.C. (2009). A cell biological view of Toll-like receptor function: regulation through compartmentalization. Nat Rev Immunol *9*, 535-542.

Basler, C.F., Mikulasova, A., Martinez-Sobrido, L., Paragas, J., Muhlberger, E., Bray, M., Klenk, H.D., Palese, P., and Garcia-Sastre, A. (2003). The Ebola virus VP35 protein inhibits activation of interferon regulatory factor 3. J Virol *77*, 7945-7956.

Basyuk, E., Galli, T., Mougel, M., Blanchard, J.M., Sitbon, M., and Bertrand, E. (2003). Retroviral genomic RNAs are transported to the plasma membrane by endosomal vesicles. Dev Cell *5*, 161-174.

Baum, A., and Garcia-Sastre, A. (2010). Induction of type I interferon by RNA viruses: cellular receptors and their substrates. Amino Acids *38*, 1283-1299.

Beach, D.L., Salmon, E.D., and Bloom, K. (1999). Localization and anchoring of mRNA in budding yeast. Curr Biol *9*, 569-578.

Beckham, C.J., Light, H.R., Nissan, T.A., Ahlquist, P., Parker, R., and Noueiry, A. (2007). Interactions between brome mosaic virus RNAs and cytoplasmic processing bodies. J Virol *81*, 9759-9768.

Bertrand, E., Chartrand, P., Schaefer, M., Shenoy, S.M., Singer, R.H., and Long, R.M. (1998). Localization of ASH1 mRNA particles in living yeast. Mol Cell *2*, 437-445.

Best, S.M., Morris, K.L., Shannon, J.G., Robertson, S.J., Mitzel, D.N., Park, G.S., Boer, E., Wolfinbarger, J.B., and Bloom, M.E. (2005). Inhibition of interferon-stimulated JAK-STAT signaling by a tick-borne flavivirus and identification of NS5 as an interferon antagonist. J Virol *79*, 12828-12839.

Beutler, B., Eidenschenk, C., Crozat, K., Imler, J.L., Takeuchi, O., Hoffmann, J.A., and Akira, S. (2007). Genetic analysis of resistance to viral infection. Nat Rev Immunol *7*, 753-766.

Bode, J.G., Brenndorfer, E.D., and Haussinger, D. (2007). Subversion of innate host antiviral strategies by the hepatitis C virus. Arch Biochem Biophys *462*, 254-265.

Boireau, S., Maiuri, P., Basyuk, E., de la Mata, M., Knezevich, A., Pradet-Balade, B., Backer, V., Kornblihtt, A., Marcello, A., and Bertrand, E. (2007). The transcriptional cycle of HIV-1 in real-time and live cells. J Cell Biol *179*, 291-304.

Brawner, I.A., Trousdale, M.D., and Trent, D.W. (1979). Cellular localization of Saint Louis encephalitis virus replication. Acta Virol *23*, 284-294.

Bressanelli, S., Stiasny, K., Allison, S.L., Stura, E.A., Duquerroy, S., Lescar, J., Heinz, F.X., and Rey, F.A. (2004). Structure of a flavivirus envelope glycoprotein in its low-pH-induced membrane fusion conformation. EMBO J *23*, 728-738.

Brinton, M.A., and Dispoto, J.H. (1988). Sequence and secondary structure analysis of the 5'-terminal region of flavivirus genome RNA. Virology *162*, 290-299.

Buckley, A., Gaidamovich, S., Turchinskaya, A., and Gould, E.A. (1992). Monoclonal antibodies identify the NS5 yellow fever virus non-structural protein in the nuclei of infected cells. J Gen Virol *73 (Pt 5)*, 1125-1130.

Cardenas, W.B., Loo, Y.M., Gale, M., Jr., Hartman, A.L., Kimberlin, C.R., Martinez-Sobrido, L., Saphire, E.O., and Basler, C.F. (2006). Ebola virus VP35 protein binds double-stranded RNA and inhibits alpha/beta interferon production induced by RIG-I signaling. J Virol *80*, 5168-5178.

Chambers, T.J., Grakoui, A., and Rice, C.M. (1991). Processing of the yellow fever virus nonstructural polyprotein: a catalytically active NS3 proteinase domain and NS2B are required for cleavages at dibasic sites. J Virol *65*, 6042-6050.

Chambers, T.J., Weir, R.C., Grakoui, A., McCourt, D.W., Bazan, J.F., Fletterick, R.J., and Rice, C.M. (1990). Evidence that the N-terminal domain of nonstructural protein NS3 from

yellow fever virus is a serine protease responsible for site-specific cleavages in the viral polyprotein. Proc Natl Acad Sci U S A *87*, 8898-8902.

Chang, T.H., Liao, C.L., and Lin, Y.L. (2006). Flavivirus induces interferon-beta gene expression through a pathway involving RIG-I-dependent IRF-3 and PI3K-dependent NF-kappaB activation. Microbes Infect *8*, 157-171.

Choo, Q.L., Kuo, G., Weiner, A.J., Overby, L.R., Bradley, D.W., and Houghton, M. (1989). Isolation of a cDNA clone derived from a blood-borne non-A, non-B viral hepatitis genome. Science *244*, 359-362.

Chu, P.W., and Westaway, E.G. (1985). Replication strategy of Kunjin virus: evidence for recycling role of replicative form RNA as template in semiconservative and asymmetric replication. Virology *140*, 68-79.

Chung, K.M., Nybakken, G.E., Thompson, B.S., Engle, M.J., Marri, A., Fremont, D.H., and Diamond, M.S. (2006). Antibodies against West Nile Virus nonstructural protein NS1 prevent lethal infection through Fc gamma receptor-dependent and -independent mechanisms. J Virol *80*, 1340-1351.

Cleaves, G.R., Ryan, T.E., and Schlesinger, R.W. (1981). Identification and characterization of type 2 dengue virus replicative intermediate and replicative form RNAs. Virology *111*, 73-83.

Cole, N.B., Smith, C.L., Sciaky, N., Terasaki, M., Edidin, M., and Lippincott-Schwartz, J. (1996). Diffusional mobility of Golgi proteins in membranes of living cells. Science *273*, 797-801.

Cui, S., Eisenacher, K., Kirchhofer, A., Brzozka, K., Lammens, A., Lammens, K., Fujita, T., Conzelmann, K.K., Krug, A., and Hopfner, K.P. (2008). The C-terminal regulatory domain is the RNA 5'-triphosphate sensor of RIG-I. Mol Cell *29*, 169-179.

Cui, Z.Q., Zhang, Z.P., Zhang, X.E., Wen, J.K., Zhou, Y.F., and Xie, W.H. (2005). Visualizing the dynamic behavior of poliovirus plus-strand RNA in living host cells. Nucleic Acids Res *33*, 3245-3252.

Daffis, S., Samuel, M.A., Suthar, M.S., Gale, M., Jr., and Diamond, M.S. (2008). Toll-like receptor 3 has a protective role against West Nile virus infection. J Virol *82*, 10349-10358.
Daffis, S., Szretter, K.J., Schriewer, J., Li, J., Youn, S., Errett, J., Lin, T.Y., Schneller, S., Zust, R., Dong, H., *et al.* (2010). 2'-O methylation of the viral mRNA cap evades host restriction by IFIT family members. Nature *468*, 452-456.

Daigle, N., and Ellenberg, J. (2007). LambdaN-GFP: an RNA reporter system for live-cell imaging. Nat Methods *4*, 633-636.

Darzacq, X., Shav-Tal, Y., de Turris, V., Brody, Y., Shenoy, S.M., Phair, R.D., and Singer, R.H. (2007). In vivo dynamics of RNA polymerase II transcription. Nat Struct Mol Biol *14*, 796-806.

Dayel, M.J., Hom, E.F., and Verkman, A.S. (1999). Diffusion of green fluorescent protein in the aqueous-phase lumen of endoplasmic reticulum. Biophys J *76*, 2843-2851.

den Boon, J.A., Diaz, A., and Ahlquist, P. (2010). Cytoplasmic viral replication complexes. Cell Host Microbe *8*, 77-85.

Diamond, M.S., and Harris, E. (2001). Interferon inhibits dengue virus infection by preventing translation of viral RNA through a PKR-independent mechanism. Virology *289*, 297-311.

Diebold, S.S., Kaisho, T., Hemmi, H., Akira, S., and Reis e Sousa, C. (2004). Innate antiviral responses by means of TLR7-mediated recognition of single-stranded RNA. Science *303*, 1529-1531.

Donelan, N.R., Basler, C.F., and Garcia-Sastre, A. (2003). A recombinant influenza A virus expressing an RNA-binding-defective NS1 protein induces high levels of beta interferon and is attenuated in mice. J Virol *77*, 13257-13266.

Dundr, M., Hoffmann-Rohrer, U., Hu, Q., Grummt, I., Rothblum, L.I., Phair, R.D., and Misteli, T. (2002). A kinetic framework for a mammalian RNA polymerase in vivo. Science *298*, 1623-1626.

Dundr, M., and Misteli, T. (2003). Measuring dynamics of nuclear proteins by photobleaching. Curr Protoc Cell Biol *Chapter 13*, Unit 13 15.

Edelmann, K.H., Richardson-Burns, S., Alexopoulou, L., Tyler, K.L., Flavell, R.A., and Oldstone, M.B. (2004). Does Toll-like receptor 3 play a biological role in virus infections? Virology *322*, 231-238.

Erbel, P., Schiering, N., D'Arcy, A., Renatus, M., Kroemer, M., Lim, S.P., Yin, Z., Keller, T.H., Vasudevan, S.G., and Hommel, U. (2006). Structural basis for the activation of flaviviral NS3 proteases from dengue and West Nile virus. Nat Struct Mol Biol *13*, 372-373.

Evans, J.D., and Seeger, C. (2007). Differential effects of mutations in NS4B on West Nile virus replication and inhibition of interferon signaling. J Virol *81*, 11809-11816.

Falgout, B., Miller, R.H., and Lai, C.J. (1993). Deletion analysis of dengue virus type 4 nonstructural protein NS2B: identification of a domain required for NS2B-NS3 protease activity. J Virol *67*, 2034-2042.

Fernandez-Garcia, M.D., Mazzon, M., Jacobs, M., and Amara, A. (2009). Pathogenesis of flavivirus infections: using and abusing the host cell. Cell Host Microbe *5*, 318-328.

Flanegan, J.B., Petterson, R.F., Ambros, V., Hewlett, N.J., and Baltimore, D. (1977). Covalent linkage of a protein to a defined nucleotide sequence at the 5'-terminus of virion and replicative intermediate RNAs of poliovirus. Proc Natl Acad Sci U S A *74*, 961-965.

Fraefel, C., Bittermann, A.G., Bueler, H., Heid, I., Bachi, T., and Ackermann, M. (2004). Spatial and temporal organization of adeno-associated virus DNA replication in live cells. J Virol *78*, 389-398.

Fredericksen, B.L., and Gale, M., Jr. (2006). West Nile virus evades activation of interferon regulatory factor 3 through RIG-I-dependent and -independent pathways without antagonizing host defense signaling. J Virol *80*, 2913-2923.

Fredericksen, B.L., Keller, B.C., Fornek, J., Katze, M.G., and Gale, M., Jr. (2008). Establishment and maintenance of the innate antiviral response to West Nile Virus involves both RIG-I and MDA5 signaling through IPS-1. J Virol *82*, 609-616.

Fredericksen, B.L., Smith, M., Katze, M.G., Shi, P.Y., and Gale, M., Jr. (2004). The host response to West Nile Virus infection limits viral spread through the activation of the interferon regulatory factor 3 pathway. J Virol *78*, 7737-7747.

Friebe, P., and Bartenschlager, R. (2002). Genetic analysis of sequences in the 3' nontranslated region of hepatitis C virus that are important for RNA replication. J Virol *76*, 5326-5338.

Fusco, D., Accornero, N., Lavoie, B., Shenoy, S.M., Blanchard, J.M., Singer, R.H., and Bertrand, E. (2003). Single mRNA molecules demonstrate probabilistic movement in living mammalian cells. Curr Biol *13*, 161-167.

Gack, M.U., Albrecht, R.A., Urano, T., Inn, K.S., Huang, I.C., Carnero, E., Farzan, M., Inoue, S., Jung, J.U., and Garcia-Sastre, A. (2009). Influenza A virus NS1 targets the ubiquitin ligase TRIM25 to evade recognition by the host viral RNA sensor RIG-I. Cell Host Microbe *5*, 439-449.

Garcia-Sastre, A., Egorov, A., Matassov, D., Brandt, S., Levy, D.E., Durbin, J.E., Palese, P., and Muster, T. (1998). Influenza A virus lacking the NS1 gene replicates in interferon-deficient systems. Virology *252*, 324-330.

Gehrke, R., Heinz, F.X., Davis, N.L., and Mandl, C.W. (2005). Heterologous gene expression by infectious and replicon vectors derived from tick-borne encephalitis virus and direct comparison of this flavivirus system with an alphavirus replicon. J Gen Virol *86*, 1045-1053.

Gillespie, L.K., Hoenen, A., Morgan, G., and Mackenzie, J.M. (2010). The Endoplasmic reticulum provides the membrane platform for biogenesis of the flavivirus replication complex. J Virol.

Gould, E.A., and Solomon, T. (2008). Pathogenic flaviviruses. Lancet *371*, 500-509.

Gretton, S.N., Taylor, A.I., and McLauchlan, J. (2005). Mobility of the hepatitis C virus NS4B protein on the endoplasmic reticulum membrane and membrane-associated foci. J Gen Virol *86*, 1415-1421.

Grief, C., Galler, R., Cortes, L.M., and Barth, O.M. (1997). Intracellular localisation of dengue-2 RNA in mosquito cell culture using electron microscopic in situ hybridisation. Arch Virol *142*, 2347-2357.

Gritsun, T.S., and Gould, E.A. (2007). Origin and evolution of flavivirus 5'UTRs and panhandles: trans-terminal duplications? Virology *366*, 8-15.

Gubler, D.J., Kuno, G., and Markoff, L. (2007). Flaviviruses. In Fields Virology, D.M. Knipe, P.M. Howley, D.E. Griffin, R.A. Lamb, and M.A. Martin, eds. (Philadelphia: Lippincott, Williams & Wilkins), pp. 1153-1252.

Guirakhoo, F., Heinz, F.X., Mandl, C.W., Holzmann, H., and Kunz, C. (1991). Fusion activity of flaviviruses: comparison of mature and immature (prM-containing) tick-borne encephalitis virions. J Gen Virol *72 (Pt 6)*, 1323-1329.

Guo, J.T., Hayashi, J., and Seeger, C. (2005). West Nile virus inhibits the signal transduction pathway of alpha interferon. J Virol *79*, 1343-1350.

Guo, Z., Chen, L.M., Zeng, H., Gomez, J.A., Plowden, J., Fujita, T., Katz, J.M., Donis, R.O., and Sambhara, S. (2007). NS1 protein of influenza A virus inhibits the function of intracytoplasmic pathogen sensor, RIG-I. Am J Respir Cell Mol Biol *36*, 263-269.

Habjan, M., Andersson, I., Klingstrom, J., Schumann, M., Martin, A., Zimmermann, P., Wagner, V., Pichlmair, A., Schneider, U., Muhlberger, E.*, et al.* (2008). Processing of genome 5' termini as a strategy of negative-strand RNA viruses to avoid RIG-I-dependent interferon induction. PLoS One *3*, e2032.

Hahn, C.S., Hahn, Y.S., Rice, C.M., Lee, E., Dalgarno, L., Strauss, E.G., and Strauss, J.H. (1987). Conserved elements in the 3' untranslated region of flavivirus RNAs and potential cyclization sequences. J Mol Biol *198*, 33-41.

Han, X., Aho, M., Vene, S., Peltomaa, M., Vaheri, A., and Vapalahti, O. (2001). Prevalence of tick-borne encephalitis virus in Ixodes ricinus ticks in Finland. J Med Virol *64*, 21-28.

Hardarson, H.S., Baker, J.S., Yang, Z., Purevjav, E., Huang, C.H., Alexopoulou, L., Li, N., Flavell, R.A., Bowles, N.E., and Vallejo, J.G. (2007). Toll-like receptor 3 is an essential component of the innate stress response in virus-induced cardiac injury. Am J Physiol Heart Circ Physiol *292*, H251-258.

Heaton, N.S., Perera, R., Berger, K.L., Khadka, S., Lacount, D.J., Kuhn, R.J., and Randall, G. (2010). Dengue virus nonstructural protein 3 redistributes fatty acid synthase to sites of viral replication and increases cellular fatty acid synthesis. Proc Natl Acad Sci U S A *107*, 17345-17350.

Heil, F., Hemmi, H., Hochrein, H., Ampenberger, F., Kirschning, C., Akira, S., Lipford, G., Wagner, H., and Bauer, S. (2004). Species-specific recognition of single-stranded RNA via toll-like receptor 7 and 8. Science *303*, 1526-1529.

Heinz, F.X., and Allison, S.L. (2003). Flavivirus structure and membrane fusion. Adv Virus Res *59*, 63-97.

Heinz, F.X., Allison, S.L., Stiasny, K., Schalich, J., Holzmann, H., Mandl, C.W., and Kunz, C. (1995). Recombinant and virion-derived soluble and particulate immunogens for vaccination against tick-borne encephalitis. Vaccine *13*, 1636-1642.

Hoenen, A., Liu, W., Kochs, G., Khromykh, A.A., and Mackenzie, J.M. (2007). West Nile virus-induced cytoplasmic membrane structures provide partial protection against the interferon-induced antiviral MxA protein. J Gen Virol *88*, 3013-3017.

Hoenninger, V.M., Rouha, H., Orlinger, K.K., Miorin, L., Marcello, A., Kofler, R.M., and Mandl, C.W. (2008). Analysis of the effects of alterations in the tick-borne encephalitis virus 3'-noncoding region on translation and RNA replication using reporter replicons. Virology *377*, 419-430.

Holden, K.L., and Harris, E. (2004). Enhancement of dengue virus translation: role of the 3' untranslated region and the terminal 3' stem-loop domain. Virology *329*, 119-133.

Hornung, V., Ellegast, J., Kim, S., Brzozka, K., Jung, A., Kato, H., Poeck, H., Akira, S., Conzelmann, K.K., Schlee, M.*, et al.* (2006). 5'-Triphosphate RNA is the ligand for RIG-I. Science *314*, 994-997.

Iacono-Connors, L.C., Smith, J.F., Ksiazek, T.G., Kelley, C.L., and Schmaljohn, C.S. (1996). Characterization of Langat virus antigenic determinants defined by monoclonal

antibodies to E, NS1 and preM and identification of a protective, non-neutralizing preM-specific monoclonal antibody. Virus Res *43*, 125-136.

Janicki, S.M., Tsukamoto, T., Salghetti, S.E., Tansey, W.P., Sachidanandam, R., Prasanth, K.V., Ried, T., Shav-Tal, Y., Bertrand, E., Singer, R.H., and Spector, D.L. (2004). From silencing to gene expression: real-time analysis in single cells. Cell *116*, 683-698.

Jones, D.M., Domingues, P., Targett-Adams, P., and McLauchlan, J. (2010). Comparison of U2OS and Huh-7 cells for identifying host factors that affect hepatitis C virus RNA replication. J Gen Virol *91*, 2238-2248.

Jones, D.M., Gretton, S.N., McLauchlan, J., and Targett-Adams, P. (2007). Mobility analysis of an NS5A-GFP fusion protein in cells actively replicating hepatitis C virus subgenomic RNA. J Gen Virol *88*, 470-475.

Kato, H., Sato, S., Yoneyama, M., Yamamoto, M., Uematsu, S., Matsui, K., Tsujimura, T., Takeda, K., Fujita, T., Takeuchi, O., and Akira, S. (2005). Cell type-specific involvement of RIG-I in antiviral response. Immunity *23*, 19-28.

Kato, H., Takeuchi, O., Mikamo-Satoh, E., Hirai, R., Kawai, T., Matsushita, K., Hiiragi, A., Dermody, T.S., Fujita, T., and Akira, S. (2008). Length-dependent recognition of double-stranded ribonucleic acids by retinoic acid-inducible gene-I and melanoma differentiation-associated gene 5. J Exp Med *205*, 1601-1610.

Kato, H., Takeuchi, O., Sato, S., Yoneyama, M., Yamamoto, M., Matsui, K., Uematsu, S., Jung, A., Kawai, T., Ishii, K.J*., et al.* (2006). Differential roles of MDA5 and RIG-I helicases in the recognition of RNA viruses. Nature *441*, 101-105.

Kaufmann, B., and Rossmann, M.G. (2011). Molecular mechanisms involved in the early steps of flavivirus cell entry. Microbes Infect *13*, 1-9.

Kawai, T., and Akira, S. (2011). Toll-like Receptors and Their Crosstalk with Other Innate Receptors in Infection and Immunity. Immunity *34*, 637-650.

Kawai, T., Takahashi, K., Sato, S., Coban, C., Kumar, H., Kato, H., Ishii, K.J., Takeuchi, O., and Akira, S. (2005). IPS-1, an adaptor triggering RIG-I- and Mda5-mediated type I interferon induction. Nat Immunol *6*, 981-988.

Keller, B.C., Johnson, C.L., Erickson, A.K., and Gale, M., Jr. (2007). Innate immune evasion by hepatitis C virus and West Nile virus. Cytokine Growth Factor Rev *18*, 535-544.

Khromykh, A.A., Kenney, M.T., and Westaway, E.G. (1998). trans-Complementation of flavivirus RNA polymerase gene NS5 by using Kunjin virus replicon-expressing BHK cells. J Virol *72*, 7270-7279.

Khromykh, A.A., Meka, H., Guyatt, K.J., and Westaway, E.G. (2001). Essential role of cyclization sequences in flavivirus RNA replication. J Virol *75*, 6719-6728.

Knoops, K., Kikkert, M., Worm, S.H., Zevenhoven-Dobbe, J.C., van der Meer, Y., Koster, A.J., Mommaas, A.M., and Snijder, E.J. (2008). SARS-coronavirus replication is supported by a reticulovesicular network of modified endoplasmic reticulum. PLoS Biol *6*, e226.

Kofler, R.M., Heinz, F.X., and Mandl, C.W. (2002). Capsid protein C of tick-borne encephalitis virus tolerates large internal deletions and is a favorable target for attenuation of virulence. J Virol *76*, 3534-3543.

Kofler, R.M., Hoenninger, V.M., Thurner, C., and Mandl, C.W. (2006). Functional analysis of the tick-borne encephalitis virus cyclization elements indicates major differences between mosquito-borne and tick-borne flaviviruses. J Virol *80*, 4099-4113.

Kopek, B.G., Perkins, G., Miller, D.J., Ellisman, M.H., and Ahlquist, P. (2007). Three-dimensional analysis of a viral RNA replication complex reveals a virus-induced mini-organelle. PLoS Biol *5*, e220.

Krishnan, M.N., Sukumaran, B., Pal, U., Agaisse, H., Murray, J.L., Hodge, T.W., and Fikrig, E. (2007). Rab 5 is required for the cellular entry of dengue and West Nile viruses. J Virol *81*, 4881-4885.

Kroschewski, H., Allison, S.L., Heinz, F.X., and Mandl, C.W. (2003). Role of heparan sulfate for attachment and entry of tick-borne encephalitis virus. Virology *308*, 92-100.

Kula, A., Guerra, J., Knezevich, A., Kleva, D., Myers, M.P., and Marcello, A. (2011). Characterization of the HIV-1 RNA associated proteome identifies Matrin 3 as a nuclear cofactor of Rev function. Retrovirology *8*, 60.

Kummerer, B.M., and Rice, C.M. (2002). Mutations in the yellow fever virus nonstructural protein NS2A selectively block production of infectious particles. J Virol *76*, 4773-4784.

Lange, S., Katayama, Y., Schmid, M., Burkacky, O., Brauchle, C., Lamb, D.C., and Jansen, R.P. (2008). Simultaneous transport of different localized mRNA species revealed by live-cell imaging. Traffic *9*, 1256-1267.

Lee, Y.F., Nomoto, A., Detjen, B.M., and Wimmer, E. (1977). A protein covalently linked to poliovirus genome RNA. Proc Natl Acad Sci U S A *74*, 59-63.

Leung, J.Y., Pijlman, G.P., Kondratieva, N., Hyde, J., Mackenzie, J.M., and Khromykh, A.A. (2008). Role of nonstructural protein NS2A in flavivirus assembly. J Virol *82*, 4731-4741.

Leyssen, P., De Clercq, E., and Neyts, J. (2000). Perspectives for the treatment of infections with Flaviviridae. Clin Microbiol Rev *13*, 67-82, table of contents.

Li, X.D., Sun, L., Seth, R.B., Pineda, G., and Chen, Z.J. (2005). Hepatitis C virus protease NS3/4A cleaves mitochondrial antiviral signaling protein off the mitochondria to evade innate immunity. Proc Natl Acad Sci U S A *102*, 17717-17722.

Lin, R., Lacoste, J., Nakhaei, P., Sun, Q., Yang, L., Paz, S., Wilkinson, P., Julkunen, I., Vitour, D., Meurs, E., and Hiscott, J. (2006a). Dissociation of a MAVS/IPS-1/VISA/Cardif-IKK{varepsilon} Molecular Complex from the Mitochondrial Outer Membrane by Hepatitis C Virus NS3-4A Proteolytic Cleavage. J Virol *80*, 6072 - 6083.

Lin, R.J., Chang, B.L., Yu, H.P., Liao, C.L., and Lin, Y.L. (2006b). Blocking of interferon-induced Jak-Stat signaling by Japanese encephalitis virus NS5 through a protein tyrosine phosphatase-mediated mechanism. J Virol *80*, 5908-5918.

Lindenbach, B.D., and Rice, C.M. (1999). Genetic interaction of flavivirus nonstructural proteins NS1 and NS4A as a determinant of replicase function. J Virol *73*, 4611-4621.

Lindenbach, B.D., Thiel, H.J., and Rice, C.M. (2007). Flaviviridae: the viruses and their replication. In Fields Virology, D.M. Knipe, P.M. Howley, D.E. Griffin, R.A. Lamb, and M.A. Martin, eds. (Philadelphia: Lippincott, Williams & Wilkins), pp. 1101-1152.

Lippincott-Schwartz, J., Altan-Bonnet, N., and Patterson, G.H. (2003). Photobleaching and photoactivation: following protein dynamics in living cells. Nat Cell Biol *Suppl*, S7-14.

Lippincott-Schwartz, J., and Patterson, G.H. (2003). Development and use of fluorescent protein markers in living cells. Science *300*, 87-91.

Lippincott-Schwartz, J., Snapp, E., and Kenworthy, A. (2001). Studying protein dynamics in living cells. Nat Rev Mol Cell Biol *2*, 444-456.

Liu, W.J., Chen, H.B., Wang, X.J., Huang, H., and Khromykh, A.A. (2004). Analysis of adaptive mutations in Kunjin virus replicon RNA reveals a novel role for the flavivirus nonstructural protein NS2A in inhibition of beta interferon promoter-driven transcription. J Virol *78*, 12225-12235.

Liu, W.J., Wang, X.J., Mokhonov, V.V., Shi, P.Y., Randall, R., and Khromykh, A.A. (2005). Inhibition of interferon signaling by the New York 99 strain and Kunjin subtype of West Nile virus involves blockage of STAT1 and STAT2 activation by nonstructural proteins. J Virol *79*, 1934-1942.

Lo, M.K., Tilgner, M., Bernard, K.A., and Shi, P.Y. (2003). Functional analysis of mosquito-borne flavivirus conserved sequence elements within 3' untranslated region of West Nile virus by use of a reporting replicon that differentiates between viral translation and RNA replication. J Virol *77*, 10004-10014.

Loo, Y.M., Fornek, J., Crochet, N., Bajwa, G., Perwitasari, O., Martinez-Sobrido, L., Akira, S., Gill, M.A., Garcia-Sastre, A., Katze, M.G., and Gale, M., Jr. (2008). Distinct RIG-I and MDA5 signaling by RNA viruses in innate immunity. J Virol *82*, 335-345.

Loo, Y.M., and Gale, M., Jr. (2011). Immune Signaling by RIG-I-like Receptors. Immunity *34*, 680-692.

Loo, Y.M., Owen, D.M., Li, K., Erickson, A.K., Johnson, C.L., Fish, P.M., Carney, D.S., Wang, T., Ishida, H., Yoneyama, M.*, et al.* (2006). Viral and therapeutic control of IFN-beta promoter stimulator 1 during hepatitis C virus infection. Proc Natl Acad Sci U S A *103*, 6001-6006.

Lorenz, I.C., Kartenbeck, J., Mezzacasa, A., Allison, S.L., Heinz, F.X., and Helenius, A. (2003). Intracellular assembly and secretion of recombinant subviral particles from tick-borne encephalitis virus. J Virol *77*, 4370-4382.

Ludwig, S., Wang, X., Ehrhardt, C., Zheng, H., Donelan, N., Planz, O., Pleschka, S., Garcia-Sastre, A., Heins, G., and Wolff, T. (2002). The influenza A virus NS1 protein inhibits activation of Jun N-terminal kinase and AP-1 transcription factors. J Virol *76*, 11166-11171.

Lund, J.M., Alexopoulou, L., Sato, A., Karow, M., Adams, N.C., Gale, N.W., Iwasaki, A., and Flavell, R.A. (2004). Recognition of single-stranded RNA viruses by Toll-like receptor 7. Proc Natl Acad Sci U S A *101*, 5598-5603.

Ma, L., Jones, C.T., Groesch, T.D., Kuhn, R.J., and Post, C.B. (2004). Solution structure of dengue virus capsid protein reveals another fold. Proc Natl Acad Sci U S A *101*, 3414-3419.

Mackenzie, J. (2005). Wrapping things up about virus RNA replication. Traffic *6*, 967-977.

Mackenzie, J.M., Jones, M.K., and Westaway, E.G. (1999). Markers for trans-Golgi membranes and the intermediate compartment localize to induced membranes with distinct replication functions in flavivirus-infected cells. J Virol *73*, 9555-9567.

Mackenzie, J.M., Jones, M.K., and Young, P.R. (1996). Immunolocalization of the dengue virus nonstructural glycoprotein NS1 suggests a role in viral RNA replication. Virology *220*, 232-240.

Mackenzie, J.M., Khromykh, A.A., Jones, M.K., and Westaway, E.G. (1998). Subcellular localization and some biochemical properties of the flavivirus Kunjin nonstructural proteins NS2A and NS4A. Virology *245*, 203-215.

Mackenzie, J.M., Khromykh, A.A., and Parton, R.G. (2007). Cholesterol manipulation by West Nile virus perturbs the cellular immune response. Cell Host Microbe *2*, 229-239.

Mackenzie, J.M., Khromykh, A.A., and Westaway, E.G. (2001). Stable expression of noncytopathic Kunjin replicons simulates both ultrastructural and biochemical characteristics observed during replication of Kunjin virus. Virology *279*, 161-172.

Mackenzie, J.M., and Westaway, E.G. (2001). Assembly and maturation of the flavivirus Kunjin virus appear to occur in the rough endoplasmic reticulum and along the secretory pathway, respectively. J Virol *75*, 10787-10799.

Mackenzie, J.S., Gubler, D.J., and Petersen, L.R. (2004). Emerging flaviviruses: the spread and resurgence of Japanese encephalitis, West Nile and dengue viruses. Nat Med *10*, S98-109.

Maiuri, P., Knezevich, A., Bertrand, E., and Marcello, A. (2010). Real-time imaging of the HIV-1 transcription cycle in single living cells. Methods.

Mandl, C.W. (2005). Steps of the tick-borne encephalitis virus replication cycle that affect neuropathogenesis. Virus Res *111*, 161-174.

Mandl, C.W., Ecker, M., Holzmann, H., Kunz, C., and Heinz, F.X. (1997). Infectious cDNA clones of tick-borne encephalitis virus European subtype prototypic strain Neudoerfl and high virulence strain Hypr. J Gen Virol *78 (Pt 5)*, 1049-1057.

Mandl, C.W., Holzmann, H., Kunz, C., and Heinz, F.X. (1993). Complete genomic sequence of Powassan virus: evaluation of genetic elements in tick-borne versus mosquito-borne flaviviruses. Virology *194*, 173-184.

Mandl, C.W., Holzmann, H., Meixner, T., Rauscher, S., Stadler, P.F., Allison, S.L., and Heinz, F.X. (1998). Spontaneous and engineered deletions in the 3' noncoding region of tick-borne encephalitis virus: construction of highly attenuated mutants of a flavivirus. J Virol *72*, 2132-2140.

Mandl, C.W., Kroschewski, H., Allison, S.L., Kofler, R., Holzmann, H., Meixner, T., and Heinz, F.X. (2001). Adaptation of tick-borne encephalitis virus to BHK-21 cells results in the formation of multiple heparan sulfate binding sites in the envelope protein and attenuation in vivo. J Virol *75*, 5627-5637.

Mandl, C.W., Kunz, C., and Heinz, F.X. (1991). Presence of poly(A) in a flavivirus: significant differences between the 3' noncoding regions of the genomic RNAs of tick-borne encephalitis virus strains. J Virol *65*, 4070-4077.

Markoff, L. (2003). 5'- and 3'-noncoding regions in flavivirus RNA. Adv Virus Res *59*, 177-228.

Mazzon, M., Jones, M., Davidson, A., Chain, B., and Jacobs, M. (2009). Dengue virus NS5 inhibits interferon-alpha signaling by blocking signal transducer and activator of transcription 2 phosphorylation. J Infect Dis *200*, 1261-1270.

Meylan, E., Curran, J., Hofmann, K., Moradpour, D., Binder, M., Bartenschlager, R., and Tschopp, J. (2005). Cardif is an adaptor protein in the RIG-I antiviral pathway and is targeted by hepatitis C virus. Nature *437*, 1167-1172.

Mibayashi, M., Martinez-Sobrido, L., Loo, Y.M., Cardenas, W.B., Gale, M., Jr., and Garcia-Sastre, A. (2007). Inhibition of retinoic acid-inducible gene I-mediated induction of beta interferon by the NS1 protein of influenza A virus. J Virol *81*, 514-524.

Miller, S., Kastner, S., Krijnse-Locker, J., Buhler, S., and Bartenschlager, R. (2007). The non-structural protein 4A of dengue virus is an integral membrane protein inducing membrane alterations in a 2K-regulated manner. J Biol Chem *282*, 8873-8882.

Miller, S., and Krijnse-Locker, J. (2008). Modification of intracellular membrane structures for virus replication. Nat Rev Microbiol *6*, 363-374.

Miorin, L., Maiuri, P., Hoenninger, V.M., Mandl, C.W., and Marcello, A. (2008). Spatial and temporal organization of tick-borne encephalitis flavivirus replicated RNA in living cells. Virology *379*, 64-77.

Molle, D., Maiuri, P., Boireau, S., Bertrand, E., Knezevich, A., Marcello, A., and Basyuk, E. (2007). A real-time view of the TAR:Tat:P-TEFb complex at HIV-1 transcription sites. Retrovirology *4*, 36.

Moradpour, D., Evans, M.J., Gosert, R., Yuan, Z., Blum, H.E., Goff, S.P., Lindenbach, B.D., and Rice, C.M. (2004). Insertion of green fluorescent protein into nonstructural protein 5A allows direct visualization of functional hepatitis C virus replication complexes. J Virol *78*, 7400-7409.

Mukhopadhyay, S., Kuhn, R.J., and Rossmann, M.G. (2005). A structural perspective of the flavivirus life cycle. Nat Rev Microbiol *3*, 13-22.

Munoz-Jordan, J.L., Laurent-Rolle, M., Ashour, J., Martinez-Sobrido, L., Ashok, M., Lipkin, W.I., and Garcia-Sastre, A. (2005). Inhibition of alpha/beta interferon signaling by the NS4B protein of flaviviruses. J Virol *79*, 8004-8013.

Munoz-Jordan, J.L., Sanchez-Burgos, G.G., Laurent-Rolle, M., and Garcia-Sastre, A. (2003). Inhibition of interferon signaling by dengue virus. Proc Natl Acad Sci U S A *100*, 14333-14338.

Muylaert, I.R., Chambers, T.J., Galler, R., and Rice, C.M. (1996). Mutagenesis of the N-linked glycosylation sites of the yellow fever virus NS1 protein: effects on virus replication and mouse neurovirulence. Virology *222*, 159-168.

Muylaert, I.R., Galler, R., and Rice, C.M. (1997). Genetic analysis of the yellow fever virus NS1 protein: identification of a temperature-sensitive mutation which blocks RNA accumulation. J Virol *71*, 291-298.

Myong, S., Cui, S., Cornish, P.V., Kirchhofer, A., Gack, M.U., Jung, J.U., Hopfner, K.P., and Ha, T. (2009). Cytosolic viral sensor RIG-I is a 5'-triphosphate-dependent translocase on double-stranded RNA. Science *323*, 1070-1074.

Nehls, S., Snapp, E.L., Cole, N.B., Zaal, K.J., Kenworthy, A.K., Roberts, T.H., Ellenberg, J., Presley, J.F., Siggia, E., and Lippincott-Schwartz, J. (2000). Dynamics and retention of misfolded proteins in native ER membranes. Nat Cell Biol *2*, 288-295.

Ng, M.L., and Hong, S.S. (1989). Flavivirus infection: essential ultrastructural changes and association of Kunjin virus NS3 protein with microtubules. Arch Virol *106*, 103-120.

Novoa, R.R., Calderita, G., Arranz, R., Fontana, J., Granzow, H., and Risco, C. (2005). Virus factories: associations of cell organelles for viral replication and morphogenesis. Biol Cell *97*, 147-172.

Onoguchi, K., Onomoto, K., Takamatsu, S., Jogi, M., Takemura, A., Morimoto, S., Julkunen, I., Namiki, H., Yoneyama, M., and Fujita, T. (2010). Virus-infection or 5'ppp-RNA activates antiviral signal through redistribution of IPS-1 mediated by MFN1. PLoS Pathog *6*, e1001012.

Opitz, B., Rejaibi, A., Dauber, B., Eckhard, J., Vinzing, M., Schmeck, B., Hippenstiel, S., Suttorp, N., and Wolff, T. (2007). IFNbeta induction by influenza A virus is mediated by RIG-I which is regulated by the viral NS1 protein. Cell Microbiol *9*, 930-938.

Orlinger, K.K., Hoenninger, V.M., Kofler, R.M., and Mandl, C.W. (2006). Construction and mutagenesis of an artificial bicistronic tick-borne encephalitis virus genome reveals an essential function of the second transmembrane region of protein e in flavivirus assembly. J Virol *80*, 12197-12208.

Overby, A.K., Popov, V.L., Niedrig, M., and Weber, F. (2010). Tick-borne encephalitis virus delays interferon induction and hides its double-stranded RNA in intracellular membrane vesicles. J Virol *84*, 8470-8483.

Park, G.S., Morris, K.L., Hallett, R.G., Bloom, M.E., and Best, S.M. (2007). Identification of residues critical for the interferon antagonist function of Langat virus NS5 reveals a role for the RNA-dependent RNA polymerase domain. J Virol *81*, 6936-6946.

Perera, R., and Kuhn, R.J. (2008). Structural proteomics of dengue virus. Curr Opin Microbiol *11*, 369-377.

Phair, R.D., and Misteli, T. (2000). High mobility of proteins in the mammalian cell nucleus. Nature *404*, 604-609.

Phair, R.D., and Misteli, T. (2001). Kinetic modelling approaches to in vivo imaging. Nat Rev Mol Cell Biol *2*, 898-907.

Pichlmair, A., and Reis e Sousa, C. (2007). Innate recognition of viruses. Immunity *27*, 370-383.

Pichlmair, A., Schulz, O., Tan, C.P., Naslund, T.I., Liljestrom, P., Weber, F., and Reis e Sousa, C. (2006). RIG-I-mediated antiviral responses to single-stranded RNA bearing 5'-phosphates. Science *314*, 997-1001.

Pichlmair, A., Schulz, O., Tan, C.P., Rehwinkel, J., Kato, H., Takeuchi, O., Akira, S., Way, M., Schiavo, G., and Reis e Sousa, C. (2009). Activation of MDA5 requires higher-order RNA structures generated during virus infection. J Virol *83*, 10761-10769.

Plotch, S.J., Bouloy, M., Ulmanen, I., and Krug, R.M. (1981). A unique cap(m7GpppXm)-dependent influenza virion endonuclease cleaves capped RNAs to generate the primers that initiate viral RNA transcription. Cell *23*, 847-858.

Politz, J.C., Browne, E.S., Wolf, D.E., and Pederson, T. (1998). Intranuclear diffusion and hybridization state of oligonucleotides measured by fluorescence correlation spectroscopy in living cells. Proc Natl Acad Sci U S A *95*, 6043-6048.

Rehwinkel, J., Tan, C.P., Goubau, D., Schulz, O., Pichlmair, A., Bier, K., Robb, N., Vreede, F., Barclay, W., Fodor, E., and Reis e Sousa, C. (2010). RIG-I detects viral genomic RNA during negative-strand RNA virus infection. Cell *140*, 397-408.

Rey, F.A., Heinz, F.X., Mandl, C., Kunz, C., and Harrison, S.C. (1995). The envelope glycoprotein from tick-borne encephalitis virus at 2 A resolution. Nature *375*, 291-298.

Rice, C.M., Lenches, E.M., Eddy, S.R., Shin, S.J., Sheets, R.L., and Strauss, J.H. (1985). Nucleotide sequence of yellow fever virus: implications for flavivirus gene expression and evolution. Science *229*, 726-733.

Robinett, C.C., Straight, A., Li, G., Willhelm, C., Sudlow, G., Murray, A., and Belmont, A.S. (1996). In vivo localization of DNA sequences and visualization of large-scale chromatin organization using lac operator/repressor recognition. J Cell Biol *135*, 1685-1700.

Rock, F.L., Hardiman, G., Timans, J.C., Kastelein, R.A., and Bazan, J.F. (1998). A family of human receptors structurally related to Drosophila Toll. Proc Natl Acad Sci U S A *95*, 588-593.

Rodriguez-Madoz, J.R., Belicha-Villanueva, A., Bernal-Rubio, D., Ashour, J., Ayllon, J., and Fernandez-Sesma, A. (2010a). Inhibition of the type I interferon response in human dendritic cells by dengue virus infection requires a catalytically active NS2B3 complex. J Virol *84*, 9760-9774.

Rodriguez-Madoz, J.R., Bernal-Rubio, D., Kaminski, D., Boyd, K., and Fernandez-Sesma, A. (2010b). Dengue virus inhibits the production of type I interferon in primary human dendritic cells. J Virol *84*, 4845-4850.

Roosendaal, J., Westaway, E.G., Khromykh, A., and Mackenzie, J.M. (2006). Regulated cleavages at the West Nile virus NS4A-2K-NS4B junctions play a major role in rearranging cytoplasmic membranes and Golgi trafficking of the NS4A protein. J Virol *80*, 4623-4632.

Rose, K.M., and Weiss, S.R. (2009). Murine Coronavirus Cell Type Dependent Interaction with the Type I Interferon Response. Viruses *1*, 689-712.

Roth-Cross, J.K., Martinez-Sobrido, L., Scott, E.P., Garcia-Sastre, A., and Weiss, S.R. (2007). Inhibition of the alpha/beta interferon response by mouse hepatitis virus at multiple levels. J Virol *81*, 7189-7199.

Rothenfusser, S., Goutagny, N., DiPerna, G., Gong, M., Monks, B.G., Schoenemeyer, A., Yamamoto, M., Akira, S., and Fitzgerald, K.A. (2005). The RNA helicase Lgp2 inhibits TLR-independent sensing of viral replication by retinoic acid-inducible gene-I. J Immunol *175*, 5260-5268.

Sage, D., Neumann, F.R., Hediger, F., Gasser, S.M., and Unser, M. (2005). Automatic tracking of individual fluorescence particles: application to the study of chromosome dynamics. IEEE Trans Image Process *14*, 1372-1383.

Saito, T., Hirai, R., Loo, Y.M., Owen, D., Johnson, C.L., Sinha, S.C., Akira, S., Fujita, T., and Gale, M., Jr. (2007). Regulation of innate antiviral defenses through a shared repressor domain in RIG-I and LGP2. Proc Natl Acad Sci U S A *104*, 582-587.

Saito, T., Owen, D.M., Jiang, F., Marcotrigiano, J., and Gale, M., Jr. (2008). Innate immunity induced by composition-dependent RIG-I recognition of hepatitis C virus RNA. Nature *454*, 523-527.

Samsa, M.M., Mondotte, J.A., Iglesias, N.G., Assuncao-Miranda, I., Barbosa-Lima, G., Da Poian, A.T., Bozza, P.T., and Gamarnik, A.V. (2009). Dengue virus capsid protein usurps lipid droplets for viral particle formation. PLoS Pathog *5*, e1000632.

Satoh, T., Kato, H., Kumagai, Y., Yoneyama, M., Sato, S., Matsushita, K., Tsujimura, T., Fujita, T., Akira, S., and Takeuchi, O. (2010). LGP2 is a positive regulator of RIG-I- and MDA5-mediated antiviral responses. Proc Natl Acad Sci U S A *107*, 1512-1517.

Schoggins, J.W., Wilson, S.J., Panis, M., Murphy, M.Y., Jones, C.T., Bieniasz, P., and Rice, C.M. (2011). A diverse range of gene products are effectors of the type I interferon antiviral response. Nature *472*, 481-485.

Seth, R.B., Sun, L., Ea, C.K., and Chen, Z.J. (2005). Identification and characterization of MAVS, a mitochondrial antiviral signaling protein that activates NF-kappaB and IRF 3. Cell *122*, 669-682.

Shav-Tal, Y., Darzacq, X., Shenoy, S.M., Fusco, D., Janicki, S.M., Spector, D.L., and Singer, R.H. (2004). Dynamics of single mRNPs in nuclei of living cells. Science *304*, 1797-1800.

Solomon, T., and Mallewa, M. (2001). Dengue and other emerging flaviviruses. J Infect *42*, 104-115.

Sourvinos, G., and Everett, R.D. (2002). Visualization of parental HSV-1 genomes and replication compartments in association with ND10 in live infected cells. Embo J *21*, 4989-4997.

Stadler, K., Allison, S.L., Schalich, J., and Heinz, F.X. (1997). Proteolytic activation of tick-borne encephalitis virus by furin. J Virol *71*, 8475-8481.

Stiasny, K., Fritz, R., Pangerl, K., and Heinz, F.X. (2009). Molecular mechanisms of flavivirus membrane fusion. Amino Acids.

Stiasny, K., and Heinz, F.X. (2006). Flavivirus membrane fusion. J Gen Virol *87*, 2755-2766.

Suthar, M.S., Gale, M., Jr., and Owen, D.M. (2009). Evasion and disruption of innate immune signalling by hepatitis C and West Nile viruses. Cell Microbiol *11*, 880-888.

Suthar, M.S., Ma, D.Y., Thomas, S., Lund, J.M., Zhang, N., Daffis, S., Rudensky, A.Y., Bevan, M.J., Clark, E.A., Kaja, M.K.*, et al.* (2010). IPS-1 is essential for the control of West Nile virus infection and immunity. PLoS Pathog *6*, e1000757.

Swaminathan, R., Hoang, C.P., and Verkman, A.S. (1997). Photobleaching recovery and anisotropy decay of green fluorescent protein GFP-S65T in solution and cells: cytoplasmic viscosity probed by green fluorescent protein translational and rotational diffusion. Biophys J *72*, 1900-1907.

Tabeta, K., Georgel, P., Janssen, E., Du, X., Hoebe, K., Crozat, K., Mudd, S., Shamel, L., Sovath, S., Goode, J.*, et al.* (2004). Toll-like receptors 9 and 3 as essential components of innate immune defense against mouse cytomegalovirus infection. Proc Natl Acad Sci U S A *101*, 3516-3521.

Tajima, S., Nukui, Y., Takasaki, T., and Kurane, I. (2007). Characterization of the variable region in the 3' non-translated region of dengue type 1 virus. J Gen Virol *88*, 2214-2222.

Takahasi, K., Yoneyama, M., Nishihori, T., Hirai, R., Kumeta, H., Narita, R., Gale, M., Jr., Inagaki, F., and Fujita, T. (2008). Nonself RNA-sensing mechanism of RIG-I helicase and activation of antiviral immune responses. Mol Cell *29*, 428-440.

Talon, J., Horvath, C.M., Polley, R., Basler, C.F., Muster, T., Palese, P., and Garcia-Sastre, A. (2000). Activation of interferon regulatory factor 3 is inhibited by the influenza A virus NS1 protein. J Virol *74*, 7989-7996.

Targett-Adams, P., Boulant, S., and McLauchlan, J. (2008). Visualization of double-stranded RNA in cells supporting hepatitis C virus RNA replication. J Virol *82*, 2182-2195.

Targett-Adams, P., and McLauchlan, J. (2005). Development and characterization of a transient-replication assay for the genotype 2a hepatitis C virus subgenomic replicon. J Gen Virol *86*, 3075-3080.

Taucher, C., Berger, A., and Mandl, C.W. (2010). A trans-complementing recombination trap demonstrates a low propensity of flaviviruses for intermolecular recombination. J Virol *84*, 599-611.

Town, T., Bai, F., Wang, T., Kaplan, A.T., Qian, F., Montgomery, R.R., Anderson, J.F., Flavell, R.A., and Fikrig, E. (2009). Toll-like receptor 7 mitigates lethal West Nile encephalitis via interleukin 23-dependent immune cell infiltration and homing. Immunity *30*, 242-253.

Tsien, R.Y. (1998). The green fluorescent protein. Annu Rev Biochem *67*, 509-544.

Tsukamoto, T., Hashiguchi, N., Janicki, S.M., Tumbar, T., Belmont, A.S., and Spector, D.L. (2000). Visualization of gene activity in living cells. Nat Cell Biol *2*, 871-878.

Tumbar, T., Sudlow, G., and Belmont, A.S. (1999). Large-scale chromatin unfolding and remodeling induced by VP16 acidic activation domain. J Cell Biol *145*, 1341-1354.

Tyagi, S., and Kramer, F.R. (1996). Molecular beacons: probes that fluoresce upon hybridization. Nat Biotechnol *14*, 303-308.

Uchil, P.D., Kumar, A.V., and Satchidanandam, V. (2006). Nuclear localization of flavivirus RNA synthesis in infected cells. J Virol *80*, 5451-5464.

Uchil, P.D., and Satchidanandam, V. (2003). Architecture of the flaviviral replication complex. Protease, nuclease, and detergents reveal encasement within double-layered membrane compartments. J Biol Chem *278*, 24388-24398.

Umareddy, I., Chao, A., Sampath, A., Gu, F., and Vasudevan, S.G. (2006). Dengue virus NS4B interacts with NS3 and dissociates it from single-stranded RNA. J Gen Virol *87*, 2605-2614.

Versteeg, G.A., Bredenbeek, P.J., van den Worm, S.H., and Spaan, W.J. (2007). Group 2 coronaviruses prevent immediate early interferon induction by protection of viral RNA from host cell recognition. Virology *361*, 18-26.

Wallner, G., Mandl, C.W., Kunz, C., and Heinz, F.X. (1995). The flavivirus 3'-noncoding region: extensive size heterogeneity independent of evolutionary relationships among strains of tick-borne encephalitis virus. Virology *213*, 169-178.

Wang, T., Town, T., Alexopoulou, L., Anderson, J.F., Fikrig, E., and Flavell, R.A. (2004). Toll-like receptor 3 mediates West Nile virus entry into the brain causing lethal encephalitis. Nat Med *10*, 1366-1373.

Wang, X., Li, M., Zheng, H., Muster, T., Palese, P., Beg, A.A., and Garcia-Sastre, A. (2000). Influenza A virus NS1 protein prevents activation of NF-kappaB and induction of alpha/beta interferon. J Virol *74*, 11566-11573.

Weber, F., Wagner, V., Rasmussen, S.B., Hartmann, R., and Paludan, S.R. (2006). Double-stranded RNA is produced by positive-strand RNA viruses and DNA viruses but not in detectable amounts by negative-strand RNA viruses. J Virol *80*, 5059-5064.

Welsch, S., Miller, S., Romero-Brey, I., Merz, A., Bleck, C.K., Walther, P., Fuller, S.D., Antony, C., Krijnse-Locker, J., and Bartenschlager, R. (2009). Composition and three-dimensional architecture of the dengue virus replication and assembly sites. Cell Host Microbe *5*, 365-375.

Wengler, G. (1993). The NS 3 nonstructural protein of flaviviruses contains an RNA triphosphatase activity. Virology *197*, 265-273.

Wengler, G., and Gross, H.J. (1978). Studies on virus-specific nucleic acids synthesized in vertebrate and mosquito cells infected with flaviviruses. Virology *89*, 423-437.

Werme, K., Wigerius, M., and Johansson, M. (2008). Tick-borne encephalitis virus NS5 associates with membrane protein scribble and impairs interferon-stimulated JAK-STAT signalling. Cell Microbiol *10*, 696-712.

Westaway, E.G., Khromykh, A.A., and Mackenzie, J.M. (1999). Nascent flavivirus RNA colocalized in situ with double-stranded RNA in stable replication complexes. Virology *258*, 108-117.

Westaway, E.G., Mackenzie, J.M., Kenney, M.T., Jones, M.K., and Khromykh, A.A. (1997). Ultrastructure of Kunjin virus-infected cells: colocalization of NS1 and NS3 with double-stranded RNA, and of NS2B with NS3, in virus-induced membrane structures. J Virol *71*, 6650-6661.

Wilson, J.R., de Sessions, P.F., Leon, M.A., and Scholle, F. (2008). West Nile virus nonstructural protein 1 inhibits TLR3 signal transduction. J Virol *82*, 8262-8271.

Wolk, B., Buchele, B., Moradpour, D., and Rice, C.M. (2008). A dynamic view of hepatitis C virus replication complexes. J Virol *82*, 10519-10531.

Yoneyama, M., and Fujita, T. (2009). RNA recognition and signal transduction by RIG-I-like receptors. Immunol Rev *227*, 54-65.

Yoneyama, M., Kikuchi, M., Matsumoto, K., Imaizumi, T., Miyagishi, M., Taira, K., Foy, E., Loo, Y.M., Gale, M., Jr., Akira, S.*, et al.* (2005). Shared and unique functions of the DExD/H-box helicases RIG-I, MDA5, and LGP2 in antiviral innate immunity. J Immunol *175*, 2851-2858.

Yoneyama, M., Kikuchi, M., Natsukawa, T., Shinobu, N., Imaizumi, T., Miyagishi, M., Taira, K., Akira, S., and Fujita, T. (2004). The RNA helicase RIG-I has an essential function in double-stranded RNA-induced innate antiviral responses. Nat Immunol *5*, 730-737.

Yu, I.M., Holdaway, H.A., Chipman, P.R., Kuhn, R.J., Rossmann, M.G., and Chen, J. (2009). Association of the pr peptides with dengue virus at acidic pH blocks membrane fusion. J Virol *83*, 12101-12107.

Yu, I.M., Zhang, W., Holdaway, H.A., Li, L., Kostyuchenko, V.A., Chipman, P.R., Kuhn, R.J., Rossmann, M.G., and Chen, J. (2008). Structure of the immature dengue virus at low pH primes proteolytic maturation. Science *319*, 1834-1837.

Zhou, H., and Perlman, S. (2007). Mouse hepatitis virus does not induce Beta interferon synthesis and does not inhibit its induction by double-stranded RNA. J Virol *81*, 568-574.

Zhou, Z., Licklider, L.J., Gygi, S.P., and Reed, R. (2002). Comprehensive proteomic analysis of the human spliceosome. Nature *419*, 182-185.

Zust, R., Cervantes-Barragan, L., Habjan, M., Maier, R., Neuman, B.W., Ziebuhr, J., Szretter, K.J., Baker, S.C., Barchet, W., Diamond, M.S.*, et al.* (2011). Ribose 2'-O-methylation provides a molecular signature for the distinction of self and non-self mRNA dependent on the RNA sensor Mda5. Nat Immunol *12*, 137-143.